

# A 2MASS All-Sky View of the Sagittarius Dwarf Galaxy: I. Morphology of the Sagittarius Core and Tidal Arms

Steven R. Majewski<sup>1</sup>, M. F. Skrutskie<sup>1</sup>, Martin D. Weinberg<sup>2</sup>, and James C. Ostheimer<sup>1</sup>

## ABSTRACT

We present the first all-sky view of the Sagittarius (Sgr) dwarf galaxy, which we have mapped by M giant star tracers detected in the complete Two Micron All-Sky Survey (2MASS). M giants make particularly good tracers of Sgr and its tidal debris because the Sgr core contains a prominent young and relatively metal-rich stellar population. Sgr M giants are separable from foreground dwarf stars using 2MASS photometry with selection criteria tuned from observations of the Sgr core's red giant branch.

Near infrared photometry of Sgr's prominent M giant population permits a view of the Sgr core with substantially reduced differential reddening. The core structure is fit with a King profile of limiting major axis radius  $30^\circ$ , ellipticity between 0.62-0.65 and a core radius substantially larger than previously found or assumed — almost  $4^\circ$ . In addition, the Sgr density profile exhibits a prominent break corresponding to the tidal debris, and in this way resembles the profiles of other Galactic dSph galaxies. However, the inner Sgr M giant density profile exhibits a cusp at the same location as, but not due to, the globular cluster M54, and provides further evidence that Sgr may be related to “nucleated dwarf elliptical” galaxies. With an inferred visual brightness of  $M_V = -13.27$ , the present Sgr *core* edges out Fornax as the brightest of the known Galactic dSph galaxies. Adopting traditional methods and previously published central velocity dispersions, we derive a total Sgr mass-to-light ratio of 25 in solar units.

Among the most striking features we identify in the all sky distribution of M giants is a prominent,  $> 150^\circ$  trailing arm extending from the Sgr core and arcing completely across the South Galactic Hemisphere with approximately constant density and a mean distance from the Sun that varies between about 20 to 40 kpc. This trailing tail of stellar debris may extend past the Galactic plane and into the Northern Galactic Hemisphere at the Galactic anticenter.

A rather prominent leading debris arm extends northward of the Galactic plane to an apoGalacticon  $\sim 45$  kpc from the Sun, then turns towards the North Galactic Pole (NGP) from where it descends back towards the Galactic plane. The near side of this Northern Loop becomes substantially foreshortened and covers the North Galactic

---

<sup>1</sup>Dept. of Astronomy, University of Virginia, Charlottesville, VA, 22903-0818 (srm4n@virginia.edu, mfs4n@virginia.edu, jco9w@virginia.edu)

<sup>2</sup>Dept. of Astronomy, University of Massachusetts at Amherst, 719 North Pleasant Street, Amherst, MA 01003-9305 (weinberg@osprey.astro.umass.edu)

Cap. The leading arm likely penetrates the Galactic disk near the Sun and may cross the trailing Sgr tidal arm in the South Galactic Hemisphere. We find ourselves at an unusual time in Galactic history: For less than 2% of the solar orbit are we closer to the mid-plane of the Sgr debris tails at the Solar Circle. It is likely that leading Sgr tidal debris is in the solar neighborhood.

We discuss the implications of this new view of the Sgr galaxy and its entrails for the character of the Sgr orbit, mass-loss rate, and contribution to the Galactic halo. The Sgr orbit shows minimal precession, with tidal debris confined to a coherent planar distribution. The relative numbers of M giants in the core and trailing tail suggests the mass in tidal arms to be at least 15% of the mass in the bound core (as defined by the King limiting radius). The fractional mass loss rate of Sgr is  $\sim 15\%$  per Gyr, which suggests that the M giant tidal structures have formed over more than one Sgr orbit. Variation of the length and density of the Sgr tails with the  $J - K_s$  colors of M giants suggests a possible age/metallicity variation along the arms and stellar ages broadly consistent with the dynamical timescale for creating tidal arms to the extent traced by the M giant stars. Sgr contributes more than 75% of the high latitude, halo M giants, despite the substantial reservoirs of M giants in the Magellanic Clouds. We find no evidence of M giant tidal debris from the Magellanic Clouds.

This first all-sky map of the Sgr dwarf is compared to all previous identifications of potential Sgr debris, including those from the Sloan Digital Sky Survey and the QUEST survey. Good correspondence is found between the M giant arms and all published Sgr finds. However, Sgr carbon stars are subluminous with respect to Magellanic Cloud carbon stars, a finding that requires adjustment of the previously published Sgr carbon star distance scale. 2MASS carbon stars trace the Sgr system less clearly than M giants, even though carbon stars associated with the Sgr tidal arms appear to account for the majority of the total high latitude Galactic halo carbon star sample to 75 kpc.

*Subject headings:* Sagittarius Dwarf – Milky Way: halo – Milky Way: structure – Milky Way: kinematics – galaxies: stellar content – Local Group

## 1. Introduction

The Sagittarius (Sgr) dwarf galaxy is a vivid and striking example of the process of satellite disruption and assimilation long presumed responsible for populating the Galactic halo (e.g. Searle & Zinn 1978). Alternatively, viewed as test particles, a sufficiently complete spatial and kinematic sample of Sgr stars can reveal underlying gravitational potentials – tracing both the luminous and dark matter of both Sgr and the Milky Way (Sackett et al. 1994, Johnston et al. 1999b, Ibata et al. 2001b). Since the discovery of Sgr (Ibata et al. 1994) there have followed a number of observations (reviewed below and in Section 8) to characterize the distribution and motion of the tidal debris and which have aided models of the disruption of the satellite in the Milky Way’s potential. Early

observations were largely restricted to small fields-of-view, but nevertheless painted the general picture of a substantially tidally disrupted satellite distributed across a sizeable portion of the celestial sphere.

However, many issues remain controversial and intertwined, particularly:

- The dark matter content in the Sgr core, which is integrally tied to the long-term integrity and mass loss rate of the satellite (e.g., Ibata & Lewis 1998, Gómez-Flechoso 1998, Gómez-Flechoso, Fux & Martinet 1999).
- The survivability of the Sgr system in its present orbit, which, even if it contains substantial dark matter, should not last a Hubble time (Velazquez & White 1995, Johnston et al. 1995). Solutions to this dilemma range from a fine tuning of the dark matter configuration within the satellite (Ibata & Lewis 1998), to an evolving orbit for the satellite (Zhao 1998, Gómez-Flechoso, Fux & Martinet 1999), or the creation of Sgr at later times as the daughter product of another, more major merger (Gómez-Flechoso, Fux & Martinet 1999).
- The original mass of the Sgr satellite, which today is smaller by an amount depending on the mass density (dark matter content) and orbital history of the system.
- The fractional contribution of Sgr stars (e.g., Ibata et al. 2001b, Vivas et al. 2001, Newberg et al. 2002) and clusters (e.g., Irwin 1999, Dinescu et al. 2000, 2001, Palma et al. 2002, Bellazzini et al. 2002a, 2003) to the Galactic halo, which must also satisfy limits imposed by the distribution of properties for Galactic halo field stars (cf. Unavane, Wyse & Gilmore 1996, Majewski et al. 2002b).
- The shape and size of the Galactic halo. Tidal tails are extremely sensitive to the amount and distribution of mass in the Galaxy (e.g., Johnston et al. 1999b, Murali & Dubinski 1999). Studies of the Sgr orbit (Ibata et al. 2001b) suggest the Milky Way dark halo to be nearly spherical, which places the Milky Way at an extreme of the wide range of dark halo flattenings (e.g., Sackett & Pogge 1995, Olling 1997, Peñarrubia et al. 2000, Sparke 2002). This result is at odds with (1) starcount studies, which typically find  $c/a \sim 0.6 - 0.8$  (e.g., Robin, Reylé & Crézé 2000, Siegel et al. 2002, Reid & Majewski 1993, and references therein), (2) *dynamical* studies of halo tracers (Binney, May & Ostriker 1987, Amendt & Cuddeford 1994; see also van der Marel 1991), and (3) Galactic microlensing studies, which imply a flattened halo (Samurovic, Cirkovic & Milosevic-Zdjelar 1999).
- The degree of visible substructure in the halo, which is directly related to the Galactic accretion history (Tremaine 1993, Bullock, Kravtsov & Weinberg 2001). For luminous halo stellar populations some mixture of Eggen, Lynden-Bell & Sandage (1962) and Searle & Zinn (1978) formation pictures is typically postulated, but evidence is increasing that the stellar halo is highly unmixed and substructured (Majewski, Munn & Hawley 1996, Vivas et al. 2001, Gilmore, Wyse & Norris 2002, Majewski 2003). To what extent Sgr has contributed to this

substructure is not well established. Recent evidence suggests that Sgr contributes of order 5% of the halo M giants in a correlated stream (Ibata et al. 2002a; but see Section 7.2).

- The degree of *invisible* substructure in the halo. Cold Dark Matter (CDM) models for the formation of galaxy halos predict the persistence of long-lived, “sub-halos” (e.g., Navarro et al. 1996, 1997) at a number greatly exceeding the number of *luminous* Galactic satellites (Klypin et al. 1999, Moore et al. 1999). The degree of coherence of tidal debris streams provide a powerful constraint on the lumpiness of the Galactic halo potential (Font et al. 2001, Johnston et al. 2002, Ibata et al. 2001b, Mayer et al. 2001).

Models for the interaction of Sgr with the Milky Way under different assumptions of orbit, Galactic potential, and Sgr dark matter content make distinct and testable predictions for the appearance of the satellite and its debris today (e.g., Velazquez & White 1995, Johnston et al. 1995, Edelshohn & Elmegreen 1997, Ibata et al. 1997, Ibata & Lewis 1998, Gòmez-Flechoso, Fux & Martinet 1999, Johnston et al. 1999a, Jiang & Binney 2000, Helmi & White 2001). Thus, improved observational constraints — e.g., on the detailed distribution (e.g., Gòmez-Flechoso et al. 1999, Jiang & Binney 2000) and degree of coherence of the Sgr debris (Ibata et al. 2002b, Johnston, Spergel & Haydn 2002) — can greatly increase our understanding of both the Milky Way and Sgr systems.

Previous studies of Sgr include a patchwork of approaches and directions of the sky, but, aided by the advent of large area surveys, including SDSS and QUEST, a more global picture of the Sgr dwarf and its remains has begun to emerge. For example, a survey locating 75 high latitude, halo carbon stars by Ibata et al. (2001b) finds more than half to lie along a great circle consistent with the likely Sgr orbit. Confirmation of this great circle comes from the location of coherent clumps of A-type (Yanny et al. 2000), RR Lyrae (Ivezić et al. 2000, Vivas et al. 2001), red clump (Mateo, Olszewski & Morrison 1998, Majewski et al. 1999a) and main sequence turn-off stars (Martinez-Delgado et al. 2001a,b, Newberg et al. 2002) in surveys that intersect this great circle at various points. Other studies have suggested an even more complex *multiply-wrapped* configuration around the Galaxy (Johnston et al. 1999, Dinescu et al. 2000, Dohm-Palmer et al. 2001, Kundu et al. 2002). In some cases, detections of Sgr debris far-flung from the Sgr core are supplemented with dynamical information (e.g., Majewski et al. 1999a, Ibata et al. 2001b, Dinescu et al. 2000, 2002, Kundu et al. 2002) useful for constraining the system dynamics.

However, to date, no single, unbiased, global, empirical characterization of Sgr exists. The Two Micron All Sky Survey (2MASS) remedies this situation by offering homogeneous photometry in bandpasses less sensitive to the effects of reddening with complete sky coverage. Studies of the high density core of the Sgr galaxy from early release 2MASS data are already in hand and delineate the bulk photometric characteristics of Sgr stars in the 2MASS bandpasses (Alard 2001, Cole 2001): Sgr apparently exhibits a metal abundance of  $[\text{Fe}/\text{H}] = -0.5$  or more (see also Bonifacio et al. 1999), and, as a result, contains a substantial number of M giants. The combination of  $J$ ,  $H$ , and  $K_s$  passbands permits color-based discrimination of M giant stars from (foreground) M dwarfs, a fact

that was exploited by Ibata et al. (2002a) to detect an excess of halo giants defining a great circle with a pole consistent with that extracted from the analysis of halo carbon stars.

Here we use the complete all-sky 2MASS source extractions to characterize the distribution of the Sgr M-giant population as projected on the sky as well as in three dimensions. This analysis reveals a King profile, dSph-like core and extensive, well-defined, trailing and leading Sgr tidal tails in the South and North Galactic Hemispheres. Among the remarkable aspects of the Sgr tidal debris stream are its coherence and nearly constant density over  $360^\circ$  of orbital longitude and that tidal debris from Sgr very likely rains down onto the solar neighborhood from the North Galactic Pole.

## 2. 2MASS Selection of Sgr M Giant Candidates

Near-IR (NIR) colors of giant and dwarf stars are degenerate for early spectral types ( $< K7$  or  $J - K_s \lesssim 0.55$ ) but become distinct in two-color diagrams for the latest spectral types because of the influence of the gravity sensitive CO bands in the  $K$  passband. The color divergence occurs for sources with  $J - K > \sim 0.85$  (Bessell and Brett 1988, Cutri 2003). A preliminary selection of candidates with  $J - K_s > 0.85$  was made from the 2MASS (Final Processing) working survey point source database covering  $> 99.9\%$  of the sky. Sgr tidal features were evident in celestial sphere projections of color/magnitude cuts even in this preliminary selection.

Subsequent reddening correction eliminates intrinsically blue objects that do not satisfy our color selection criteria (below). To account for differential reddening around the Galaxy we have interpolated  $E(B - V)$  for each of the selected stars with algorithms and reddening data provided by Schlegel et al. (1998), who give  $E(B - V)$  values derived from IRAS 100 micron emission all-sky maps. Each source was then dereddened after adopting the following selective and total extinction laws:

$$E(J - K_s) = 0.54E(B - V)$$

$$E(J - H) = 0.34E(B - V)$$

$$A(K_s) = 0.28E(B - V).$$

For the remainder of our analysis, sources with  $E(B - V) > 0.555$ , corresponding to  $E(J - K_s) = 0.30$ , were excluded to avoid potential contamination from excessively reddened sources.

Noise in stellar colors smears the distinction between dwarfs and giants. 2MASS aperture magnitudes are demonstrably more precise than the PSF-fit magnitudes for the brighter stars. The photometry used here is exclusively aperture photometry where the quoted photometric uncertainty was  $< 0.06$  mag in all three bands. This strong constraint on photometric accuracy imposes a

completeness limit on the 2MASS selection used here of approximately  $K_s < 13.5$ , substantially brighter than the 99% survey completeness requirement of  $K_s < 14.3$ .

Evaluation of the  $J - H$  vs.  $J - K_s$  color-color diagram of the Sgr core permits further refinement of the color selection criteria for Sgr M giants. Figure 1 shows the  $(J - K_s, K_s)_o$  color-magnitude and color-color diagrams for 2MASS point sources in  $3 \times 3 \text{ deg}^2$  areas centered on the Sgr core and in a control field centered on a point reflected across the Galactic  $l = 0$  axis at the same Galactic latitude. To make the Sgr red giant branch even more clear, we include in Figure 1c the results of a statistical subtraction in color-magnitude space of the control field from the Sgr core field using the same method as Layden & Sarajedini (2000) with aspect ratio parameter  $\alpha = 5$ . Significant small-scale variations in reddening and population densities mean that the subtraction is not perfect, but the position of the Sgr giant branch in both Figures 1c and 1f are obvious.<sup>3</sup> The prominent Sgr red clump also becomes more visible in Figure 1c.

The initial selection for M giants is conservative, to balance a desire for a large statistical sample of M giants but with minimal contamination by other stars (improperly dereddened dwarfs and stars with large photometric errors; see Figure 2a), and satisfies (Figure 2):

$$\begin{aligned} J - K_s &> 0.85 \\ J - H &< 0.561(J - K_s) + 0.36 \\ J - H &> 0.561(J - K_s) + 0.22 \end{aligned}$$

where all magnitudes are in the intrinsic, dereddened 2MASS system.

From a partial survey of the Sgr core, Whitelock et al. (1999) estimate that the Sgr dwarf galaxy contains of order 100 N-type carbon stars (a slight underestimate — see Figure 21). Carbon stars, because they have extreme, easily identifiable NIR colors, make them a potentially useful tracer of the Sgr debris stream (e.g., Ibata et al. 2001b). However, Sgr carbons have a large spread in luminosity and a number are long-period variable (see Figure 20 below), which yields large uncertainties in estimated photometric parallaxes relative to the better defined M giant color-magnitude relation. Thus, in this paper we rely predominantly on the much more populous M giants to trace the Sgr tidal streams, but include a discussion of the carbon stars in Section 8.3.

---

<sup>3</sup>We show in Section 4 that the semi-major axis of the Sgr core is about  $30^\circ$ , which means that the control field here, though near the minor axis of Sgr, is still within the tidal radius. However, the density of Sgr in the control field at this radius is about 1% the core, so its presence in the control field does not effect our interpretation of the CMD here or our analysis of the Sgr luminosity function in Figure 22.

### 3. Salient Features of All-Sky Maps of 2MASS M Giant Candidates

The Sgr core is a readily apparent feature of all-sky images of the 2MASS point source catalogue already in the public domain (see, for example, <http://www.ipac.caltech.edu/2mass/gallery/showcase/allsky/index.html>). Various aspects of Sgr’s debris stream also become readily apparent in color-magnitude windows of the point source catalogue that highlight Sgr M giants at specific distances. Figure 3 shows two such windows.

Several large scale features are evident in Figure 3. Some are artifacts of heavy and patchy differential reddening near the Galactic plane. Reddening can shift early type stellar colors into the giant star two-color locus (Figure 2). Several prominent extensions from the disk correspond to high latitude dust in the Galaxy also seen in IRAS 100 micron maps.

Figure 3 shows Sgr debris at varying distances in a great circle around the entire celestial sphere. The most prominent M giant features, apart from the Galactic Center and plane, are the Magellanic Clouds and the Sgr core at  $(\alpha, \delta) = (284, -30)^\circ$  (discussed in Section 4). Stretching from the Sgr core itself, southward for a short span and then northward, is a “Southern Arc”. In Section 6 we explore the distance distribution of the Arc and show that it extends physically from the Sgr core. The distance modulus of the Southern Arc is more or less constant from the Sgr core to the Galactic anticenter. The arc may, in fact, cross the Galactic plane at the anticenter and cross into the Northern Galactic Hemisphere, albeit at very low surface density.

More than a magnitude fainter than the Arc is a spike of M giants extending prominently northward from the Galactic Center direction. This “Northern Spur” has a longitudinal gradient in median  $K_s$  magnitude indicating a growing distance with increasing Galactic latitude until reaching the North Galactic Cap. The brighter magnitude slice in Figure 3 shows a subtle, more extended, “fluffy” distribution of M giant candidates situated near the termination point of the Northern Spur. The fluffy concentration spans several tens of degrees, obviously wider than either the Northern Spur and Southern Arc, but with less area density. As we show in Section 6, the bright northern fluff represents a severely foreshortened extension of the Northern Spur. Indeed, in even brighter magnitude windows, this “North Fluff” is still present, but is spread out over steradians. At the brightest 2MASS magnitudes it encompasses nearly all of the Northern Galactic Hemisphere, as would be expected for a large structure very near the Sun (Section 6.4).

### 4. Analysis of the Sagittarius Core

The extended, low surface brightness, Sgr core lies nearly behind the Galactic Center, which leads to significant contamination by foreground Milky Way bulge and disk stars and obscuration by patchy foreground dust. Early star count analyses by Ibata, Gilmore & Irwin (1995) and Ibata et al. (1997) explored the core and southwards (Mateo, Olszewski and Morrison 1998). More recently, studies of RR Lyrae stars examined the more obscured northern core (Cseresnjes, Alard & Guibert

2000, see also Alard 1996, Alcock et al. 1997). However, the integrated structure of the Sgr core remains uncertain. For example, while roughly agreeing on the derived Sgr major axis scale length of fit exponential profiles, Mateo et al. (1998) identify a break in the southern profile of Sgr at a radius of 20 degrees while Cseresnjes et al. (2000) identify one at a substantially different density in the northern profile at only six degrees.

Despite its rather irregular appearance in optical maps, Sgr is most often assumed to be a dwarf spheroidal type galaxy, because: (1) Sgr lacks significant HI (Koribalski, Johnston, & Otrupcek 1994, Burton & Lockman 1999), (2) it contains both old stars and has experienced extended star formation epochs (cf. Mateo et al. 1995) but is not presently forming strars (Bellazzini et al. 1999b), and (3) like other dSph galaxies, Sgr appears to have a rather large  $M/L$  (Ibata et al. 1997). Alternatively, it is often postulated (Bassino & Muzzio 1995, Sarajedini & Layden 1995, Layden & Sarajedini 2000) that the center of Sgr coincides with the globular cluster M54 (Ibata et al. 1995, 1997) and the M54+Sgr combination may represent a *nucleated dwarf elliptical* galaxy (Zinnecker et al. 1988, Freeman 1993). Because Sgr exhibits an apparent metallicity gradient with overall higher core metallicity (Bellazzini et al. 1999a,b, Alard 2001 - though see Cseresnjes 2001) along with rather young,  $\sim 0.5$  to  $\sim 3$  Gyr stellar populations there (cf. Bellazzini et al. 1999b, Layden & Sarajedini 2000), Alard (2001) postulates a third scenario - that Sgr may be more like an LMC-type galaxy with an inner disk, or perhaps a recently disrupted disk. While other dwarf spheroidals have been shown to have metallicity gradients (e.g., Light 1988, Da Costa et al. 1996, Majewski et al. 1999b, Hurley-Keller, Mateo & Grebel 1999, Harbeck et al. 2001), Sgr is unique in having such young and metal-rich populations. Recent simulations (Mayer et al. 2001) suggest that it does not take much tidal stirring in a satellite to transform disk dwarf spheroidals into dwarf spheroidals.

The 2MASS database presents the first opportunity for a large-scale, uniform study of the extended Sgr core at NIR wavelengths where the effects of reddening are diminished. These data clarify a number of the above issues regarding the nature of the Sgr galaxy.

#### 4.1. Radial Profile Fits to the Sgr Core

Figure 4 illustrates the distribution of candidate M giants near the nominal Sgr core stars with  $E(B - V) < 0.555$ ,  $0.95 < (J - K_s)_o < 1.10$  and  $10.5 < (K_s)_o < 12.0$ . This magnitude range excludes strong foreground contamination from brighter Galactic bulge/disk stars and a smaller number of likely disk stars at fainter magnitudes (see Figure 8). The NIR appearance of Sgr is far smoother than that seen in optical starcount analyses (e.g., Ibata, Gilmore & Irwin 1995, Ibata et al. 1997): At NIR wavelengths the Sgr core closely resembles other dwarf spheroidal galaxies, as is shown quantitatively below. We fit two functional forms to the least reddened Sgr core data with  $b < -10^\circ$  (Figure 4) using the Bayesian methods and analytical forms described by Ostheimer et al. (2003): a King (1962) profile and a power law plus core (PLC) model. Table 1 and Figure 5 summarize these results.

Understanding the matter distribution of both the bound and unbound portions of Sgr requires separating the two contributions with care. A King profile fit to starcounts at all positions angles (Figure 5a) does not account for unbound tidal debris manifested as a “break” from a nominal King shape at a major axis radius of about 1300 arcmin (more visible in Figure 5c and Figure 12), and at smaller radii at position angles away from the major axis because of the ellipticity of the system. To counter the growing influence with radius of unbound stars on the King profile fit, we excise data along the major axis, thus weighting the fit at large radii predominantly by the minor axis structure, which is primarily constituted by bound stars (Figure 5b). The King parameterization now fits well over most radii; Table 1 gives the fit to the Figure 4 data trimmed by Right Ascension to  $\alpha_{2000} < 300^\circ$  and by Galactic latitude to  $b < -10^\circ$ . Transferring this fit of *bound* Sgr stars back to the full radial profile reveals more clearly the transition from bound to unbound stars (Figure 5c). Despite the major improvement in the fit of the King profile at interior radii, the position angle ( $100.5^\circ$  versus  $104.3^\circ$ ), the ellipticity (0.62 versus 0.65) and the declination of the core ( $\Delta\delta = 3$  arcmin) change only slightly. The fit is robust to varying the right ascension cutoff to more conservatively exclude tidal features.

A single power law fit to the radial density profile can only accommodate the general character of the density decline (Figure 5d), but not the detailed shape of the radial profile; for example, it “averages over” the kink in the density profile discussed above. The mean power law fit (with  $\nu = 1.44$ ; see Ostheimer et al. 2003 for the precise function of the model) corresponds at large radii to an  $r^{-\gamma}$  decline with  $\gamma \sim 2.88$ , which is overly steep beyond the break near 1300 arcmin, where the data appear to decline more like  $\gamma \sim 2$ . This  $\gamma \sim 2$  decline is similar to that observed beyond the King limiting radius of the Carina dSph (Majewski et al. 2000).

The Table 1 King and PLC model fits yield Sgr position angles in the range of those found by previous analyses: Mateo, Olszewski & Morrison (1998) obtained a position angle of  $104.8^\circ \pm 1.2^\circ$  while Cseresnjes, Alard & Guibert (2000) obtained a PA of  $108.4^\circ$ . Not surprisingly, both of our model fits find Sgr to be of high ellipticity,  $\epsilon = 0.62 - 0.65$ , though not quite as high as the  $\epsilon = 0.80 \pm 0.15$  previously reported (Mateo 1998). Several other Local Group dSph galaxies have similar ellipticities, namely And III (Caldwell et al. 1992, Ostheimer et al. 2003) and Ursa Minor (Irwin & Hatzidimitriou 1995, Kleyna et al. 1998, Bellazzini et al. 2002b, Palma et al. 2003). Indeed, the structure of Sgr bears similarity to Ursa Minor (Palma et al. 2003) and Carina (Majewski et al. 2000).

## 4.2. Departures from a King Profile

### 4.2.1. Nucleus

Two differences of the observed versus fit radial profiles are noteworthy: the presence of a break population (Section 4.2.2) and the appearance of a “core” within about 20-25 arcminutes that is elevated above the density trend immediately exterior to this radius. The centers of the King

and PLC fits lie within a few arcminutes of the center of the massive globular cluster NGC6715 (M54) at  $(\alpha, \delta)_{2000} = (18:55:03.3, -30:28:42)$ . The excess 2MASS starcounts might be attributed to the cluster itself, however, (1) the core, half-light and tidal radii of M54 have been derived (Trager, King & Djorgovski 1995) as 0.11, 0.46 and 7.5 arcmin — too small to account for the extent of the excess observed; and (2) the metallicity of M54 is  $[\text{Fe}/\text{H}] = -1.7$  and its age is 14-16 Gyr (Layden & Sarajedini 2000), so it should not contain stars as red as the M giants used for the fits (and shown in Figure 4) and is thus “invisible” to our survey (the tip of the corresponding RGB is at  $[J - K_s]_{2MASS} = 0.724$ ; Bertelli et al. 1994). The 2MASS results demonstrate that there is a nuclear condensation in the Sgr system that is independent of the presence of the metal poor population typically identified with the M54 globular cluster, whether or not M54 is a distinct stellar system from Sgr.

Layden & Sarajedini (2000) have recently shown that all metallicity Sgr populations are clumped around M54, with the most metal-rich ( $[\text{Fe}/\text{H}] \sim -0.5$ ) and young (1 and 2.5-3 Gyr) stellar populations particularly so (see also Sarajedini & Layden 1995, Marconi et al. 1998, Bellazzini et al. 1999a). The metal-rich populations are the likely source of the M giant enhancement we observe. Our finding of a cuspy distribution in the center of the Sgr profile is similar to the findings of Cseresnjes et al. (2000) who with their various fits also faced problems with the peaked central density of RR Lyrae stars. That our highest Sgr density is coincident with the position of M54 is consistent with other large area studies of the Sgr core (Ibata et al. 1995, 1997, Bellazzini et al. 1999a).

Whether M54 represents the actual nucleus of Sgr, or just happens to reside at the bottom of the Sgr potential well remains uncertain, and M54’s relation to, and potential role in creating, the much more metal rich populations condensed around it are matters of conjecture. These and related issues are explored in more detail by Layden & Sarajedini (2000). Though the overall radial profile of Sgr resembles that of other dSphs (and even including the presence of a “break population” at large radii - see below), the presence of a nucleated core in at least one way restores Sgr to a unique status among the Galactic dSphs.

#### 4.2.2. Break Population

The 2MASS Sgr radial profile shows a “break” from a King model near a semi-major axis of about 1300 arcmin. Mateo, Olszewski & Morrison (1998) observed a similar “kink” at  $\sim 20^\circ$  radius and speculated that it might arise from a transition from a distinct Sgr dwarf to tidal stream debris. The Mateo et al. surface density data match well the representation of 2MASS density with longitude along the major axis (Figure 13). The break from a King profile matches the expectations of the profile of a tidally disrupted dwarf (Johnston, Sigurdsson & Hernquist 1999). The 1300 arcmin radius thus demarcates the approximate projected radius where unbound tidal material begins to dominate the density profile (Mateo et al. 1998, Helmi & White 2001). The actual Sgr tidal radius formally obtained (Table 1) from the King limiting radius, is 1800 arcmin.

The Sgr radial profile resembles those of other Galactic dSphs found to have breaks from a King profile at large radii (see Irwin & Hatzidimitiou 1995), for example Carina (Kuhn et al. 1996, Majewski et al. 2000), Ursa Minor (Kocevski & Kuhn 2000, Martínez-Delgado et al. 2001a, Palma et al. 2003) Sculptor (Westfall et al. 2000, 2003, Walcher et al. 2003), and Leo I (Sohn et al. 2003). Sgr now demonstrates at least one case where the break population represents tidal debris, and lends support to claims that break populations in other dwarfs similarly imply tidal disruption (see discussion in Majewski et al. 2002a, for example).

### 4.3. Sgr Mass-to-Light Ratio Revisited

The dark matter content of the Sgr dwarf core remains controversial (Ibata & Lewis 1998, Gómez-Flechoso, Fux & Martinet 1999). The mass density of the satellite determines its long-term integrity. Early investigations (Ibata et al. 1997) postulated that “Sgr is being tidally distorted and is tidally limited, but is not disrupted as yet”, and derived a Sgr model with a central mass-to-light ratio of  $(M/L_V) \sim 50M_\odot/L_{\odot,V}$ . This dark matter-dominated, prolate but tidally-limited model, where mass does not follow light, was motivated by the apparent delicacy and short-livedness of low mass King models when placed in the most likely Sgr orbits (Velazquez & White 1995, Johnston et al. 1995). It was further suggested that Sgr could not have been significantly larger than observed today, otherwise “we would expect to find its ‘missing mass’ as a substantial population of Sagittarius dwarf debris — globular clusters and stars — along its dispersion orbit” (Ibata et al. 1997). Subsequently, with the observed extent of the Sgr system growing and the clear indication of mass loss into tidal debris tails, the picture of Sgr changed dramatically, with the dwarf recognized to be “in the process of being tidally disrupted and assimilated into the Milky Way” (Ibata 1999). But a conundrum remains: Even were Sgr to contain substantial dark matter — sufficient to account for the observed large internal velocity dispersion in the core and suggesting a global  $M/L_V$  at the level of the most extreme cases among the Galactic dSph population — it would not be enough to solve the puzzle of how the dwarf could have survived as long as it has in its present orbit.

Fine tuning of the dark matter configuration within the satellite provides one possible solution (Ibata & Lewis 1998). Such models with very extended dark matter haloes yield concomitantly high  $M/L \sim 100$ , yet still cannot match some characteristics of the observed Sgr system (see Helmi & White 2001).

More prosaic alternatives can also address the dilemma of a fragile Sgr surviving a Hubble time. For example, Zhao (1998) proposed that Sgr has not always been in its present orbit, but rather it was deflected from a “safer” orbit by an encounter with the Magellanic Clouds several Gyr ago. Gómez-Flechoso et al. (1999) similarly that as long as the full Galactic tidal field is experienced slowly (e.g., through a prolonged decay of an orbit via dynamical friction) even a non-dark-matter-dominated satellite could survive many orbits (see also Jiang & Binney 2000). Alternatively, Gómez-Flechoso et al. (1999) propose that Sgr may have formed in the tidal tail of a larger parent undergoing a major merger.

The 2MASS structural parameters allow a rederivation of Sgr’s  $M/L$  according to standard prescriptions based on the virial theorem. The applicability of these standard prescriptions for systems that appear *not* to be in virial equilibrium has been discussed by, e.g., Kroupa (1997), Gómez-Flechoso (1998), Klessen & Kroupa (1998), Majewski et al. (2002a) and Gómez-Flechoso & Martínez-Delgado (2003). Our goal here is to employ these standard methods as a touchstone for further discussion about the dark matter issue elsewhere.

Using the King profile parameters in Table 1 to represent the *bound* part of the Sgr system, we convert the integrated light profile to a total brightness by matching the M giant density at a specific radius to the equivalent surface brightness measured at the same radius. The King profile fit does not track the elevated density cusp in the center of Sgr so the peak surface brightness of Sgr is unrepresentative of the inner King brightness. Fortunately, Mateo et al. (1995) have measured the surface brightness of Sgr outside the central condensation, while Mateo, Olszewski & Morrison (1998) have estimated the “central” surface brightness as part of an extrapolation of a fit to the brightness profile that also ignores the cusp; both methods obtain  $\Sigma_{o,V} = 25.2 \pm 0.3$  mag arcsec $^{-2}$ . With the latter value for the flat part of our density profile, an integration of the King profile yields a total apparent magnitude for Sgr of  $M_V = 3.63$ , which is virtually identical to one of the results obtained by Mateo et al. (1998, their  $V_{tot,1}$ ), though the similarity may be fortuitous since Mateo et al. integrate a two-component exponential profile fit to their one-dimensional cross-sectional profile of Sgr and their integration *includes* the tidal debris profile, whereas we fit and integrate a King profile fit to the full two-dimensional shape of Sgr and include only the supposed *bound* stars in the integration. On the other hand, the Mateo et al. (1998) adoption of a 3:1 axis ratio for the inner shape of Sgr (Ibata et al. 1997) reasonably matches our findings for the Sgr ellipticity. The tidal debris contribution in the area they surveyed makes a relatively minor contribution to the total luminosity. Ignoring the central cusp likely underestimates the total Sgr luminosity by < 5%.

A Sgr distance modulus of  $(m - M)_o = 16.90 \pm 0.15$  (Ibata et al. 1997), implies an absolute magnitude of  $M_V = -13.27$  for the bound part of the galaxy. Thus, the Sgr dSph is likely the most luminous of the Milky Way family. That the bound fraction of Sgr and the Fornax dSph ( $M_V = -13.2$ ; Mateo 1998) are of comparable luminosity is consistent with the currently established globular cluster specific frequency of the two systems: Fornax has six clusters and Sgr almost certainly has five (see Section 8 below), and possibly several more (Palma et al. 2002, Bellazzini et al. 2002a, 2003).

The pre-disruption luminosity of Sgr was brighter than the above estimate. In Section 7.1 we estimate that the tidal tails contain about 15% of the bound mass. Prior to disruption Sgr was at least several tenths of a magnitude brighter (ignoring effects of stellar evolution and a variable star formation history).

To estimate the bound mass of Sgr, we use the formalism of King (1966) as outlined by Richstone & Tremaine (1986). Thus, the mass of Sgr is given by

$$M_{tot} = 166.5 r_c \mu / \beta$$

where the scaling parameter  $\mu$  is given by King (1966) as  $\sim 9.38$  for an object with the concentration of Sgr, i.e.  $\log(r_t/r_c) = 0.905$  (Table 1). The velocity parameter  $\beta$  is related to the observed velocity dispersion, most commonly taken as the  $11.4 \text{ km s}^{-1}$  value in Ibata et al.’s (1997) field “f7” in the Sgr core. This dispersion yields  $\beta \sim 0.8^2/\sigma^2$  (Binney & Tremaine 1987, see their Figure 4.11),  $M_{tot} = 4.9 \times 10^8 M_\odot$ , and  $M_{tot}/L_{tot} = 25$  in solar units (where we adopt the total V band luminosity from above as  $2 \times 10^7 L_\odot$ ). The fact that there appears to be a nuclear concentration of stars (and therefore mass) in the central region of Sgr that spans Ibata et al.’s field f7 raises concern that the velocity dispersion there may be enhanced. Ibata et al.’s next field out from the Sgr center, at several core radii, is “f5” for which the velocity dispersion is only  $9.2 \text{ km s}^{-1}$ . Adopting this dispersion, however, leads to little difference:  $\beta \sim 0.6^2/\sigma^2$ ,  $M_{tot} = 5.8 \times 10^8 M_\odot$  and  $M_{tot}/L_{tot} = 29$ .

These  $(M/L)_{tot}$  values are two to four times smaller than suggested by earlier studies, except that of Mateo et al. (1998). But it is important to point out that the Table 1 *structural parameters* are also significantly different than those that have been adopted in previous studies and models of the Sgr system. For example, while the stellar distributions in Helmi & White’s (2001) Sgr models have similar concentrations,  $c = \log_{10}(r_t/r_c)$ , to the  $c = 0.90$  here, the actual scale of their Sgr stellar systems are more than a factor of four smaller than found here. The models by Ibata & Lewis (1998) and Gómez-Flechoso et al. (1999) are similarly spatially compressed. Indeed, no model in the Ibata & Lewis (1998) library has a tidal radius anywhere near that derived here (their model K9, with a tidal radius roughly half of ours but a similar mass and approximately similar  $[\Psi/\sigma^2]$  parameter is probably the closest match to the observed 2MASS M giant parameters). Most of these models have been influenced by the original structural parameters derived for the Sgr dwarf by Ibata et al. (1997), which yielded a half-light radius that is almost exactly three times smaller than derived here. The large difference in the derived core radius is likely because we have fit (Figure 5) a King profile to the entire system *and that fit is generally insensitive to the localized central cusp of Sgr*, whereas Ibata et al. use the cusp to define the central surface brightness from which they search for a half-light decrement. In effect, the Table 1 profile fits to the Sgr dSph result in a satellite that has an overall structure that is much more distended – and therefore apparently more fragile – than typically assumed.

## 5. Great Circle M Giant Streams, the Sgr Orbital Plane and a Sgr Coordinate System

### 5.1. Great Circle Cell Counts of M Giants

We first define a new coordinate system specific to the Sgr system in which the core and tidal debris can readily be assembled into a coherent picture. Because Sgr and its debris lie close to

one great circle defined by its orbit (Figure 3), we adopt the method of Great Circle Cell Counts (“GC3”; Johnston, Hernquist & Bolte 1996) for an initial approximation to the orbital plane. A similar method was adopted by Ibata et al. (2002a) on the 2MASS Second Incremental Data Release; in their analysis of 26.4% of the sky Ibata et al. identified a peak in the M giant candidate source counts corresponding to Sgr at  $(l, b) = (95, 13)^\circ$ . Ibata et al. (2001b) have also explored carbon star counts in great circle cells and identified a peak at  $(l, b) = (90, 13)^\circ$  corresponding to Sgr.

To establish the Sgr orbital geometry we select M giant candidates with  $0.95 < (J - K_s)_o < 1.10$ , and  $E(B - V) < 0.555$ . We further limit the survey to M giant candidates with projected photometric parallaxes from 13 to 65 kpc — the primary distance range for the majority of material in the Southern Arc and Northern Spur. While limiting the volume of our GC3 assessment of tidal streams, the above photometric parallax limit also reduces the contribution of “false positive” detections that flood the survey sample at the faint end of the magnitude range (see discussion in Section 6.6). GC3 runs with a variety of Galactic latitude limitations were made, both including and excluding the main body of Sgr. By excluding the main body of Sgr, we give more weight to the tidal debris in the derivation of the best fit plane, but the results of the analysis were rather robust to these variations as well as in variations in the angular width of the cells and in the step size of the poles: For runs with various cell sizes and exclusion zones the peak in GC3 counts yielded poles within a degree of  $(l, b) = (273, -13)^\circ$ .<sup>4</sup>

Figure 6a shows the GC3 pole count analysis for a sample limited to  $|b| > 30^\circ$  and excluding the Large and Small Magellanic Clouds.<sup>5</sup> A great circle cell width of  $5^\circ$  is used. The pole from this particular figure is  $(l, b) = (272, -12)^\circ$ . By a quirk of Nature, the Sgr debris plane lies relatively near the ecliptic plane (which has a pole of  $[l, b] = [276, -30]$ ).

## 5.2. Best Fitting Sagittarius Plane

### 5.2.1. Fit in Galactic Cartesian Coordinates

The GC3 methodology assumes that the debris under study is sufficiently far away that the effects of Galactocentric parallax are negligible; i.e., strictly speaking, debris streams will follow great circles across the sky only when viewed from the Galactic Center. However, parts of the Sgr debris stream come sufficiently close to the Sun and the Galactic Center that several interesting effects of perspective come into play (Figure 7). The facts that 1) the Sun is not directly in the orbital plane of Sgr, and 2) the Southern Arc and Northern Spur stars are at rather different

<sup>4</sup> Any great circle distribution on the sky produces two antipodal peaks in the cell counts. Unlike Ibata et al. (2002a), we elect to identify Sgr with the peak in the South Galactic hemisphere because this corresponds to the *angular momentum pole* of the satellite itself (see also Palma et al. 2002).

<sup>5</sup> The Magellanic Clouds were removed by excluding the zone  $260^\circ < l < 320^\circ$  and  $-53^\circ < b < -25^\circ$ .

distances from us means that different GC3 poles are derived by analysis of the two tidal tails independently: We obtain  $(279, -18)^\circ$  and  $(271.5, -11.5)^\circ$  as the GC3 poles when we divide the data set into Northern and the Southern Galactic Hemispheres, respectively (Figures 6b and 6c).

To remove Galactocentric parallax effects, we find the best-fitting Sgr orbital plane in the Cartesian Galactic coordinate system. To place stars in these coordinates, a photometric parallax is calculated for each star from an absolute magnitude-color relation derived from the red giant branch color-magnitude data shown in Figure 1c. The fit was restricted to 1675 stars in the restricted range  $0.9 \leq (J - K_s)_o \leq 1.10$ , the primary M giant color range explored in this paper. With  $2.5\sigma$  iterative rejection of 158 stars, the following fit is obtained with an RMS of 0.36 mag:

$$K_S = -8.650(J - K_s)_o + 20.374$$

The resultant distance scale (after assuming a Sgr core distance modulus of 16.90) is approximately 13% smaller (at  $[J - K_s]_o = 1.0$ ) than the one obtained from adopting the primary locus for an  $[\text{Fe}/\text{H}] \approx -0.5$  or  $-0.4$  population identified as a good match by Cole (2001) to 2MASS observations of the Sgr core,

$$M_{K_S, \text{CIT}} = -9.43(J - K_s)_{o, \text{CIT}} + 3.623,$$

and which translates to

$$K_S = -8.930(J - K_s)_o + 20.383$$

after transforming the Elias et al. (1982) Caltech/CTIO (CIT) system into the natural 2MASS filter system using the equations given by Carpenter (2001). Use of the color-magnitude calibration from Figure 1c is preferred over the latter relation because: (1) The former  $K_S([J - K_s]_o)$  relation is from a fit specific to the restricted color range explored in this paper; (2) it is derived from a *background-subtracted* color-magnitude diagram of the core; (3) it was fit in the natural 2MASS photometric system and free of transformation equation uncertainites; and (4) it derives from a Sgr core catalogue almost ten times larger than Cole used.

Adopting this mean RGB color-magnitude relation implicitly translates the astrophysical scatter within the Sgr RGB into an imposed artificial scatter about calculated mean photometric parallaxes for Sgr features. This intrinsic “standard candle” scatter dominates the 2MASS photometric errors, selected to be  $< 0.06$  mag in each band and typically closer to the 0.02-0.03 mag uncertainty for bright survey sources. The intrinsic vertical width of the Sgr RGB in Figure 1c for the  $0.9 \leq (J - K_s)_o \leq 1.1$  color range at the heart of most of the results presented in this paper is  $\text{FWHM}(K_s) \sim 0.85$  mag. Thus, the imposed fractional distance spread is approximately  $\sigma_d/d \sim 0.17$ . This is probably a slight underestimate, since the RGB spread is not strictly Gaussian (being somewhat flatter than Gaussian within the FWHM), and, of course, this does not account for the weak tail to brighter  $M_{K_s}$  for the more metal poor component of Sgr.

To fit the Sgr orbital plane, we adopt as a first approximation the GC3 pole from above and find all M giant candidates within 15 kpc to either side of the plane in the sky defined by this pole. Obviously, this plane includes the Sun, but not the Galactic Center, however, because the Sun is

*almost* in the Sgr orbital plane (see below), this is a reasonable first subsample that is more than generous enough to include all of the Sgr tidal debris. Though, as we show below (e.g., Sections 5.3 and 7.1), Sgr debris represents the *bulk* of the M giant population in the outer halo, we can refine this “Sgr debris” sample by making a further, narrower color selection of  $1.0 \leq (J - K_s)_o < 1.1$ : This color range removes a large amount of contamination by photometric errors in the distance range of the Sgr debris (see Section 6.6 and Figures 14 and 15), but also restricts the absolute magnitude range and thereby lessens the effects of any systematic photometric parallax errors. To remove the remaining photometric error contaminants of *this* color-restricted sample, and with some foreknowledge of the position of the Sgr debris streams (Section 6), we remove stars with  $Z_{GC} \geq 50$  kpc and  $Z_{GC} \leq -30$  kpc. Finally, we remove stars from the disk and bulge with a requirement that  $|Z_{GC}| > 11$  kpc, which also removes stars from the Sgr core and prevents them from biasing the fit (in the end, this has only a minor effect on the results).<sup>6</sup>

From this sample we determine a least-squares best-fitting plane by iteratively removing larger than  $2\sigma$  outliers, redrawing the sample to those stars within 15 kpc of the new plane (and with the other  $Z_{GC}$  limits above), and repeating the fit. From a final sample of 1161 stars, from which 695 lie within  $2\sigma$  (and where the RMS is 1.78 kpc), we find the best-fitting plane in Galactic Coordinates (where the Sun is at  $X_{GC} = 0$  and this axis is positive towards the Galactic anticenter) to be:

$$0.064X_{GC} + 0.970Y_{GC} + 0.233Z_{GC} + 0.776\text{kpc} = 0.$$

The derived errors on the coefficients are (0.002, 0.008, 0.002, 0.038), respectively. This plane corresponds to a Galactocentric orbital pole of  $(l_{GC}, b_{GC}) = (273.8, -13.5)^\circ$ , only slightly different from that obtained with the GC3 analysis. The pole derived here is also independent of any distance scale errors - such errors only affect the distance of the Sun (the fourth constant in the equation, 0.776 kpc) and the distance of the Galactic Center from the best-fitting plane. Note that we did not constrain the best-fitting plane to include the Galactic Center; if we assume the Galactic Center to lie at  $(X_{GC}, Y_{GC}, Z_{GC}) = (-8.5, 0, 0)$  kpc, this point lies 0.23 kpc from the plane. Had the Sgr plane been more inclined to the  $X_{GC}$  axis, defining the Sgr orbital plane would have allowed a new way to determine the distance to the Galactic Center, which would be assumed to lie in or near the orbital plane. However, the actual Sgr orbital plane is so close to the  $X_{GC}$  axis that the distance of the plane offers little leverage on the distance to the Galactic Center. But this technique may be applicable to other extended halo tidal streams found in the future.

---

<sup>6</sup>S-shape structures have been seen in the case of, e.g., the globular cluster Palomar 5 (Odenkirchen et al 2001, Rockosi et al. 2002) and the Ursa Minor dSph (Palma et al. 2003) – both systems for which our perspective is nearly edge-on to the orbital plane. Part of an S-shape is also apparent in Figure 4 and Figure 7e-f. Because the northern limb of the bound part of the Sgr system lies in the Galactic midplane, both ends of the S-shape canting of the Sgr core are not evenly sampled in our data. Thus, including the heavy statistical weight of the Sgr core in our analysis would result in a slight biasing to the best-fitting plane.

### 5.2.2. The Flatness and Proximity of the Sgr Plane

Our proximity to the Sgr plane is a somewhat remarkable coincidence. If we adopt the solar position as  $3.75^\circ$  from the Sgr-Galactic plane line of nodes, we are closer to the Sgr orbital plane during less than 4% of our own orbit around the Galaxy. This number drops to 2% when we consider that it is only on this side of the Galactic Center that the Sgr tidal debris arms (as traced by M giants) apparently reach the Solar Circle (see Sections 6.4 and 9). Our 0.78 kpc distance from the Sgr plane is less than half the RMS spread in Sgr debris about the plane fit above, so that if Sgr debris passes within a few kpc of the Solar Circle, we are very likely to be amidst that debris. Sections 6.4 and 9 address the implications of this unusual time in Solar System history.

That the Sun is not *precisely* in the orbital plane leads to some perspective effects. In Figure 7 we show only those points used in the derivation of the best fitting plane, and lying within  $2\sigma$ . Figures 7a and 7b compare the slightly different perspectives offered by a projection on the  $X_{GC} - Z_{GC}$  and the plane obtained by rotation of  $3.8^\circ$ , which allows a direct edge-on view of Sgr. Because of the variation in distance of Sgr tidal debris from the Sun, a slight “bowing” of the apparent Sgr orbital plane is removed when viewed in the more edge-on view. This bowing (seen more obviously in Figure 16 below) explains the differences in derived great circle poles for Northern and Southern Hemisphere GC3 analyses above.

Figure 7c shows a projection of the  $|Z_{GC}| > 11$  kpc portions of the tidal arms onto the Galactic plane as another means to illustrate the tilt in the Sgr orbital plane. Equivalent side views of the Milky Way and Sgr with no restriction to  $< 2\sigma$  outliers are shown in Figures 16 and 17, and show that the relative thinness of the distribution is not simply contrived by the present analysis. The coherence of the Sgr debris tightly to one plane highlights how little precession the Sgr system experiences for the 1-2 Gyr of orbit traced by the observable debris; we show elsewhere (Majewski et al. 2003) that the M giant tails show no more than a few degrees total precession. Orbital precession in tidal tails is acutely sensitive to the shape of the halo potential (cf. Johnston, Sackett & Bullock 2001, Mayer et al. 2002), and the flatness of the Sgr debris stream strongly points to a *spherical* mass potential for the Milky Way to at least  $\sim 50$  kpc. Our results here concur with and *strengthen* the similar arguments previously made by Ibata et al. (2001b), because even tighter coherence of the Sgr stream is demonstrated after properly removing Galactocentric parallax effects. We shall explore in more detail the actual limits on the shape and flattening of the Galactic potential in another paper.

Figure 7d shows the variation in the width of the Sgr stream when projected onto the sky. As may be seen, the debris stream is most foreshortened and spans the largest angle when it is near us, in the general direction of the North and South Galactic Poles. Figure 7d demonstrates how much of the high latitude celestial sphere contains lines of sight that intercept the Sgr stream (especially accounting for the fact Figure 7d does not display  $> 2\sigma$  outliers from the Sgr midplane); particularly at the Galactic poles, Sgr debris is hard to avoid! Figure 12, discussed later, shows more than  $> 2\sigma$  outliers from the Sgr plane and makes this point even more clearly. We review

various proposed detections of Sgr debris in this context in Sections 8 and 9.

### 5.2.3. *Sagittarius Spherical Coordinate Systems*

Determining the Sgr orbital plane, as we have done here, permits us to derive a more natural spherical coordinate system for the interpretation of Sgr tidal debris - one with the equator defined by the Sgr debris midplane. We actually define two such systems (Table 2). In the first, Sgr latitudes,  $B_{\odot}$ , are defined by the Sgr debris *projected on the sky as viewed from the Sun*. We adopt a debris midplane based on the  $(l_{GC}, b_{GC}) = (273.8, -13.5)^\circ$  pole derived in this subsection. Sgr longitudes,  $\Lambda_{\odot}$ , are defined to increase in the direction of trailing Sgr debris, with the prime meridian,  $\Lambda_{\odot} = 0^\circ$ , defined by the longitude of the center of the King profile fit to the Sgr core determined in the previous section. This first coordinate system is entirely empirically based, but, being Sun-centered, preserves Galactocentric parallax effects.

The Sgr plane defined in Cartesian Galactic coordinates allows us to define a *Galactocentric* spherical coordinate system. While immune from Galactocentric parallax effects, this system is, however, subject to scale and random errors in the determination of photometric parallaxes. Using the above plane, we define a Galactocentric  $(\Lambda_{GC}, B_{GC})$  system, with  $\Lambda_{GC} = 0$  taken as centered on Sgr, as before. Because the plane does not actually contain the Galactic Center (it was not constrained to do so), we take as the center of the  $(\Lambda_{GC}, B_{GC})$  system the point in the plane closest to  $(X_{GC}, Y_{GC}, Z_{GC}) = (-8.5, 0, 0)$  kpc, which is  $(X_{GC}, Y_{GC}, Z_{GC}) = (-8.51, -0.21, -0.05)$  kpc.

Table 2 gives the Eulerian rotation angles (under the “x-convention”),  $(\phi, \theta, \psi)$ , and Galactic coordinate centers of rotation used to define the two Sgr  $(\Lambda, B)$  coordinate systems used here. Note that these systems as adopted are right handed, and therefore determined from the standard left-handed Galactic system after the translation  $X_{GC} \rightarrow -X_{GC}$ . For some illustrations it is convenient and intuitive to leave the intersection of the Sgr and Galactic plane horizontal, and this is achieved by adopting  $\psi = 0$ . Thus, we define two Cartesian Sgr coordinate systems used throughout this paper, as follows:

$$X_{Sgr,\odot} = d_{\odot} \cos(\Lambda_{\odot} + 14.42^\circ) \cos(B_{\odot})$$

$$Y_{Sgr,\odot} = d_{\odot} \sin(\Lambda_{\odot} + 14.42^\circ) \cos(B_{\odot})$$

$$Z_{Sgr,\odot} = d_{\odot} \sin(B_{\odot})$$

where  $d_{\odot} = (X_{Sgr,\odot}^2 + Y_{Sgr,\odot}^2 + Z_{Sgr,\odot}^2)^{0.5}$  is the distance of the star from the Sun, and (distinct from the normal Galactic  $[X_{GC}, Y_{GC}, Z_{GC}]$  coordinates), and

$$X_{Sgr,GC} = d_{Sgr,GC} \cos(\Lambda_{GC} + 21.60^\circ) \cos(B_{GC})$$

$$Y_{Sgr,GC} = d_{Sgr,GC} \sin(\Lambda_{GC} + 21.60^\circ) \cos(B_{GC})$$

$$Z_{Sgr,GC} = d_{Sgr,GC} \sin(B_{GC})$$

where  $d_{Sgr,GC} = (X_{Sgr,GC}^2 + Y_{Sgr,GC}^2 + Z_{Sgr,GC}^2)^{0.5}$  is the distance from the center of the  $(\Lambda_{GC}, B_{GC})$  system as given above and in Table 2.

Finally, in Figures 7e and 7f we show projections perpendicular to both the best fitting Sgr plane and the Galactic plane, respectively, in the region of the Sgr core. The canting of the Sgr core with respect to the best-fitting plane towards the direction of the normal to the Galactic plane can be seen. Indeed, the angle of this tilt is nearly identical to the angle between the Sgr core and the normal to the Galactic plane, or a little more than about  $6^\circ$ . This canting is the rationale for removing the Sgr core from our calculation of the best-fitting plane above. Figures 7e and 7f shows how the beginning of the Sgr tidal stream emanates from the main body more or less evenly to either side of the debris midplane, despite the tilt of Sgr. Figures 7e and 7f provides a slight qualification to the usual assumption that the ellipticity of satellite systems are aligned with the direction of orbital motion and point in the direction of their tidal tails. Note that this tilting of the major axis of Sgr, *which is away from the orbital plane*, does not appear to be the same phenomenon that leads to the S-shapes seen *within the orbital plane* of disrupting model satellites as a result of energy differences of released particles in advance and behind the parent object (e.g., Figure 3 of Johnston 1998).

### 5.3. No Magellanic Cloud M Giant Streams

No other strong GC3 peak appears in the M giant candidate pole counts (a result that applies, at least, within 75 kpc and for the specific M giant photometric criteria employed here), in agreement with the preliminary analysis of 2MASS M giants by Ibata et al. (2002a). We confirm this result for all late type giants (M giants and carbons) in our analysis in Cartesian coordinates in Section 7. In addition, no GC3 peak corresponds to tidal debris from the Magellanic Clouds, even though the Magellanic Clouds are copiously populated by such stars (e.g., Nikolaev & Weinberg 2000), and are, by far, the predominant reservoirs of late type giants in the Galactic halo. Previous analysis of a sample of halo carbon stars by Ibata et al. (2001b) suggested the existence of a Magellanic carbon star stream. We note that while our GC3 analysis specifically leaves out the region around the Magellanic Clouds (excluding the zone  $-25^\circ > b > -53^\circ$ ,  $260^\circ < l < 312^\circ$ ) to avoid the interference of a large great circle band dominating Figure 6, any roughly coherent tidal streams extending more than about 25 degrees from the Clouds should be apparent as a GC3 peak in that figure. Analysis of the distribution of 2MASS starcounts by van der Marel (2001) shows the Large Magellanic Cloud to be elongated by Galactic tidal forces, but the lack of any GC3 peaks associated with the Magellanic Clouds suggests that any tidal forces on them either are not sufficient to create extratidal stars, or at least that young, metal rich populations are not presently participating in such streams.

The coherence of the Sgr orbital plane and the implied sphericity of the Galactic potential

implies that tidal streams in the outer Galaxy should face little precessional smearing, remain spatially coherent for at least several gigayears, and be evident as great circles on the sky. Ibata et al. (2002a) have argued that the lack of any other discovered M giant GC3 streams means that the present accretion rate of luminous, low-mass satellites must be very low, and that most of the luminous part of the Milky Way halo must have been in place more than 3 Gyr ago, before the accretion of Sgr. However, this conclusion applies only to systems sufficiently metal-rich to produce M giants. Most halo globular clusters and Galactic dSph galaxies contain few if any such stars because they are dominated by old, metal-poor populations (note, as just one example, the total absence of the four Sgr globular clusters in the M giant distribution of the Sgr core shown in Figure 4). Indeed, only Sgr and the Magellanic Clouds are identifiable away from the Milky Way disk in the full sky, 2MASS M giant distribution explored here. Thus, the lack of other M giant streams places no limit on the present accretion rate of older, more metal-poor systems.

## 6. Analysis of Observed Tidal Features in the Sagittarius Plane

### 6.1. Tidal Tails

While useful to demonstrate the locations of these features, Figures 2 and 3 give the unfortunate, illusory appearance of discontinuity between the Northern Spur and the Southern Arc. Figure 8 makes the connection by showing the distribution of the dereddened  $K_s$  magnitudes of M giant candidates with  $(J - K_s)_o \geq 1.0$  and  $-10^\circ \leq B_\odot \leq +10^\circ$  as a function of Sgr longitude. Figure 9 presents the same distribution in a polar projection. Figures 8 and 9 show directly observed quantities, so are free of interpretation. Both figures show the more complex character of the Southern Arc and Northern Spur, and give proof of their contiguous connection: While the two features are on average at different mean  $K_s$  magnitudes, projections of the magnitude-longitude trends through the Zone of Avoidance show that the two features meet at the Sgr core, and represent the leading (Northern Spur) and counterpart trailing (Southern Arc) tidal tails. Figures 10 and 11 present the same data in terms of distances from the Sun and distance from the center of the best fitting plane (approximately  $R_{GC}$ ), after deriving photometric parallaxes with the M giant absolute magnitude-color relation in Section 5.2

Figures 8-11 make clear the leading/trailing tail structure of the Sgr dwarf and the rosette nature of its orbit. Figure 11, which shows the distribution of stars projected onto the presumed Sgr orbital plane, gives a particularly clear impression of the rosette shape. We fit this distribution to a model of the Sgr dwarf in the Galactic potential in a subsequent contribution (Majewski et al. 2003), but as a general guide to understanding the interweaving and overlapping tidal arms illustrated in Figure 11 here, we call attention to Ibata & Lewis (1998) model K6-a shown in their Figure 3, and highlighted more clearly in Figure 3 of Ibata et al. (2001b). Though shown in the slightly different (canted by about  $13.5^\circ$ )  $X_{GC} - Z_{GC}$  plane, the overall appearance of the Ibata & Lewis K6-a model illustration bears great resemblance to the M giant distribution shown in Figure

11 (see also Figure 14, particularly panel c).

## 6.2. Trailing Tidal Debris

As may be seen in Figures 8 and 9, the center thread of the Southern Arc M giants varies by only about a magnitude across the Southern Galactic Hemisphere. The actual mean photometric parallax of this trailing debris tail is roughly 25 kpc where it attaches to the Sgr core, slightly less than 20 kpc when it achieves its closest distance to us near the SGP, and then gets progressively more distant towards the Galactic anticenter (e.g.,  $\sim 40$  kpc at  $\Lambda_\odot \sim 160^\circ$ ). The Galactocentric distance of the Southern Arc ranges from  $R_{GC} = 16$  kpc at the Sgr core and a similar distance when it passes beneath the Galactic Center ( $\Lambda_{GC} \sim 70^\circ$ ) to  $\sim 50$  kpc at the Galactic anticenter.

The disposition of this trailing tidal arm at longitudes even farther from the core is less clear. Inspection of Figures 8 through 11 (and particularly the bottom panel of Figure 10) all seem to suggest that the trailing arm crosses the Galactic plane, since there appears to be a continuation of the sweeping Southern Arc north of the Galactic plane, and an overdensity of points near  $\Lambda_\odot \sim 185^\circ$  and  $K_s \sim 13 - 14$ . Unfortunately, this is where our selection of M giants becomes both incomplete and noisy (see discussion of Figure 15 below). A large number of stars appear at  $(K_s)_o > 13.0$  at all longitudes, but their reality as M giants, much less Sgr M giants, must be considered highly uncertain and remains to be verified spectroscopically. We address the issue of the length of the tidal tails further in Section 6.4 below.

## 6.3. Leading Tidal Debris

The Northern Spur can be seen (Figures 8-11) to represent the leading tidal debris tail of Sgr. Figures 10 and 11 show that the approximate center of the locus of the leading tidal debris arm reaches a mean apoGalacticon distance of about 40 kpc around  $\Lambda_{GC} = 280^\circ$  ( $l \sim 350^\circ, b \sim 45^\circ$ ).

Figure 11 makes clear the relationship between the diffuse North Galactic Cap (NGC) material and the Northern Spur: The diffuse NGC material represents an extension of the Northern Spur as it loops around the Galactic Center and begins to fall downward onto the Galactic plane. The NGC material is more spread out on the celestial sphere simply because it is closer and foreshortened along the line of sight. Figures 8-10 show the looping northern arm spreading across the NGC, covering a large angular range when it gets to the smallest distances from us (see top panel of Figure 10). The top panel of Figure 10 gives the strongest impression that debris from the leading arm of Sgr appears to be falling onto the Galactic plane near the Solar Circle: No distance scaling problem can move stars *on the celestial sphere*, and that material is seen to either side of  $\Lambda_\odot = 256^\circ$  (the direction closest to the North Galactic Pole) points to Sgr material falling to either side of the Solar Circle.

#### 6.4. The Sagittarius Leading Arm Near the Solar Neighborhood

We have already shown (Section 5.2) that the Sun lies within a kiloparsec of the Sgr orbital plane, a distance well within the width of the Sgr tidal debris stream; thus the actual proximity of Sgr debris to us depends on the length of the leading arm and where it crosses the Galactic plane on this side of the Galactic Center, if it is long enough to do so. For a variety of reasons, whether and where the northern tidal arm crosses the Galactic plane toward the southern hemisphere must still be considered somewhat uncertain, and Figures 8-11 might be consistent with a variety of possible interpretations. However, we note the following points:

- 1) In the fit to the Sgr plane in Section 5, we obtained an RMS residual of nearly 2 kpc. While there is a 17% distance smearing imposed from the intrinsic spread about the adopted color-magnitude relation, it is clear that Sgr debris girdles the Sgr orbital midplane with a total width of 4-8 kpc or more. This is supported by the fact that the Southern Arc (at a distance of about 20 kpc) is 10-20 degrees or more wide on the sky (e.g., Figures 3, 7d and 12). Simplistically, one might assume a circular cross-section for the tidal arms, in which case the width of the Sgr arms *within* the orbital plane (e.g., that projection shown in Figure 11) might be similar (4-8 kpc). Thus, should the leading stream be long enough to reach the Galactic plane on this side of the Galactic Center, and should it do so within 2-4 kpc from the Sun, then Sgr debris will pass through the solar neighborhood.
- 2) Previous models (e.g., Ibata et al. 2001b, see, e.g., their Figure 3) derive an orbit for Sgr similar to that traced by the rosette of debris seen here and predict current passage of leading arm debris through the Galactic plane at a mean distance from of  $\sim 4$  kpc outside the Solar Circle. However, our own best fitting models to the present data set (Majewski et al. 2003) obtain a passage of the center of the leading Sgr arm within a kiloparsec.
- 3) Figures 10 and 11 show the presence of 15 – 30 kpc distant M giants stretching from  $\Lambda_\odot = 225^\circ$  to  $280^\circ$  or more. An even wider angular distribution at closer distances suggests the passage of leading arm material both exterior *and* interior to the Solar Circle at these distances (the NGP is near  $\Lambda_\odot = 256^\circ$ ). Unfortunately, increased confusion between Sgr debris and disk and bulge M giants in the inner Galaxy means that the exact disposition of the nearby Sgr debris requires spectroscopic weeding of Milky Way contaminants.
- 4) Figures 8 and 9 show a slight excess of stars with  $7.5 < K_s < 10$  and  $\sim 5^\circ < \Lambda_\odot < \sim 75^\circ$  that may be a southern extension of the infalling Northern debris. The tidal debris model shown by Ibata et al. (2001b; their Figure 3) shows just such an extension that passes not only through the Galactic plane, but also through the trailing debris arm and to larger distances. Such a feature may be the origin of the slight excess of more distant stars (with  $11.5 < K_s < 13$ ) in exactly the predicted longitude range ( $\Lambda_\odot \sim 15 - 65^\circ$ ). The lower right quadrant of Figure 14c, which matches closely the overall appearance of the Ibata et al. model, shows this apparent excess of more distant stars most clearly.

Each of the above scenarios can be checked readily with a spectroscopic assessment of the bright, nearby M giant sample in both hemispheres. Radial velocities of both very bright and faint M giant stars in each hemisphere would be particularly useful for understanding whether a vertical flow of Sgr stars exists through the nearby Galactic plane and onward, past the trailing debris arm. We discuss recent spectroscopic observations bearing on these subjects in our next contribution.

### 6.5. Density Variation Along the Tidal Arms

Both the length of and density variation along the tidal debris arms of a disrupting satellite system bears on the duration, strength and overall nature of the interaction with the Milky Way (Johnston 1998). For example, the recent mapping of the tidal arms of the globular cluster Palomar 5 gives a useful demonstration of the effects of tidal “pulsing” on the mass loss rate of the cluster: Each perigalacticon passage of the cluster appears to have produced a density node in each of the tidal arms (Odenkirchen et al. 2001), each node pair corresponding to one periGalacticon passage, so that one can read the past history of the mass loss rate down the length of the arms.

Figure 12 is an attempt to unwrap the Sgr tidal material into a surface brightness ribbon around the sky as a means to look for similar variations in the Sgr tidal arms. Only stars lying within 7 kpc of the best fit plane to the Sgr debris are shown. Because the Sun is more centrally placed with respect to the arc of the trailing tail than is the Galactic Center, we unwrap the debris along the  $\Lambda_\odot$  longitude (rather than  $\Lambda_{GC}$ ) to minimize projection effects in the representation of the relative density as a function of position along this tidal arm. To remove the bulk of Galactic disk/bulge contamination, we only show stars more than 10 kpc from the Galactic Center (assuming a Galactic Center distance of 8.5 kpc), more than 15 kpc from us, and with  $|b| > 10^\circ$ . To increase the S/N of the tail density, we include bluer M giants by opening our selection criterion to  $0.95 \leq (J - K_s)_o \leq 1.10$ .

Because of its nearly equal distance from us as a function of Sgr longitude, the Southern Arc of Sgr provides a facile means by which to measure density/mass loss variations relatively free of the effects of foreshortening. In Figure 13 we show the numbers of M giants as a function of  $\Lambda_\odot$  position. Counts are shown for tallies within *slabs* of various thicknesses centered on the Sgr midplane. To isolate those stars in each slab associated specifically with the Southern Arc, we fit a quadratic function to the photometric parallaxes of all stars in the slab as a function of  $\Lambda_\odot$  (with an iterative rejection of  $2.5\sigma$  outliers). For  $\pm 3$ ,  $\pm 5$  and  $\pm 7$  kpc thick slabs, the  $\sigma$  of the Southern Arc distances are 3.6, 3.7, and 3.9 kpc, respectively. This *depth spread* is larger than the  $\sim 2$  kpc sigma *width spread* found in our fits of the best fit plane to the Sgr debris, but the depth spread is of course affected by the artificial, ( $\sigma_d/d \sim 0.2$ ) spreading due to “standard candle” scatter (Section 5.2).

To determine a background level of non-Sgr “contaminants” in the Southern Arc we count M giant candidate stars in tidal-stream-like tubular volumes of the Galactic halo, but in a direction

that avoids Sgr, the Magellanic Clouds and regions of large reddening. Through trial and error we found reasonable results by rotating the slabs containing the Southern Arc tubular volumes  $35^\circ$  about the line of nodes represented by the intersection of Sgr and Galactic planes. In this orientation, the “Southern Arc” tubes now sample random halo volumes associated with the great circle pole  $(l, b) = (272, +23)^\circ$ . Although nearly as polar as the original Sgr plane (and therefore sampling a similar Galactic halo density law), this “background plane” suffers from the shortcoming that thicker slabs centered on it become ever more contaminated by Sgr contributions near the Galactic plane (thus, in one direction, near the Sgr core). Because we are concerned here with assessing the density of the more diffuse parts of Sgr, it is less critical to obtain an accurate accounting of the background near the Sgr core (which has, in any case, been done more properly in the radial profile fits in Section 4). Figure 13 includes the derived background counts for the  $\pm 3$  kpc wide slab as representative; the background is typically about 10% in the tail regions away from the core. Tests of various sized background slabs show that the background level away from the core is fairly constant, at  $0.33 \times (\text{slab width})$  per ( $5^\circ$  longitude). This adopted background is subtracted in the density plots shown.

Both Figures 12 and 13 demonstrate that, for the most part, the tidal arms of Sgr show no substantial density variation with longitude, especially over the range  $\sim 45 < \Lambda < \sim 140^\circ$ . This suggests a more or less constant mass loss rate for the timescale represented by this portion of the tail. The decline at large longitudes is in part due to reddening and Galactic latitude limitations (note that the Galactic anticenter is at  $\Lambda_\odot = 166^\circ$ ). However, both figures also hint at a slightly higher density of M giants some  $25\text{--}50^\circ$  in longitude downstream from the Sgr core. Figure 13 shows this increase in the number of stars as a “hump” in the tidal tail distribution for  $25^\circ < \Lambda_\odot < 50^\circ$  (recall that the King limiting radius of Sgr along the major axis is  $30^\circ$ , and therefore there is presumably no contribution from bound stars beyond this point). An apparent widening in the tail at these longitudes is also suggested by Figure 12 as well as by the separation of the  $z = \pm 3$  kpc points from the  $z = \pm 5$  and  $\pm 7$  kpc points in Figure 13 at this longitude compared to other places along the trailing debris tail.

We propose two possible explanations for the existence of such a “nodal” feature:

1) Longitudinal nodes of increased numbers of released stars give a similar impression of wider portions along the tidal tails extending from the globular cluster Palomar 5 (Rockosi et al. 2002, Odenkirchen et al. 2001). As mentioned above, these nodes appear at regular intervals along the Pal 5 tail and correspond to “pulses” of stars released upon the shrinkage of the tidal radius at each periGalacticon passage. Published Sgr orbits that approximately match our data (e.g., Figure 3 in Ibata et al. 2001b) show Sgr to have passed through periGalacticon very recently (within  $\sim 0.1$  Gyr). If the “hump” in Figure 13 is related to a periGalacticon pulse, then (as in Pal 5) a symmetrically placed feature might be expected in the leading tail; unfortunately, this feature, if it exists, would lie close to the Galactic plane, where our data become more confused, though a larger density of stars at  $-50^\circ < \Lambda_\odot < -30^\circ$  is not inconsistent with the data (see Figure 12). A smaller, less significant overabundance also appears at  $\Lambda_\odot \sim 133^\circ$ , but generally, the relative

density variation along the Sgr tail is steadier than in the case of Pal 5.

2) If, as is suggested by the Sgr disruption model of Ibata et al. (2001b) as well as the various pieces of evidence within the M giant distribution discussed in Section 6.4, the leading tidal arm penetrates back into the southern hemisphere and crosses the trailing arm, we would expect an increased density of stars at about the longitudes where the excess density is observed. Radial velocities of stars in the node would reveal a clear signal of this overlap. Early evidence from our M giant radial velocity work suggest this may be the case (see also the discussion of overlapping Sgr tails in this part of the sky by Johnston et al. 1999a).

In Figure 13 we have shown for comparison the Sgr longitudinal profile over the range  $10 < \Lambda_\odot < 34^\circ$  obtained by Mateo, Olszewski & Morrison (1998) for main sequence turn-off stars. The detailed shape of their profile is remarkably consistent with the 2MASS M giant profile over the longitudinal range of overlap. However because the main body of Sgr is canted somewhat with respect to the mean trend of the debris, and because Mateo et al. extrapolated their outer fields from the direction of the major axis of the Sgr core, their outer fields progressively fall away from the center of the debris stream (see Figure 12 and Figure 7f, where the  $\Lambda_\odot = 34^\circ$  Mateo et al. point corresponds to a location about 12 kpc below the Sgr core).

## 6.6. Length of, and Possible Population Variation Along, the Tidal Arms

The question of the lengths of the Sgr tidal debris arms is of interest not only because it bears on the duration of the mass loss process, but because it bears on the question of whether the leading tail is long enough to reach the solar neighborhood. As described earlier, uncertainty over the length of the leading tail is complicated by contamination by disk/bulge M giants at low Galactic latitudes, and the possibility of tail overlap below the Galactic plane. It would be useful, therefore, if the length of the Southern tail could serve as a guide. Section 6.2 offered evidence that the Southern Arc may extend to the Northern Hemisphere at the Galactic anticenter, but confidence in this result is limited by increased magnitude errors at large  $K_s$ , which makes selection of M giants both incomplete and more contaminated by “false positives”. Figure 14 demonstrates this effect with planar distributions of giant star candidates binned by  $(J - K_s)_o$  color.

Figure 14a shows the spatial distribution of stars in the color range  $0.90 < (J - K_s)_o \leq 0.95$ , and quite evident is a “shell” of excess, contaminating stars introduced at the nominal photometric parallax limit ( $\sim 35$  kpc) of stars of this color range. Since for the same apparent magnitude error limit redder giant candidates are projected to greater distances, we see how the shell of excess contaminants is larger in the  $0.95 < (J - K_s)_o \leq 1.00$  color bin shown in Figure 14b, and expands outward with color until, for stars redder than  $(J - K_s)_o \sim 1.0$ , the contaminating shell is outside the distance range shown. The distance progression of these “contamination shells” with  $(J - K_s)_o$  color is illustrated in Figure 15, where we have shown the starcounts as a function of distance for four  $(J - K_s)_o$  color bins within a cone selected to be more or less free of Sgr stars and the

Magellanic Clouds, specifically  $Y_{GC} > 0$ ,  $Z_{GC} > 0$ , and  $Z_{GC} > Y_{GC}$ , where the latter limit is used to avoid much of the Galactic disk; Figure 16 is a useful aid for orientation to this wedge. The peak of the “contamination shell” for  $0.90 < (J - K_s)_o \leq 0.95$  is plainly visible at a distance of about 35 kpc, for example, and at 47 kpc for  $0.95 < (J - K_s)_o \leq 1.00$ . Only for  $(J - K_s)_o > 1.05$  is the outer limit of the Northern Loop confidently free of significant contamination when viewed in a slab of finite width (note that the counts shown in Figure 15 are for a volume element increasing as the cube of the distance).

Convolved and competing with the above technical problem of determining the true length of the Sgr tidal arms is a second complication arising from stellar population considerations: M type red giant stars occur only in metal-rich populations. While the Sgr core has ample numbers of sufficiently metal-enriched stars to create a substantial M giant population, the Sgr metallicity gradient found by Alard (2001) suggests that the tidal debris leaving the Sgr dwarf now is likely to be, on average, more metal poor than that remaining in the most central regions. Moreover, Layden & Sarajedini (2000) have demonstrated a clear age-metallicity relationship among the Sgr populations. Thus, one might expect a natural limit to the extent that the Sgr tidal tails *could* be traced with M giants, with that limit corresponding to the oldest possible tidal debris that contains M giants.

In Table 2 we give the age-metallicity characteristics of the three primary Sgr populations identified by Layden & Sarajedini (2000). For each of these populations we use the isochrones and other data in Bertelli et al. (1994) to determine the  $(J - K_s)$  color of the RGB tip, accounting for the conversion to the 2MASS photometric system using the equations in Carpenter (2001). As may be seen, the most metal-poor population in the Sgr system is virtually invisible to the color-selected M giant candidate sample shown in Figures 8-11 (recall the invisibility of the M54 globular cluster in Figure 4). Thus, uncovering the distribution of these older detached giant star populations requires use of earlier and intrinsically fainter giant stars, but doing so with 2MASS, as shown in Figure 14a, is complicated by the severe contamination at distances of particular interest. On the other hand, younger populations will have had less time to separate from the Sgr core. Therefore, the apparently decreasing length of both leading and trailing M giant tidal tails as we map them with progressively cooler stellar tracers (Figure 14) suggests *a mean stellar age/metallicity variation along the tidal tails*.<sup>7</sup>

The actual tidal release age of any particular part of the Sgr arms as deduced from the apparently youngest stars is an upper limit because (1) the steepness of the luminosity function means that the incidence of stars at the actual tip of the RGB is relative rare, so that any particular M giant is likely blueward of the RGB-tip color for its age/metallicity population (Table 3), and (2) it takes time for stars presumably formed in the deepest part of the Sgr potential well to work their

---

<sup>7</sup>A tendency for the tidal arms to appear more tightly wrapped for bluer colors may further hint at a shift in the mean color-magnitude relation for M giants in the tails compared to the color-magnitude relations adopted from the Sgr core, in the sense that the tails contain more metal-poor (brighter) M giants than the core.

way out of that well and become tidally separated from Sgr. Therefore, it is reasonable to suspect that the M giant population explored in this paper is actually tracing only the very most recently lost stars (perhaps only the last Gigayear or so) from what may be a longer tidal interaction and net tidal arm length. Such youthful ages for the length of tails reported here are consistent with Sgr disruption models (e.g., Johnston et al. 1999a).

Nevertheless, the highly “tuned” samples shown in Figures 14b-14d offer the strongest evidence that the trailing Sgr arm is at least long enough to presently lie across the Galactic plane in the Northern Galactic Hemisphere towards the Galactic anticenter. Moreover, Figure 14c in particular offers tantalizing evidence that the *leading* Sgr arm crosses the Galactic plane on this side of the Galactic center and extends past the trailing Sgr arm as a “spray” of stars in the lower right quadrant of the orbital plane (as shown by in the K6-a model illustrated in Figure 3 by Ibata et al. 2001b).

## 7. From Sgr to the Galactic Halo

### 7.1. Minimum Integrated Mass Loss Of Sgr

As discussed above, M giants only permit estimates of a *lower limit* on the net stellar mass lost by Sgr and the fractional contribution of Sgr debris to the Milky Way halo.

The longitudinal profile in Figure 13 enables an estimate of the fractional mass of the Sgr system in its tidal arms under the assumption that the M giants provide a suitable and equitable tracer over the entire Sgr core + tail system. Presuming the southern and northern arm are equal in mass and using the determined King profile (Section 4, Table 1) to represent the bound part of Sgr, we find that the unbound debris contains 15% of the number of stars in the bound part of the Sgr core (within the King profile). These values correspond to the  $\pm 5$  kpc slab.

Johnston, Sigurdsson & Hernquist (1999) have given a formalism for calculating the mass loss rate in a dwarf satellite based on a measured profile such as that shown in Figures 5 and 13. Using their formula (18), an orbital period of the Sgr system of 0.7 Gyr, and only the clearly visible tail to  $\Lambda_{\odot} = 155^{\circ}$ , we obtain that the present mass loss rate for Sgr is 17% of its mass per Gyr. With a 0.7 Gyr period orbit and at least 15% of the mass now presently in the tails, this implies that Sgr has been losing mass for about 1.5 orbits. This figure must be taken as a lower limit, given the real uncertainty in the lengths of the tidal tails and the age/metallicity effects discussed above.

### 7.2. Sagittarius Stellar Contribution to the Milky Way Halo

Figure 16 shows the distribution of 2MASS late type giants projected onto the Galactic  $Y - Z$  plane. In this orientation, we see the Sgr orbital plane almost “edge-on” as the vertical spike

spanning both hemispheres, as in Figure 7a. The panels illustrate the same color ranges as Figure 14, however, unlike Figure 14, in which the sample has been limited to stars in a 14 kpc wide slab centered on the Sgr plane, Figure 16 shows the entire 2MASS sample, except for stars more reddened than  $E(B - B) = 0.555$ . The increased “limb brightening” of the faint magnitude “contamination shells” is more obvious in Figure 16 than Figure 14 because for the former the full spherical volume of the survey is projected rather than just a cross-sectional slab. It is difficult to assess the fractional contribution of Sgr stars to the Galactic halo in light of this contamination problem, particularly for the  $(J - K_s)_o \lesssim 1.00$  sample, which is heavily laden with this noise.

For redder samples, however, the dominance of Sgr tidal debris in the Galactic halo M giant population becomes obvious. For example, as may be seen in Figures 16d and 16e, apart from the Magellanic Clouds, which are the sources of the large “finger of God” features<sup>8</sup> in the lower right of each panel, unbound Sgr debris is the predominant source of halo late type giant stars.

To make this even more readily apparent, in Figure 17 we reproduce Figures 16c-e after removal of all sources with estimated photometric parallaxes larger than 40 kpc, 50 kpc, and 60 kpc, respectively; these distance limits effectively remove the bulk of the faint end contaminants (see Figure 15), at the expense of slightly truncating the most distant parts of the Northern Loop. On the basis of the data in Figure 17 and assessing only the Northern Galactic Hemisphere to avoid the complication of the Magellanic Clouds, we estimate that Sgr debris represents more than about 75% of the high halo ( $Z_{GC} > 13$  kpc) in the color ranges shown. The estimate rises to 80% or more if the high halo is defined by  $Z_{GC} > 20$  kpc. Of course, this estimate does not (1) include Sgr debris stars lopped off the top of the Northern Loop by the distance limits (which would increase the fractional Sgr contribution), (2) account for residual contamination of the halo by false positives introduced by photometric errors, or (3) account for any possible increases in the number of M giants at larger radii than the limits shown, or Galactic latitudes lower than those analyzed. In addition, (4) our criterion for selecting M giants was guided specifically by the location of *Sgr* M giants in the NIR two-color diagram; however, age-metallicity effects in the relevant parts of the two-color diagram are minor for these types of stars. Nevertheless, that Sgr debris is the major contributor of the high latitude halo M giant population to 60 kpc seems a reasonable conclusion.

The dominance of Sgr in creating the Galactic halo M giant population is reflected in the Great Circle Cell Counts analysis discussed in Section 5. However, our results differ somewhat from those of Ibata et al. (2002a), whose analysis of the 2MASS early release data led them to conclude that Sgr debris represented only about 5% of the halo M giant population. Though the two analyses use different selection criteria to isolate M giant stars, we are uncertain exactly why they arrive at such substantially different limits on the M giant contribution to the halo. It may be that Galactic disk giant exclusion based on a Galactic latitude limit, as used by Ibata et al., is not as restrictive

---

<sup>8</sup>That the Magellanic Clouds are seen as “finger of God” spikes in Figure 16 is attributable to the fact that the color-absolute magnitude relation we have adopted is specifically tuned to the most metal rich Sgr population, and is not necessarily a good description of Magellanic populations.

as our  $Z_{GC}$  criterion, but a more likely contributor to the difference is our elimination of the excess background by the “contamination shell” (Section 6.6) in both the Cartesian as well as the GC3 analysis presented in Section 5.

We are in agreement with Ibata et al. (2002a) that, apart from the presumably bound population of red stars in the Magellanic Cloud represented by the finger of God spikes, it would appear that the Clouds have *not* been a major contributor to the halo M giant population.

These results pertain only to Sgr contribution to the halo of the latest type giant stars, and say nothing about the net mass contributed to the halo, either in the form of dark matter or in stars of all spectral types. However, along these lines, we find interesting the result of Vivas et al. (2001; discussed further below), in which almost every one of the RR Lyraes they find along the line of sight to the apoGalacticon of the Northern Loop could conceivably be a part of Sgr tidal debris, possibly including even the nearby RR Lyraes, depending on the disposition of the Sgr debris near the Sun. In any case, that Vivas et al. find a “hole” in their RR Lyrae counts precisely at the distance of the interior of the Northern Loop is dramatic and suggests that even for such old stars Sgr may be a dominant contributor to at least the outer ( $> 25$  kpc) halo.

## 8. Comparison to Previous Sgr Searches and Potential Identifications

Dinescu et al. (2002) have summarized the various searches for extended Sgr debris to date; their Figure 4 gives a representation of the placement of various detections and non-detections on the celestial sphere, along with a great circle for the Ibata et al. (1997) Sgr orbit, which reasonably approximates that which we have found here. Given our new understanding of the three dimensional position of Sgr debris, it is worth reviewing the previous detections of Sgr debris in more detail here, and, in particular, taking into account the *distances* of the stars that constitute the various detections. A comparison with other surveys is especially useful (1) as a check on distance scales from the disparate tracers that have been used, (2) because we are now able to place almost all previous detections into a unified context, and (3) comparisons to surveys of other Sgr tracers provide new insights into the Sgr disruption and debris trails. Figure 18, which repeats the M giant distribution of Figure 10, also provides our summary comparison of the detections by Sgr longitude and distance. Figure 18 includes only detections of extratidal Sgr material, and excludes the numerous studies near the Sgr core.

### 8.1. Connecting to the Sloan and QUEST Detections

Perhaps the most striking visual impression of extended Sgr (and other potential) tidal debris in the halo has been that afforded by the Sloan Digital Sky Survey. In several studies analyzing data from the first Sloan observations in a strip along the celestial equator, the presence of Sgr’s extended tidal arms have made themselves known. Figure 19b shows a slice through the 2MASS

M giants along the celestial equator, which mimics the region of the sky surveyed by the Sloan survey on the equator. While the latter covers a roughly 2.5 degree wide strip along the equator, we opened the declination range of our comparison image to  $-10^\circ < \delta < +10^\circ$  to increase the density of plotted points for our lower density population of M giants.

The first published results from Yanny et al. (2000), while only in two limited angle wedges of the equatorial stripe, nevertheless showed excess starcounts of A type stars in several regions that can now be firmly identified with parts of the Southern Arc at  $\Lambda_\odot \sim 104^\circ$  and the far side of the Northern Loop at  $\Lambda_\odot \sim 295^\circ$ . The heliocentric distances Yanny et al. (2000) infer for their two structures are 28 kpc and 48 kpc, respectively. These distances generally agree with our results (Figure 18). Though they do not comment on it, the Yanny et al. data also show an excess of stars  $< 20$  kpc away in the same direction of the sky (see, e.g., their Figures 18 and 19), consistent with our finding of *closer* M giant candidates at the same longitudes ( $\Lambda_\odot \sim 295^\circ$ ). Because of uncertainty over the mean distance of this nearby Yanny et al. clump, it is not represented in Figure 18.

A similar detection of two density enhancements towards the Northern Loop has been discovered in the study of RR Lyraes discovered in the Sloan equatorial strip by Ivezić et al. (2000), as well as in the QUEST RR Lyrae Survey (Vivas et al. 2001), which explores nearly the same region of sky ( $13 < \alpha < 16$  hours). Both surveys comment primarily on an excess of RR Lyrae stars at 45 and 50 kpc, respectively, a feature that we can now confidently associate with the same expanse of the Sgr Northern Loop identified by the Newberg et al. (2002) and Martínez-Delgado et al. (2001b) surveys, and shown in the upper right quadrant of Figure 11. The distances of these more distant RR Lyraes are also in reasonably good agreement with the M giant distribution presented here ( $\Lambda_\odot \sim 270 - 310^\circ$ , Figure 18).

As with Yanny et al.’s A stars, both Ivezić et al. and Vivas et al. also have in their distance distribution of RR Lyrae stars a large number at distances that correspond to the  $< 20$  kpc M giant candidates seen at  $\Lambda \sim 295^\circ$  in Figure 18. Figure 4 of Vivas et al. and especially the middle panel of Ivezić et al.’s (2000) Figure 8 are very similar in appearance to the distribution of stars along the same line of sight in Figure 11 here. Vivas et al. find that from 16-23 kpc there is a *bona fide* excess of stars over an  $R_{gc}^{-3}$  law, but they attribute the majority of this excess to be likely bound and unbound RR Lyrae stars from the tidally disrupted Pal 5 system, while Ivezić et al. apparently do not find an excess over a -2.7 power law. Clearly radial velocity data are needed to determine whether any of the  $< 20$  kpc M giants and RR Lyrae may be related to Sgr or other tidal debris interior to the Solar Circle (e.g., wrapped up leading arm material as described in Johnston et al. 1999a and Kundu et al. 1999), or whether they are all part of the Galactic bulge and/or inner halo.

Interior to their  $\sim 45 - 50$  kpc clumps, both RR Lyrae surveys also show a prominent “hole” in their distribution that appears to correspond to the interior of the Northern Loop. This is an interesting result, because Sgr disruption models (e.g., Ibata et al. 2001b) predict that trailing arm debris, extending beyond the length limit revealed by M giants here, should be found in the

Northern Loop hole. Indeed, the cluster NGC 5364, which lies right in the middle of the Northern Loop hole (see Figure 18), is consistent with the position and velocity of wrapped Sgr trailing debris (Bellazzini et al. 2002a, 2003). If NGC 5634 is Sgr debris, one might expect to see a population of Sgr RR Lyraes along with it. Further work is needed to clarify this dilemma.

Our analysis (Section 7.2) for the fractional contribution of Sgr *M giants* to the halo pertains to a stellar species expected only for relatively metal rich ( $[\text{Fe}/\text{H}] > \sim -1$ ) populations — and it is not altogether too remarkable that the relatively minor fraction of halo stars that are that metal-rich could have come from a very small number of contributors like Sgr. However, that the overall distribution of *RR Lyrae stars* in this part of the sky, including the contrast of near and far clumps and the intervening hole, appears to match so closely the distribution of the M giants suggests that the dominance of Sgr M giants in the halo may extend to older, more metal-poor populations (at least for the outer halo and in this one direction of the sky).

The most extensive use of the SDSS for stream detections is that presented for presumed main sequence turn off stars in a nearly complete equatorial stripe by Newberg et al. (2002). Figure 19a here is a reproduction of their their Figure 1; we include on Figure 19b the azimuthal locations of features pointed out and discussed by Newberg et al. It is clear that the strong Newberg et al. feature S167-54-21.5 is indeed the Southern Arc tidal arm of Sgr, and their feature S341+57-22.5 is the far side of the Northern Loop (as suggested by their own discussion of these features); the Sgr longitudes of these features are (see Figure 10)  $\Lambda_\odot \sim 110^\circ$  and  $\sim 286^\circ$ , respectively. But we can also make the likely connection of the more diffuse clumping S297+63-20.0, which Newberg et al. attribute tentatively as “a stream or other diffuse concentration of stars in the halo”, as well as a lot of the similar-magnitude fluff contiguously connected to this feature from  $\alpha \sim 150^\circ$  to  $\alpha \sim 210^\circ$ , to the foreshortened Northern Loop near  $\Lambda_\odot = 265^\circ$  and stretching more generally from  $\Lambda_\odot \sim 230^\circ$  to  $\Lambda_\odot \sim 285^\circ$  (see Figure 18). The consistency with the M giant debris here is noteworthy, and the wide spread of the S297+63-20.0 feature elicits further interest into the question of precisely where the Northern Loop crosses the Galactic plane near the Sun.

Newberg et al. draw attention to several other features located at the low  $|b|$  edges of their survey wedges. For example their feature S223+20-19.4 is discussed in the context of a possible “newly discovered dwarf galaxy in the Galactic plane” at a distance of about 11 kpc, but they also admit the possibility that it is a metal weak, disklike structure with large scaleheight and scalelength. Ibata et al. (2003) have suggested the possibility that the Sloan detection may be part of a ring or tidal tail nearly in the Galactic disk plane. Figure 19 gives the appearance of a distinct structure at the same position and at a corresponding distance modulus ( $m - M \sim 15$ ) if we assume these are M giant stars. This structure appears to span both sides of our Zone of Avoidance (though predominantly situated North of the Galactic plane in this slice through the Galaxy), with an overdensity of stars that also corresponds more or less to the Newberg et al. S200-24-19.8 structure.<sup>9</sup> It is unlikely that the 2MASS feature is from improper dereddening,

---

<sup>9</sup>The apparent overdensity in the 2MASS M giant sample corresponding to the S200-24-19.8 structure shows more

since the S223+20 structure extends to reasonably high latitudes ( $b > 20^\circ$ ). Figure 19 supports the reality of the Sloan find.

## 8.2. Other Searches for Distant Sgr Debris

We have already compared our results to those of Mateo, Olszewski & Morrison (1998) in Figure 13 and Section 6.5. Near the Mateo et al. strip of fields, and slightly closer to the center of the Sgr tidal debris stream is the possible detection of Sgr red clump stars in the ASA184 field ( $[l, b] = [11, -40]^\circ$ ) by Majewski et al. (1999a). The distance modulus with reddening of these stars at  $\Lambda_\odot \sim 26^\circ$  is projected to be  $(m - M - A)_V = 16.8$ , which is 22 kpc assuming  $A_V = 0.15$ ; this distance is in agreement with the M giant distribution in Figure 10. Majewski et al.’s non-detections in the other three fields they studied - SA184, SA107 and ASA107 – can be understood by comparison to the Sgr debris streams as delineated by M giants: SA184 and SA107 are off the Sgr orbital plane (as expected by Majewski et al.). The fourth field they studied, ASA107, however *does* ( $[l, b] = [353, +41]^\circ$ ) lie in the thick of the Northern Loop at  $\Lambda_\odot = 300^\circ$  (which is why it was selected). Unfortunately, the mean distance of the loop at this point, i.e.  $\sim 45$  kpc translates to an expected red clump magnitude of  $V \sim 19.5$ , which was just beyond the limit of their study.<sup>10</sup> This point has previously been made by Martinez-Delgado et al. (2001b).

Another Kapteyn Selected Area previously suspected to contain Sgr debris is SA71 ( $[l, b] = [167, -35]^\circ$ ). Dinescu et al. (2002) report an excess of  $B - V \leq 1.1$  stars for  $18 < V < 20$ , and most prominently in the range  $18 < V < 19$ . These stars also appear to have distinct proper motions consistent with the Sgr orbit. SA71 lies near the main Sgr debris stream towards the Galactic anticenter ( $\Lambda_\odot \sim 128^\circ$ ) where the M giants are centered at about 28 kpc distance. By assuming that their excess population corresponds to the Sgr horizontal branch/red clump, Dinescu et al. derive a distance for their potential Sgr debris of 29-32 kpc, in good agreement with the M giants. Dinescu et al. explore three other Selected Areas — SA29, SA45, and SA118 — and found no similar Sgr-like detection. As these authors point out, SA29 and SA45 are considerably off the primary Sgr orbit. However, in their Figure 3 SA118 is shown to be nearly similarly displaced from the Ibata et al. (1997) Sgr orbit. Our ability to pinpoint more precisely the path of the Sgr debris allows us to determine that, in fact, SA71 is much closer to the primary debris great circle than is SA118; this could explain their Sgr debris non-detection in SA118.

Martínez-Delgado et al. (2002) have identified potential main sequence Sgr stars in deep  $BR$  imaging near the globular cluster Pal 12, previously identified by Dinescu et al. (2000) as a likely Sgr globular cluster. Martínez-Delgado et al. estimate the distance of these stars as 17-24 kpc,

---

clearly when bluer M giants are included in the analysis.

<sup>10</sup>Interestingly, there is an excess of stars at this magnitude visible in the Figure 4 of Majewski et al. (1999a), but the excess was deemed not statistically significant by those authors.

depending on assumptions about the expected absolute magnitudes of the stars. At this longitude ( $\Lambda_\odot \sim 40^\circ$ ), we find the mean M giant distance to be about 19 kpc, which is also the same distance as Pal 12, and this is consistent with the Martínez-Delgado results. In a similar, deep CMD search in a field in the SDSS equatorial strip, Martínez-Delgado et al. (2001) also find a signal they tentatively associate with Northern Hemisphere Sgr dwarf material. The distance to the feature, which they associated with “the Sagittarius stream or traces of a new nearby dwarf galaxy” is  $51 \pm 12$  kpc, and  $R_{GC} = 46 \pm 12$  kpc. Their identified stellar population indeed corresponds to the distant part of the Northern Loop at  $\Lambda_\odot = 295^\circ$ , and is only slightly farther than other detections in this part of the sky, including our own. The lack of detection of the near side of the Northern Loop by both Majewski et al. (1999a) and Martínez-Delgado et al. (2001) relates to the bright-end magnitude limits in both surveys.

Finally, two searches for giant stars have recently published possible detections of Sgr debris in the Northern Hemisphere. Dohm-Palmer et al. (2001) have found four giant stars with similar velocities and distance in fields near the Sgr mid-plane near  $\Lambda \sim 295^\circ$ . At least some of these stars, at a typical distance of 50 kpc and a moderate positive velocity, are a plausible Sgr Northern Loop detection consistent with the M giant distribution. Finally, Kundu et al. (2002) have found a position-velocity sequence of eight giant stars with unusually large negative velocities as part of a large K giant survey. These stars lie very near the Sgr mid-plane and may correspond to the very nearest parts of the infalling Northern Loop (see Figure 18).

We may summarize the comparisons discussed to this point as almost uniform in agreement with regard to both the locations of Sgr debris in position on the sky *and* with respect to distance (despite the disparate methods for identifying and gauging Sgr debris).

### 8.3. Carbon Stars

Carbon stars have also been associated with the Sgr plane. The large-area APM Survey (Totten & Irwin 1988) revealed dozens of carbons stars with positions and radial velocities consistent with the Sgr tidal tails and which Ibata et al. (2001a,b) used to define a Sgr orbital plane and a debris model that generally resembles the distributions of 2MASS M giants. However, the carbon star luminosities adopted in these studies yield photometric parallaxes that are, on average,  $\sim 35\%$  larger than the M-giant distance scale (which has been shown to agree with numerous other studies; Figure 18), even when very dusty N type stars are ignored.<sup>11</sup>

Calibration of the carbon star distance scale has been historically complex, being complicated by variability, obscuring dust shells and metallicity effects. While Totten, Irwin & Whitelock (2000)

---

<sup>11</sup>The assertion of an overestimated distance scale assumes that the carbons near the Sgr plane shown in Figure 18 are predominantly Sgr debris. Totten & Irwin (1998) have mentioned that CH-type carbon stars “are likely to be somewhat fainter intrinsically than N-types and hence closer than estimated...”.

have demonstrated good agreement between  $JK$ -based distance estimates and an assumed  $R$ -band carbon star absolute magnitude of  $M_R = -3.5$ , Demers, Dallaire and Battinelli (2002) have noted a metallicity trend whereby the  $[\text{Fe}/\text{H}] = -1.4$  carbon stars in Fornax are 0.25 mag fainter in  $K_s$  absolute magnitude than  $[\text{Fe}/\text{H}] \sim -0.5$  LMC carbon stars.<sup>12</sup>

Figure 20 highlights 95 extreme-colored ( $[J - K_s]_o > 1.3$ ) stars within  $5^\circ$  of the Sgr core that lie in a well-defined carbon star locus extending from the Sgr Red and Asymptotic Giant Branches. Stars with  $(K_s)_o < 8$  are most likely foreground carbon stars associated with the Galactic bulge. Though it contains several times more carbon stars, this Sgr carbon star sequence is consistent with the Sgr carbon star locus of Whitelock et al. (1999). However, both sequences fall below the carbon star loci determined for Milky Way satellites (Totten et al. 2000) and the LMC (Weinberg & Nikolaev 2001) when these loci are adjusted for the Sgr core distance. The mean  $(K_s)_o$  of the highlighted points in Figure 20 is  $9.59 \pm 0.06$  mag. In the color range  $1.3 < (J - K_s)_o < 2.0$ , the Sgr carbon locus is  $0.39 \pm 0.07$  mag fainter than the Weinberg & Nikolaev LMC locus, while for  $(J - K_s)_o \geq 2.0$  the Sgr locus is  $0.64 \pm 0.10$  mag underluminous.

Regardless of the calibration of absolute magnitude, the spatial distribution of 2MASS-selected carbon stars (Figure 21) provides a poor estimate of Sgr morphology relative to M giants because: (1) Sgr carbon stars are much less populous (thirty times less numerous than  $0.95 \leq (J - K_s)_o < 1.10$  M giant candidates in the same area of the Sgr core), (2) carbon stars have a larger intrinsic scatter in their color-magnitude relation (an RMS of 0.59 mag in the Figure 20 carbon sample compared to 0.46 mag for the Figure 1c M giants), and (3) a substantial number of carbon stars are long period variables. 2MASS in particular provides mainly single epoch observations of a carbon star sample that likely contains a substantial fraction of  $\Delta K > 0.4$  Mira, as well as lower amplitude, variable stars (Whitelock et al. 1999).

Figure 21 shows the orbital plane distribution of Galactic carbon stars (selected as sources with  $[J - K_s]_o \geq 1.3$ ), with absolute magnitudes derived from the Weinberg & Nikolaev (2001) loci dimmed by 0.5 mag (panel a) and by adopting a simple  $M_{K_s} = (9.59 - 16.90) = -7.31$  for all stars (panel b).<sup>13</sup> A “finger of God” effect for the Sgr core is a result of intrinsic spread in the

<sup>12</sup>Kunkel, Demers & Irwin (1997) also find a median  $R = 15.2$  magnitude for more than 400 carbons in the LMC periphery, which, with an LMC distance modulus of 18.55, yields an  $M_R$  closer to -3.35 for these carbon stars. Totten, Irwin & Whitelock (2000) note a “vertical scatter about the fitted curve [that] covers a range of  $\sim \pm 0.5$  mag, with occasional more extreme outliers that in the main are probably caused by variable stars.” Their data also reveal something of a population gradient in that the bright, blue CH-type LMC carbons of Hartwick & Cowley (1988), which have been argued (Suntzeff et al. 1993) to be a very young (0.1 Gyr) AGB population, lie well above their fit color-magnitude relation, while the more “normal” LMC carbons as well as a number of other dSph and SMC carbons create much of the vertical scatter 0.5 mag or more *fainter* than the fit. This trend echoes the Demers et al. (2002) conclusion regarding likely metallicity effects on carbon star luminosities.

<sup>13</sup>In contrast to previous plots presented here for M giants (e.g., those shown Figure 14) that only included stars within a *linear* distance from the  $\Lambda_{GC}$  plane, Figure 21 shows stars with *angular* ( $|B_\odot| < 10^\circ$ ) separations from the Sgr plane; with the larger uncertainty in the carbon star photometric parallaxes, we risk losing Sgr carbons with a

color-magnitude relation (Figure 20) and variability. About five or six dozen high latitude carbon stars lie near the Sgr plane but only loosely trace the M giant tidal arms (compare Figure 21 to Figure 11).

To give some impression of the relative contribution of carbon stars to the Galactic halo from the Sgr dwarf, we show in Figure 21c the Galactic  $Y_{GC} - Z_{GC}$  distribution of all stars with  $(J - K_s)_o \geq 1.3$ . For clarity a constraint of  $(K_s)_o < 11.75$  is imposed (without this criterion the distribution is significantly noisier, likely due to a “contamination shell” problem as found for the M giants in Section 6.6). Outside the quadrant containing the Magellanic Clouds, Sgr appears to have been the predominant source of high latitude,  $R_{GC} \lesssim 75$  kpc halo field carbon stars.

#### 8.4. Globular Clusters

It is presently known that four globular clusters with positions near the Sgr core, NGC 6715 (M54), Terzan 7, Terzan 8 and Arp2 are associated with the dwarf galaxy: These globulars have similar distances and radial velocities to the main body of Sgr (Ibata et al 1995). A fifth cluster that lies in the heart of the Southern Arc (Figure 18), Pal 12, has been shown to have orbital characteristics that make it a reasonably good candidate for association with Sgr (Dinescu et al. 2000; see also Martinez-Delgado et al. 2002). Several studies of the Galactic globular cluster population have sought additional possible cluster members of the Sgr debris streams, with a number of additional candidates proposed (Irwin 1999, Dinescu et al. 2001, Palma et al. 2002, Bellazzini et al. 2002a, 2003). The recent analysis by Bellazzini et al. (2003), in particular, makes a strong case for several additional Sgr clusters. Because, as Bellazzini et al. (2003) have shown, precise knowledge of the Sgr orbit is of great use to sorting out interesting candidates, we defer an analysis of connections of the Sgr debris streams and globular clusters to a companion contribution containing our best fit model to the M giant data.

### 9. Density of Nearby Sgr Stellar Debris

In Section 6.4 we discussed the proximity of the Sgr Northern Arm to the Solar Neighborhood. In Section 6.6 we argued that the Southern Arm seemed to be at least  $180^\circ$  long, sweeping into the Northern Hemisphere; if so, then models of the Sgr disruption show that the Northern Loop is long enough to cross the Galactic plane on this side of the Galactic Center. In Figures 14c and 14d we find evidence that the leading arm may even cross the *trailing* arm in the Southern Hemisphere. And in Section 8 and Figure 18 we showed apparently confirmatory evidence from other surveys that Sgr debris is falling about the Solar neighborhood from the NGP. How might the suggested local presence of debris from the Sgr dwarf spheroidal have impacted previous studies

---

linear constraint on distance from the Sgr plane.

of the Galactic halo, many which have been conducted with halo stars relatively near the Sun in potentially “Sgr-contaminated” regions of the Galaxy? The question turns on the relative density of leading Sgr arm debris passing through/near the solar neighborhood.

We can estimate the local density of Sgr stars by extrapolating the M giant density just above the Galactic plane and converting that density to other spectral types (colors) via an adopted luminosity function. This is most straightforward for evolved stars, where the luminosity function can be derived directly from 2MASS observations of the Sgr core — for example, the background-subtracted Sgr color-magnitude diagram shown in Figure 1c. To eliminate residual, unsubtracted contamination from non-Sgr stars and isolate the Sgr RGB we apply the following criterion:

$$K_s > -7.22(J - K_s) + 17.64.$$

This selection also effectively separates the Sgr RGB from the prominent Sgr red clump near  $K_s = 12.75$ ; to restore this population to the luminosity function, we allow stars satisfying

$$12 < K_s < 13.5$$

$$J - K_s > 0.45.$$

The resulting luminosity functions so calculated are shown in Figure 22a. The Figure 1c color-magnitude diagram begins to “run out” beyond  $(K_s)_o = 14.3$ .

The *color function* for evolved stars corresponding to the luminosity function is shown in Figure 22b. From the slope of the RGB, the  $(K_s)_o = 14.3$  magnitude limit means that the color function is complete only for RGB stars redder than  $(J - K_s)_o \sim 0.80$  — roughly spectral types later than K3. The red clump, however, is completely sampled.

The ratios of stars of different spectral types can be computed by comparing counts by colors. Bessell & Brett (1988; see also Bessell et al. 1991) have given approximate colors for stars by spectral type and luminosity class. Obviously metallicity effects are important, but for a rough calculation the corresponding 2MASS color for the Bessell & Brett types is simplistically adopted. Accordingly, the 2MASS color of a type M0III star is  $(J - K_s)_o \sim 0.98$  (Carpenter 2001). Table 4 presents the Figure 1c counts for evolved Sgr stars as determined by the color functions presented in Figure 22b. Roughly, for every Sgr M giant we expect three stars of type K3III through M0III, and more than seven K giants of any type (a substantially conservative lower limit due to the incompleteness of the early K type giant counts due to the magnitude limit of the Figure 1 sample). We also obtain a 3:1 ratio of red clump to later than M0III stars.

We now extrapolate the M giant density in the Sgr leading tidal arm to the solar neighborhood by counting the number of all Sgr M giant stars ( $0.98 \leq [J - K_s]_o < 1.30$ ) in a 5 kpc radius cylinder

centered on the Sun and whose axis is roughly perpendicular to the Galactic plane.<sup>14</sup> To avoid disk contamination, but sample the nearby Sgr leading arm, only stars with  $-30 < Y_{Sgr,GC} < -9$  kpc are tallied; 70 are found, which results in an M giant density of about  $0.036 \text{ kpc}^{-3}$ . Using Table 4, this implies a nearby Sgr  $>\text{K3}$  giant density of  $0.14 \text{ kpc}^{-3}$  and a nearby Sgr red clump density of  $0.11 \text{ kpc}^{-3}$ . Because the M:K giant ratio decreases with age/metallicity, and, given the evidence for possible age/metallicity/giant color variations depicted in Figure 14, the above K giant density is a lower limit.<sup>15</sup> This density is comparable to the density of a velocity clump of nine mostly metal poor ( $[\text{Fe}/\text{H}] < -1$ ) red giants having Hipparcos proper motions and radial velocities and located within 2.5 kpc of the Sun, discussed by Helmi et al. (1999). These authors postulate that this clump, which has a velocity perpendicular to the plane consistent with that expected for nearby Sgr debris (roughly  $225 \text{ km s}^{-1}$  downward), came from a progenitor system that “probably resembled the Fornax and Sagittarius dwarf spheroidal galaxies” and that may have contributed 12% of all metal-poor halo stars outside the Solar Circle (a number that may be three times smaller according to a reanalysis by Chiba & Beers 2000). These nine stars are distributed all over the sky with no obvious spatial structure within the 2.5 kpc radius volume, as might be expected for a large stream passing near the Sun. Together, the aforementioned properties of this clump of giant stars are enticingly consistent with Sgr leading arm in the solar neighborhood; however, the derived (by both Helmi et al. and Chiba & Beers)  $L_Z$  angular momentum for this clump is apparently too large and the apoGalacticon for its progenitor system too small compared to expectations for the nearly polar Sgr orbit that would have produced the M giant tidal arms observed here. Both inconsistencies depend to some extent on the adopted Galactic rotation curve (mass profile) and Local Standard of Rest velocity and should be re-addressed with a Galactic model that self-consistently explains the Sgr debris stream in all directions.

The halo luminosity function is poorly constrained for giant stars. Reid & Majewski (1993; see their Figure 5) have compiled numerous estimates of the halo luminosity function and derive a mean “globular cluster” luminosity function. Adopting this function for the local halo produces a density of  $>\text{K3}$  halo giants (assuming  $M_V[\text{K3III}] \sim 0.0$ ) of order  $45 \text{ kpc}^{-3}$  — a number that is about a factor of two higher than Morrison’s (1993) estimate (taking into account the fainter absolute magnitude limit in her study) and so perhaps represents an upper limit. From the same luminosity function, we estimate a nearby halo red clump star density of  $91 \text{ kpc}^{-3}$ . To the extent that the true local halo giant density is thus described, one might therefore conclude that if the Sgr leading arms is in the solar neighborhood it contributes only of order 0.1-0.3% of the *local* evolved halo stars, and would not likely have significantly impacted studies (e.g., Yoss et al. 1992, Morrison et al. 1993) of nearby “halo giants”. However, it may well have affected more distant

---

<sup>14</sup>The actual cylinder used is centered on  $[X, Z]_{Sgr,GC} = [-8.5, 0]$  kpc and parallel to the  $Y_{Sgr,GC}$  axis in Figure 11.

<sup>15</sup>Majewski et al. (2002b) stress how the *observed* age distribution of bound populations in a steadily disintegrating stellar system is more heavily weighted toward younger populations, and does not accurately reflect the balance of populations to be found in tidal debris from that stellar system.

halo giant samples, e.g., that towards the SGP field SA141 field by Ratnatunga & Freeman (1989), a field for which they noted a particularly small velocity dispersion and which contains stars of the approximate velocity expected for the trailing Sgr tail in this general direction. Assuming an effective vertical halo scaleheight of 3.5 kpc (Reid & Majewski 1993) and the above local halo giant density, Sgr dominates the halo K giant density by 5-6 scaleheights, or 17-20 kpc above the plane — distances comparable to those probed by the SA141 survey.

Rather than rely on incomplete knowledge of the halo star density to ascertain the relative impact of Sgr debris on Galactic structure studies, we may more directly calculate the number of Sgr stars contributing to a particular survey. Here we focus on the magnitude limited survey of stars at the NGP by Majewski (1992), for which a relatively complete radial velocity and proper motion analysis of stars (mainly F-K dwarfs) to  $V \sim 19$  is described in Majewski, Munn & Hawley (1994, 1996). To estimate the number of such stars that could have been contributed by Sgr, we integrate the 15 Gyr old (the age adopted has little affect on the analysis) theoretical luminosity function for a cluster with metal abundance  $Z = 4 \times 10^{-3}$  by Silvestri et al. (1998); this luminosity function was found to give a good match to observationally-derived RGB and main sequence luminosity functions for the globular cluster 47 Tucanae by those authors. Taking into account the volume completeness limits as a function of ( $M_V$ ), we integrate the Silvestri et al. luminosity function from the main sequence turn off at  $M_V = 3.4$  to  $M_V = 8.0$  and scale this density by the ratio of Sgr >KIII giants above to the integral of the luminosity function for  $M_V \leq 0$ . The result leads to an estimate that some 5-10 Sgr dwarfs should be present in the sample discussed by Majewski, Munn & Hawley (1996). It is interesting, therefore, that the halo sample in that survey is constituted by three phase space clumps with of order this number of stars each, and two of the clumps (and the net average of all halo stars in the survey) show a net negative radial velocity, as expected for Sgr debris at the North Galactic Pole. A more detailed assessment of the particular energy and momentum distribution of those phase space clumps in the context of Sgr models that accommodate nearby debris flow is warranted, but clearly the several recent findings of excess numbers of stars with a downward motion from the NGP - for example, from the Majewski et al. survey of dwarf stars and the Kinman et al. (1994, 1996) studies of horizontal branch stars — offer tantalizing possibilities of earlier detections of the leading Sgr arm near the Sun.

## 10. Epilogue

The 2MASS database has been used to make the first all-sky map of the M giant populations of the Sagittarius dwarf spheroidal galaxy system. The present discussion provides the first relatively reddening-free description and analysis of the core regions of the dwarf, as well as extensive new information on the extended tail structure of tidally stripped stars. The latter is particularly useful for placing all previous studies of the Sgr system into a well-defined context, and places the most stringent constraints yet on models of the disruption of Sgr in the Galactic potential.

We have concentrated on an empirical description of the Sgr system and have resisted extensive

interpretation via disruption model-fitting. This tack has been adopted because: (1) The degree to which a simple *empirical* description of the 2MASS results nonetheless advances our understanding of the Sgr system is manifest. (2) Previous successes in the area of model fitting to previously extant data, especially the works by Ibata et al. (2001) and Ibata & Lewis (1998) to which we have frequently referred, provide a sufficiently accurate match to the spatial distributions described here that a general sense of the Sgr orbit and destruction are in hand. Further modeling will benefit from the addition of dynamical information along the tidal arms of the Sgr system. (3) A survey to obtain the dynamics of stars in the extended Sgr tidal arms is underway, and first results for hundreds of M giants will be included in a future contribution. The sample of likely Sgr M giants identified here, being both intrinsically bright and numerous, provides an ideal database for obtaining the dynamics of the tidal streams from radial velocities (using *small* telescopes) and, eventually, from proper motion studies (either ground or space-based). Once the Sgr orbit and debris stream are mapped and understood with accuracy and precision it can become a primary fiducial for delineating the structure and dynamics of the Milky and its halo.

The results presented in this publication make use of data from the Two Micron All Sky Survey (2MASS), which is a joint project of the University of Massachusetts and the Infrared Processing and Analysis Center (IPAC), Funded by the National Aeronautics and Space Administration and the National Science Foundation. The 2MASS database owes its existence to the dedicated work of 2MASS scientists and IPAC staff in producing data products of unparalleled photometric quality and uniformity. MS acknowledges support from NASA/JPL contract 123402, and SRM acknowledges support from a Space Interferometry Mission Key Project grant, NASA/JPL contract 1228235. SRM appreciates useful conversations with William Kunkel, Kathryn Johnston and David Law. We thank Heidi Newberg for providing and giving permission to use the Sloan Digital Sky Survey equatorial distribution image. Richard Patterson, Jeffrey Crane, Megan Kohring, Howard Powell and Kiri Xiluri are thanked for assistance with various figures.

## REFERENCES

Alard, C. 1996, A&A, 458, L17  
Alard, C. 2001, A&A, 377, 389  
Alcock, C. et al. 1997a, ApJ, 474, 217  
Amendt, P. & Cuddeford, P. 1994, ApJ, 435, 93  
Bassino, L. P. & Muzzio, J. C. 1995, The Observatory, 115, 256  
Bellazzini, M., Ferraro, F. R., & Buonanno, R. 1999, MNRAS, 304, 633  
Bellazzini, M., Ferraro, F. R., & Buonanno, R. 1999, MNRAS, 307, 619  
Bellazzini, M., Ferraro, F. R., & Ibata, R. 2002a, AJ, 124, 915

Bellazzini, M., Ferraro, F. R., & Ibata, R. 2003, AJ, 125, 188

Bellazzini, M., Ferraro, F. R., Origlia, L., Pancino, E., Monaco, L., & Oliva, E. 2002b, AJ, 124, 3222

Bertelli, G., Bressan, A., Chiosi, C., Fagotto, F., & Nasi, E. 1994, A&AS, 106, 275

Bessell, M. S. & Brett, J. M. 1988, PASP, 100, 1134

Binney, J., May, A., & Ostriker, J. P. 1987, MNRAS, 226, 149

Binney, J. & Tremaine, S. 1987, Princeton, NJ, Princeton University Press, 1987, 747 p. 236

Bonifacio, P., Pasquini, L., Molaro, P., & Marconi, G. 1999, Ap&SS, 265, 541

Bullock, J. S., Kravtsov, A. V. & Weinberg, D. H. 2001, ApJ, 548, 33

Burton, W. B. & Lockman, F. J. 1999, A&A, 349, 7

Caldwell, N., Armandroff, T. E., Seitzer, P., & Da Costa, G. S. 1992, AJ, 103, 840

Carpenter, J. M. 2001, AJ, 121, 2851

Chiba, M. & Beers, T. C. 2000, AJ, 119, 2843

Cole, A. A. 2001, ApJ, 559, L17

Cseresnjes, P. 2001, A&A, 375, 909

Cseresnjes, P., Alard, C., & Guibert, J. 2000, A&A, 357, 871

Cutri, R. 2003, *in preparation*

Da Costa, G. S., Armandroff, T. E., Caldwell, N., & Seitzer, P. 1996, AJ, 112, 2576

Demers, S., Dallaire, M., & Battinelli, P. 2002, AJ, 123, 3428

Dinescu, D. I., Majewski, S. R., Girard, T. M., & Cudworth, K. M. 2000, AJ, 120, 1892

Dinescu, D. I., Majewski, S. R., Girard, T. M., & Cudworth, K. M. 2001, AJ, 122, 1916

Dinescu, D. I. et al. 2002, ApJ, 575, L67

Dohm-Palmer, R. C., Helmi, A., Morrison, H., Mateo, M., Olszewski, E. W., Harding, P., Freeman, K. C., Norris, J. & Shectman, S. A. 2001, ApJ, 555, L37

Edelsohn, D. J. & Elmegreen, B. G. 1997, MNRAS, 290, 7

Eggen, O. J. Lynden-Bell, D. & Sandage, A. R. 1962, ApJ, 136, 748

Elias, J. H., Frogel, J. A., Matthews, K., & Neugebauer, G. 1982, AJ, 87, 1029

Font, A.S., Navarro, J.F., Stadel, J. & Quinn, T. 2001, ApJ, 563, L1

Freeman, K. C. 1993, ASP Conf. Ser. 48: The Globular Cluster-Galaxy Connection, 608

Gilmore, G., Wyse, R. F. G., & Norris, J. E. 2002, ApJ, 574, L39

Gómez-Flechoso, M. A. 1998, Ap&SS, 263, 155

Gómez-Flechoso, M. A., Fux, R., & Martinet, L. 1999, A&A, 347, 77

Gómez-Flechoso, M. A. & Martínez-Delgado, D. 2003, ApJL, *in press*

Harbeck, D. et al. 2001, AJ, 122, 3092

Helmi, A. & White, S.D.M. 2001, MNRAS, 323, 529

Helmi, A., White, S. D. M., de Zeeuw, P. T., & Zhao, H. 1999, Nature, 402, 53

Hurley-Keller, D., Mateo, M., & Grebel, E. K. 1999, ApJ, 523, L25

Ibata, R. A. 1999, IAU Symp. 186: Galaxy Interactions at Low and High Redshift, 186, 39

Ibata, R. A., Gilmore, G., & Irwin, M. J. 1994, Nature, 370, 194

Ibata, R. A., Gilmore, G. & Irwin, M. J. 1995, MNRAS, 277, 781

Ibata, R. A., Irwin, M. J., Lewis, G. F., Ferguson, A. M. N. & Tanvir, N. 2003, astro-ph/0301067

Ibata, R., Irwin, M., Lewis, G. F., & Stolte, A. 2001a, ApJ, 547, L133

Ibata, R. A. & Lewis, G. F. 1998, ApJ, 500, 575

Ibata, R. A., Lewis, G. F., Irwin, M. J., & Cambrésy, L. 2002, MNRAS, 332, 921

Ibata, R. A., Lewis, G. F., Irwin, M. J., & Quinn, T. 2002, MNRAS, 332, 915

Ibata, R., Lewis, G. F., Irwin, M., Totten, E., & Quinn, T. 2001b, ApJ, 551, 294

Ibata, R. A., Wyse, R. F. G., Gilmore, G., Irwin, M. J., & Suntzeff, N. B. 1997, AJ, 113, 634

Irwin, M. 1999, IAU Symposium, 192, 409

Irwin, M. & Hatzidimitriou, D. 1995, MNRAS, 277, 1354

Ivezić, Ž., et al. 2000, AJ, 120, 963

Jiang, I. & Binney, J. 2000, MNRAS, 314, 468

Johnston, K. V. 1998, ApJ, 495, 297

Johnston, K. V., Hernquist, L., & Bolte, M. 1996, ApJ, 465, 278

Johnston, K. V., Majewski, S. R., Siegel, M. H., Reid, I. N., & Kunkel, W. E. 1999, AJ, 118, 1719

Johnston, K. V., Sackett, P. D., & Bullock, J. S. 2001, ApJ, 557, 137

Johnston, K. V., Sigurdsson, S. & Hernquist, L. 1999a, MNRAS, 302

Johnston, K. V., Spergel, D. N., & Haydn, C. 2002, ApJ, 570, 656

Johnston, K. V., Spergel, D. N., & Hernquist, L. 1995, ApJ, 451, 598

Johnston, K. V., Zhao, H., Spergel, D. N., & Hernquist, L. 1999, ApJ, 512, L109

King, I. 1962, AJ, 67, 471

King, I. R. 1966, AJ, 71, 64

Kinman, T. D., Pier, J. R., Suntzeff, N. B., Harmer, D. L., Valdes, F., Hanson, R. B., Klemola, A. R., & Kraft, R. P. 1996, AJ, 111, 1164

Kinman, T. D., Suntzeff, N. B., & Kraft, R. P. 1994, AJ, 108, 1722

Klessen, R. S. & Kroupa, P. 1998, ApJ, 498, 143

Kleyna, J. T., Geller, M. J., Kenyon, S. J., Kurtz, M. J., & Thorstensen, J. R. 1998, AJ, 115, 2359

Klypin, A., Kravtsov, A. V., Valenzuela, O., & Prada, F. 1999, ApJ, 522, 82

Kocevski, D. D. & Kuhn, J. R. 2000, American Astronomical Society Meeting, 197,

Koribalski, B., Johnston, S., & Otrupcek, R. 1994, MNRAS, 270, L43

Kroupa, P. 1997, New Astron. 2, 139-164, 2, 139

Kuhn, J. R., Smith, H. A., & Hawley, S. L. 1996, ApJ, 469, L93

Kundu, A., *et al.* 2002, ApJ, 576, L125.

Kunkel, W. E., Irwin, M. J., & Demers, S. 1997, A&AS, 122, 463

Layden, A. C. & Sarajedini, A. 2000, AJ, 119, 1760

Light, R.M. 1988, Ph.D. Thesis, Yale Univ.

Majewski, S. R. 1992, ApJS, 78, 8

Majewski, S. R. 2003, in New Horizons in Globular Cluster Astronomy, ed. G. Piotto, ASP Conf. Ser. Vol., *in press*.

Majewski, S. R., Law, D. R., Johnston, K. V., Patterson, R. J., Kunkel, W. E., Polak, A. A., Frinchaboy, P. M., Rhee, J. & Hummels, C. B. 2003, *in preparation*.

Majewski, S. R., et al. 2002a, in Yale Cosmology Workshop: The Shapes of Galaxies and their Dark Halos, ed. P. Natarajan, (World Scientific: New Jersey), p. 214.

Majewski, S. R., et al. 2002b, in Modes of Star Formation and the Origin of Field Populations, eds. E. K. Grebel & W. Brandner, ASP Conf. Ser. Vol. 285, p. 199.

Majewski, S. R., Munn, J. A. & Hawley, S. L. 1994, ApJ, 427, L37

Majewski, S. R., Munn, J. A. & Hawley, S. L. 1996, ApJ, 459, L73

Majewski, S. R., Ostheimer, J. C., Patterson, R. J., Kunkel, W. E., Johnston, K. V. & Geisler, D. 2000, AJ, 119, 760

Majewski, S. R., Siegel, M. H., Kunkel, W. E., Reid, I. N., Johnston, K. V., Thompson, I. B., Landolt, A. U., & Palma, C. 1999a, AJ, 118, 1709

Majewski, S. R., Siegel, M. H., Patterson, R. J., & Rood, R. T. 1999b, ApJ, 520, L33

Marconi, G., Buonanno, R., Castellani, M., Iannicola, G., Molaro, P., Pasquini, L., & Pulone, L. 1998, A&A, 330, 453

Martínez-Delgado, D., Alonso-García, J., Aparicio, A., & Gómez-Flechoso, M. A. 2001a, ApJ, 549, L63

Martínez-Delgado, D., Aparicio, A., Gómez-Flechoso, M. Ángeles, & Carrera, R. 2001b, ApJ, 549, L199

Martínez-Delgado, D., Gómez-Flechoso, M. A., & Aparicio, A. 2001b, in ASP Conf. Ser., Observed HR Diagrams and Stellar Evolution, ed. T. Lejeune & J. Fernandes (M01)

Martínez-Delgado, D., Zinn, R., Carrera, R., & Gallart, C. 2002, ApJ, 573, L19

Mateo, M. L. 1998, ARA&A, 36, 435

Mateo, M., Olszewski, E. W., & Morrison, H. L. 1998, ApJ, 508, L55

Mateo, M., Udalski, A., Szymanski, M., Kaluzny, J., Kubiak, M., & Krzeminski, W. 1995, AJ, 109, 588

Mayer, L., Governato, F., Colpi, M., Moore, B., Quinn, T., Wadsley, J., Stadel, J., & Lake, G. 2001, ApJ, 559, 754

Mayer, L., Moore, B., Quinn, T., Governato, F., & Stadel, J. 2002, MNRAS, 336, 119

Moore, B. 1996, ApJ, 461, L13

Moore, B., Ghigna, S., Governato, F., Lake, G., Quinn, T., Stadel, J., & Tozzi, P. 1999, ApJ, 524, L19

Morrison, H. L. 1993, AJ, 106, 578

Murali, C. & Dubinski, J. 1999, AJ, 118, 9111

Navarro, J. F., Frenk, C. S. & White S. D. M. 1996, ApJ, 462, 563

Navarro, J. F., Frenk, C. S. & White S. D. M. 1997, ApJ, 490, 493

Newberg, H. J. et al. 2002, ApJ, 569, 245

Nikolaev, S. & Weinberg, M. D. 2000, ApJ, 542, 804

Odenkirchen, M. et al. 2001, ApJ, 548, L165

Olling, R. P. 1997, Dark Matter in Astro- and Particle Physics : (DARK '96), eds. H.V. Klapdor-Kleingrothaus, Y. Ramachers, (Singapore: World Scientific), p. 44.

Ostheimer, J. C., Link, R., Majewski, S. R., Patterson, R. J. & Crane, J. D. 2003, *in preparation*

Palma, C., Majewski, S. R., & Johnston, K. V. 2002, ApJ, 564, 736

Palma, C., Majewski, S. R., Siegel, M.S., Patterson, R.J., Ostheimer, J.C. & Link, R. 2003, astro-ph/0205194

Peñarrubia, J., Boily, C. M., Just, A., & Kroupa, P. 2000, Astronomische Gesellschaft Abstract Series, Vol. 17. Abstracts of Contributed Talks and Posters presented at the Annual Scientific Meeting of the Astronomische Gesellschaft at Bremen, p. 50

Ratnatunga, K. U. & Freeman, K. C. 1989, ApJ, 339, 126

Reid, N. & Majewski, S. R. 1993, ApJ, 409, 635

Richstone, D. O. & Tremaine, S. 1986, AJ, 92, 72

Robin, A. C., Reylé, C., & Crézé, M. 2000, A&A, 359, 103

Rockosi, C. M. et al. 2002, AJ, 124, 349

Sackett, P. D. & Pogge, R. W. 1995, Dark Matter, 141

Sackett, P. D., Rix, H., Jarvis, B. J., & Freeman, K. C. 1994, ApJ, 436, 629

Samurović, S., Ćirković, M. M., & Milošević-Zdjelar, V. 1999, MNRAS, 309, 63

Sarajedini, A. & Layden, A. C. 1995, AJ, 109, 1086

Schlegel, D. J., Finkbeiner, D. P., & Davis, M. 1998, ApJ, 500, 525

Searle, L. & Zinn, R. 1978, ApJ, 225, 357

Siegel, M. H., Majewski, S. R., Reid, I. N. & Thompson, I. 2002, ApJ, 578, 151

Silvestri, F., Ventura, P., D'Antona, F., & Mazzitelli, I. 1998, ApJ, 509, 192

Sohn, S., Majewski, S.R., Patterson, R.J. & Siegel, M.H. 2003, *in preparation*

Sparke, L. S. 2002, Proceedings of the Yale Cosmology Workshop "The Shapes of Galaxies and Their Dark Matter Halos", ed. P. Natarajan (Singapore: World Scientific), p.178

Totten, E. J. & Irwin, M. J. 1998, MNRAS, 294, 1

Totten, E. J., Irwin, M. J., & Whitelock, P. A. 2000, MNRAS, 314, 630

Trager, S. C., Djorgovski, S., & King, I. R. 1995, AJ, 109, 218

Tremaine, S. 1993, in *Back to the Galaxy*, eds. S. S. Holt & F. Verter, (New York: AIP Conference Proceedings), 599

Unavane, M., Wyse, R. F. G., & Gilmore, G. 1996, MNRAS, 278, 727

van der Marel, R. P. 1991, MNRAS, 248, 515

van der Marel, R. P. 2001, AJ, 122, 1827

Velazquez, H. & White, S. D. M. 1995, MNRAS, 275, L23

Vivas, A. K. et al. 2001, ApJ554, L33

Walcher, J., Fried, J.W., Burkert, A. & Klessen, R.S. 2002, astro-ph/0207467.

Weinberg, M. D., & Nikolaev, S. 2001, ApJ, 548, 712

Westfall, K. B., Majewski, S. R., Ostheimer, J. C., Frinchaboy, P. M., Patterson, R. J., & Kunkel, W. E. 2003, *in preparation*

Westfall, K. B., Ostheimer, J. C., Frinchaboy, P. M., Patterson, R. J., Majewski, S. R., & Kunkel, W. E. 2000, American Astronomical Society Meeting, 197,

Whitelock, P., Menzies, J., Irwin, M., & Feast, M. 1999, IAU Symposium, 192, 136

Yanny, B. et al. 2000, ApJ, 540, 825

Yoss, K. M., Neese, C. L., & Hartkopf, W. I. 1987, AJ, 94, 1600

Zhao, H. 1998, ApJ, 500, L149

Zinnecker, H., Keable, C. J., Dunlop, J. S., Cannon, R. D., & Griffiths, W. K. 1988, IAU Symp. 126: The Harlow-Shapley Symposium on Globular Cluster Systems in Galaxies, 126, 603



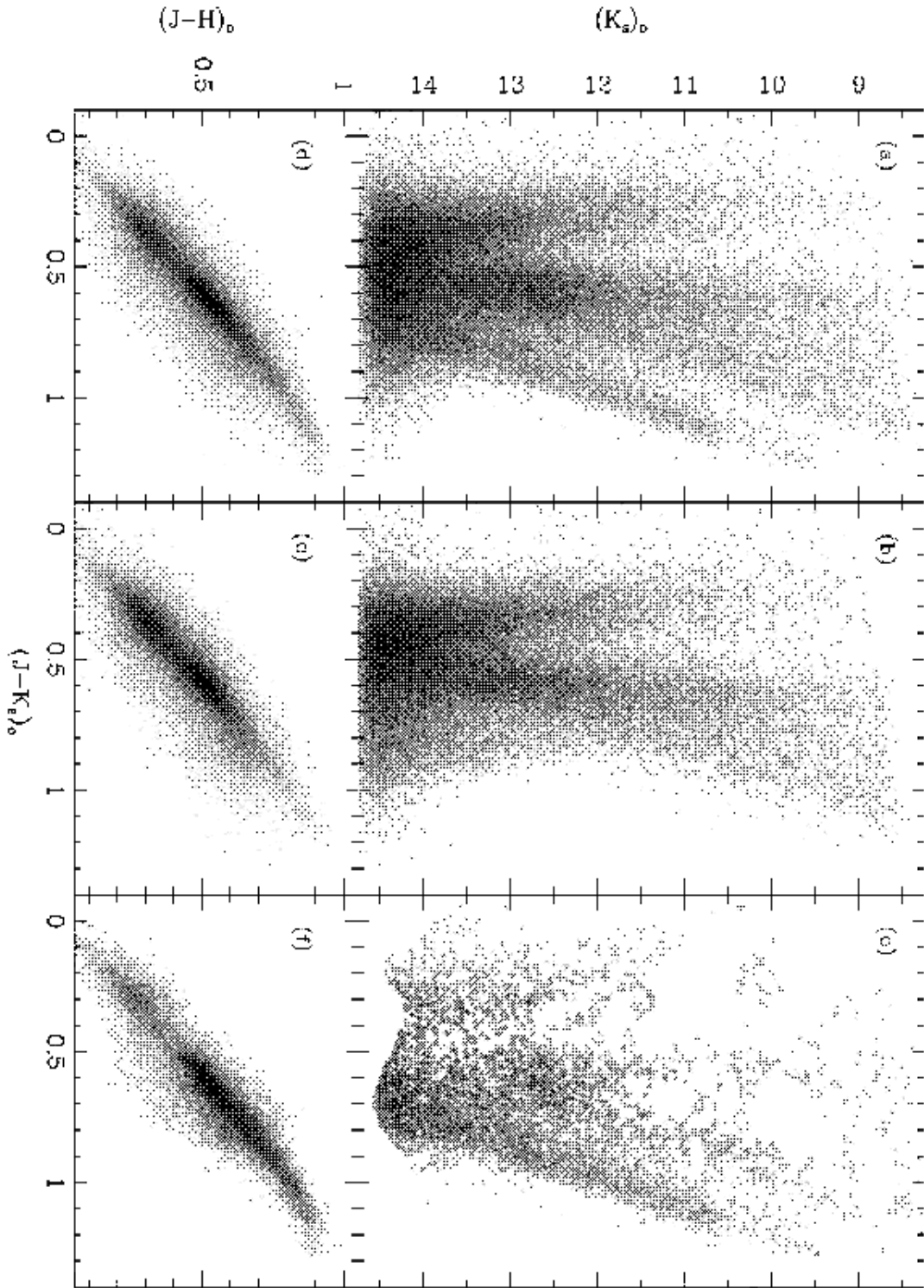


Fig. 1.— Near-infrared  $(J-K_s, K_s)$  color-magnitude diagrams of (a) the Sgr core, (b) a control field of identical area, and Galactic coordinates reflected about  $l = 0^\circ$ , and (c) a star by star subtraction of (b) from (a). Panels (d)-(f) show the corresponding  $(J-K_s, J-H)$  two-color diagrams for the samples shown in (a)-(c). All sources are dereddened using the Schlegel et al. (1998) maps.

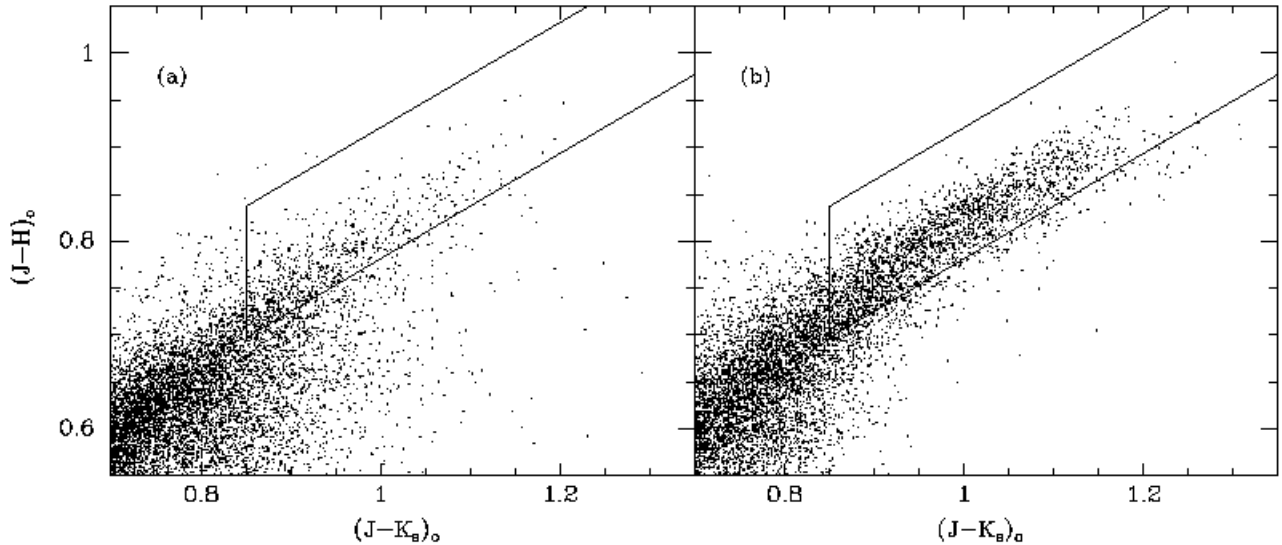


Fig. 2.— The solid lines indicate the color-color selection criteria adopted to find M giants for most of this paper. Panel (a) shows the distribution of stars in the control field, from Figure 1e, and panel (b) shows the distribution of stars from the statistically subtracted sample in Figure 1f. Note that the control field, selected to be a Galactic longitude match to the Sgr core field, still contains about a 1% contribution from the Sgr dwarf itself.

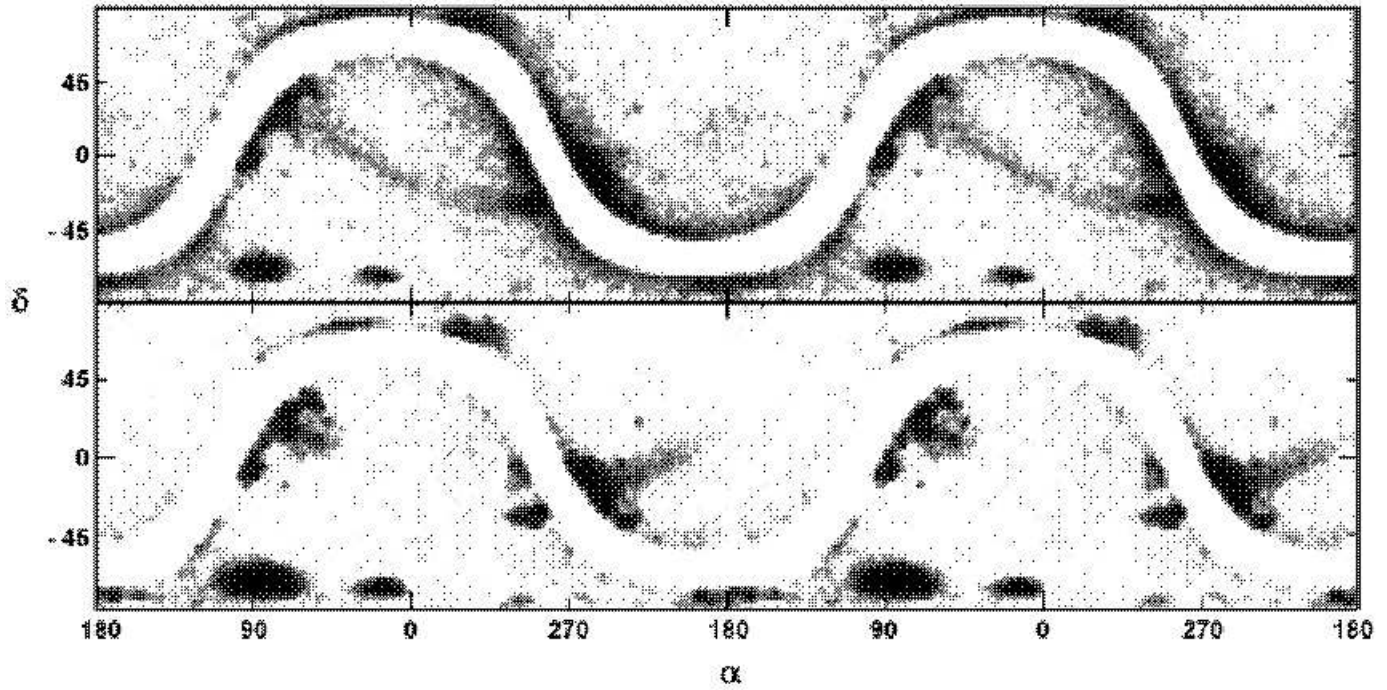


Fig. 3.— Smoothed maps of the sky in equatorial coordinates for two color-magnitude windows of the (non-dereddened) 2MASS point source catalogue filtered optimally to show (top) the “Southern Arc” and (bottom) the “Northern Spur”: (top)  $11 \leq K_s \leq 12$  and  $1.00 < J - K_s < 1.05$ , and (bottom)  $12 \leq K_s \leq 13$  and  $1.05 < J - K_s < 1.15$ . We show two cycles around the sky to demonstrate the continuity of features.

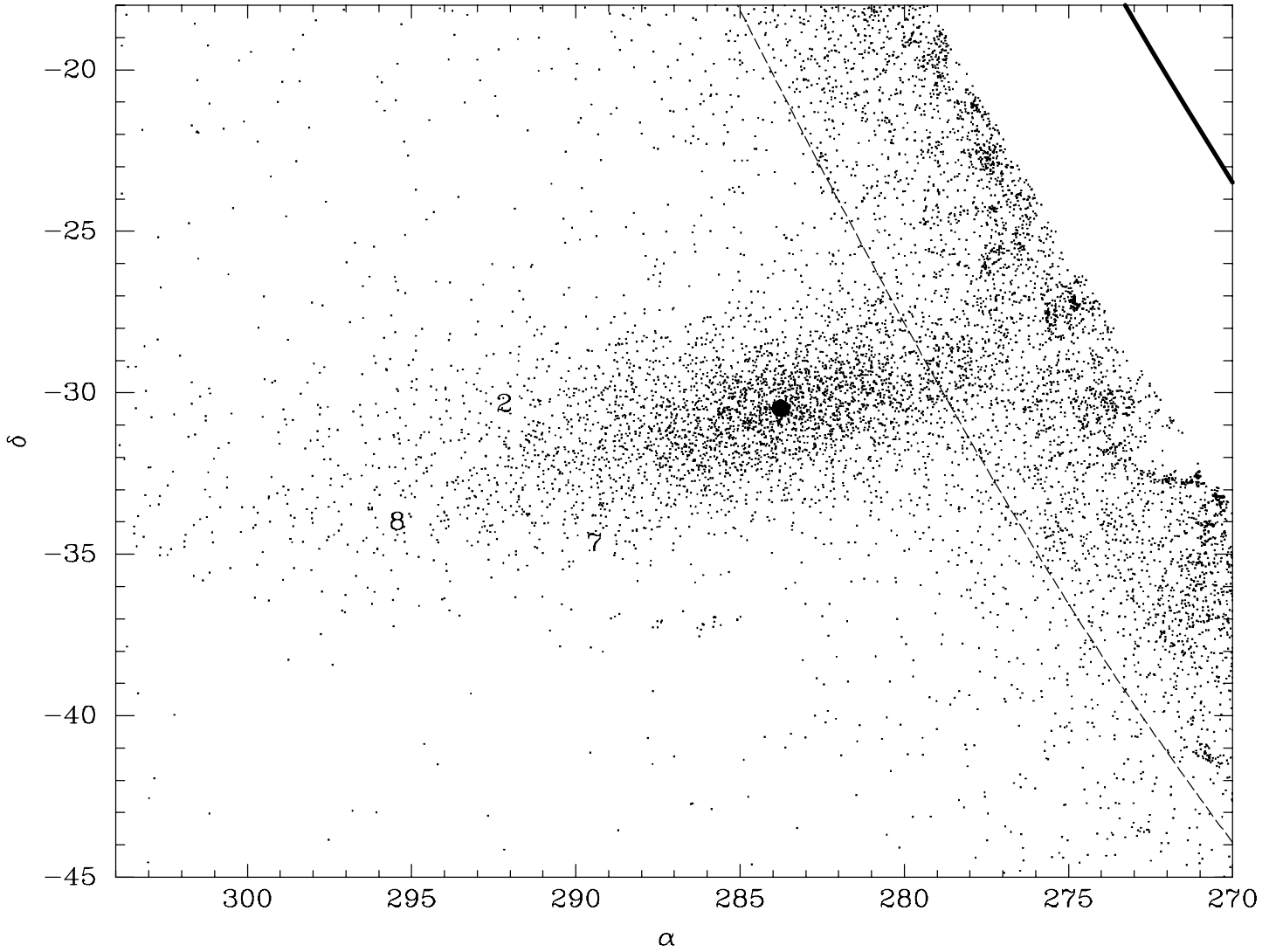


Fig. 4.— View of the Sgr core near where it crosses the Galactic mid-plane (shown as the heavy line to the upper right). Sources up to  $b = -5^\circ$  are shown; the results of very patchy reddening can be seen for  $b > -10^\circ$  (demarcated by the dashed line). The symbols mark the locations of globular clusters as follows: “2” is Arp 2, “7” is Terzan 7, “8” is Terzan 8, and the *solid circle* is the location of the cluster M 54.

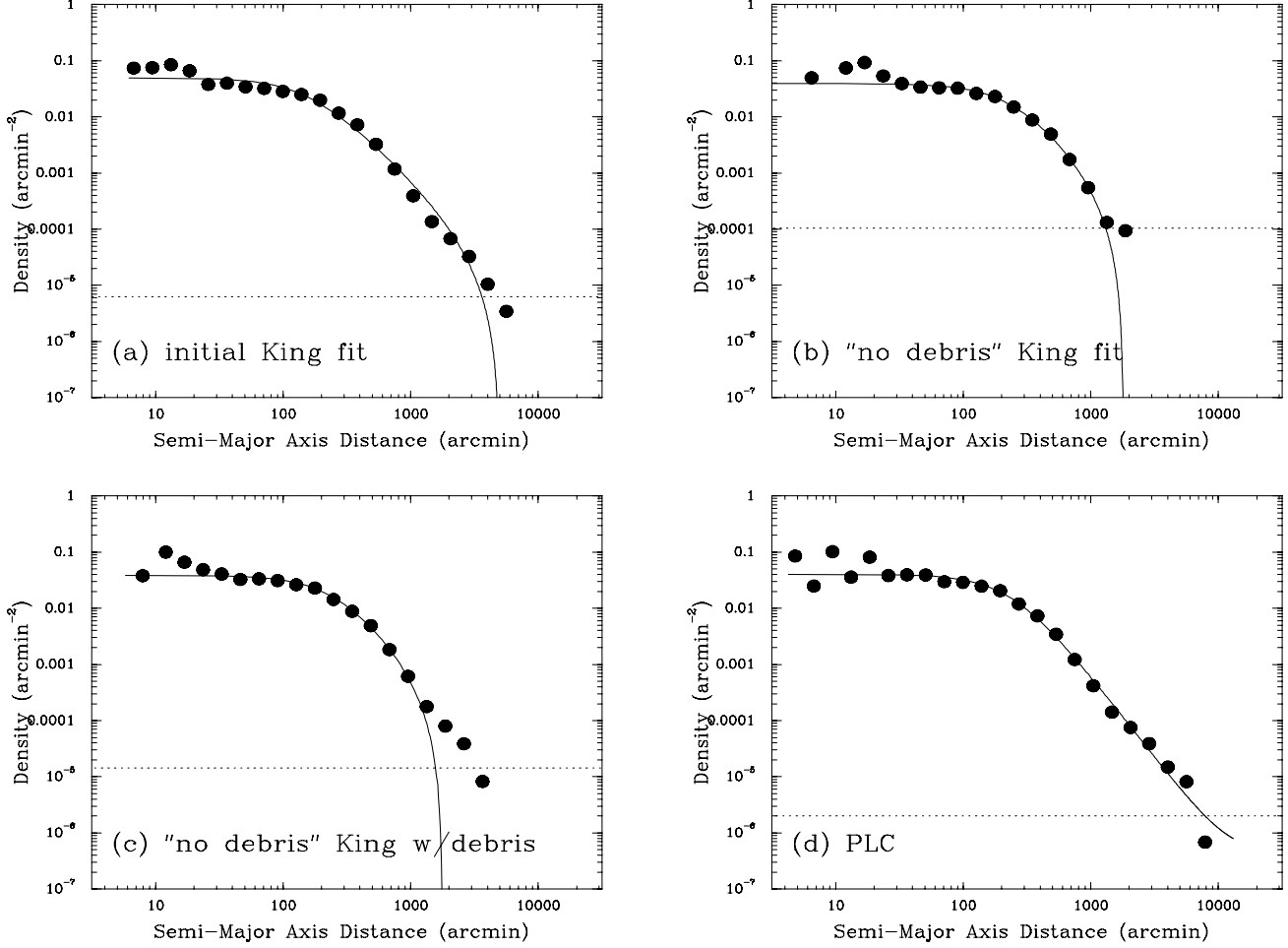


Fig. 5.— Model fits to the radial profile of the Sgr main body. (a) Original fit to the area shown in Figure 4, but with  $|b| > 12^\circ$ . (b) Fit to data with an additional restriction to Figure 5 of  $\alpha_{2000} < 300^\circ$  to remove the tidal debris along the major axis. (c) The derived fit panel (b), but with the data in panel (a). All parameters from the panel (b) fit are utilized, except the background level, which has been refit because of variations in the background level when different Galactic latitude ranges are considered. (d) Power Law + Core fit to the same data as in panel (a). In all cases, the dotted lines are the derived level of the background, which has been subtracted off the data and the fit curves. Note that the data points in each panel change positions due to rebinning that reflects different ellipticities and position angles derived from the fits.

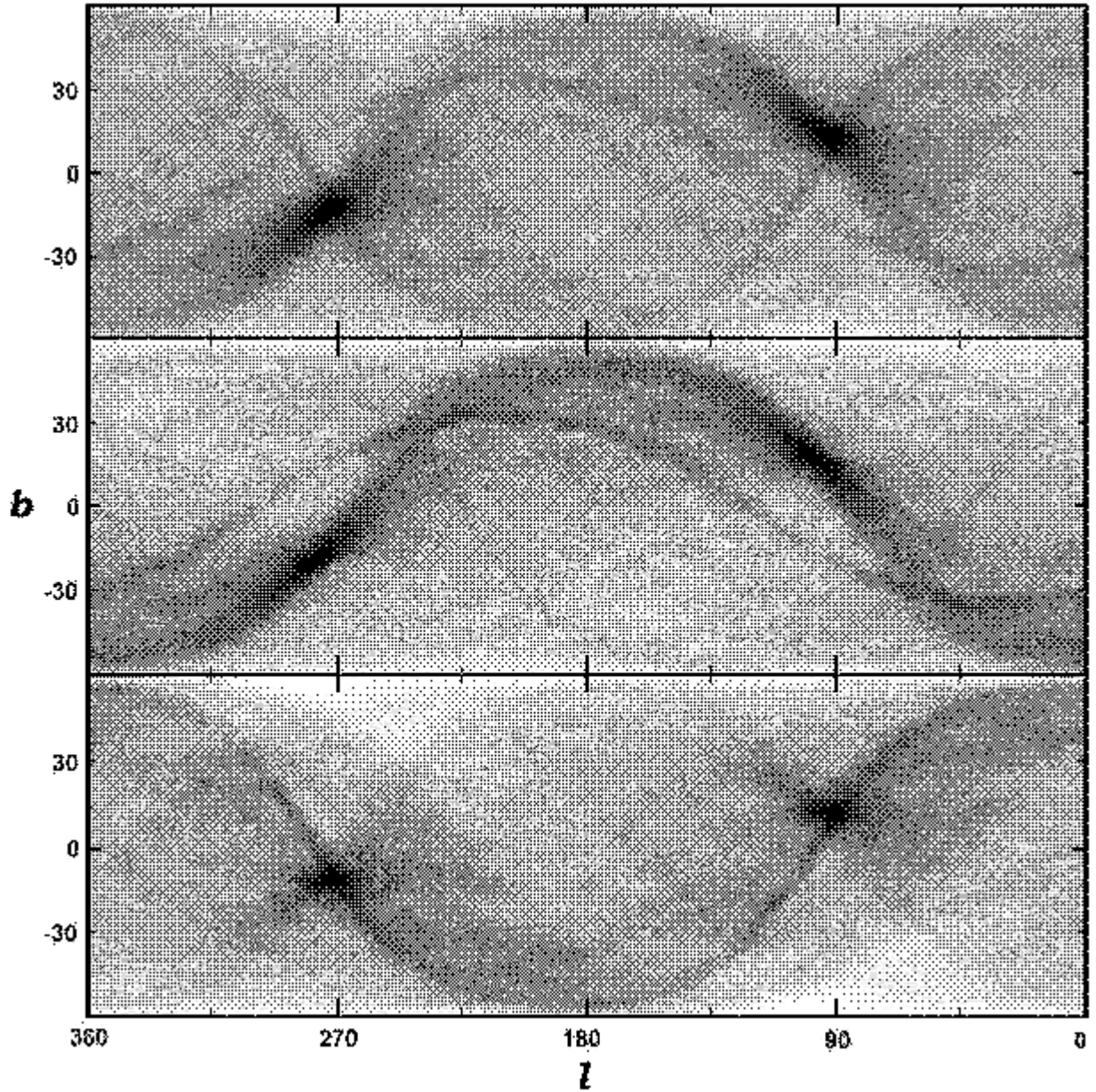


Fig. 6.— Great circle cell counts for M giant candidates in the projected distance range 13–65 kpc and  $|b| > 30^\circ$ . The plots are in sky-right, Galactic coordinates, from  $360^\circ > l > 0^\circ$  and  $-60^\circ < b < 60^\circ$ . The top panel shows the results for both hemispheres together, the middle panel is for inclusion only of Northern Hemisphere data, and the lower panel is for inclusion of only Southern Hemisphere data. From all panels we have removed the Magellenic Clouds from the sample to remove the rather strong great circle pole families they contribute. The darkest patches correspond to the pole and antipole of the Sgr tidal debris stream at approximately  $(l, b) = (272, -13)^\circ$ . No other strong peaks occur in this particular stellar sample of M giants. Arc-like features in the GCCC distributions result from various localized density peaks in the sky distribution.

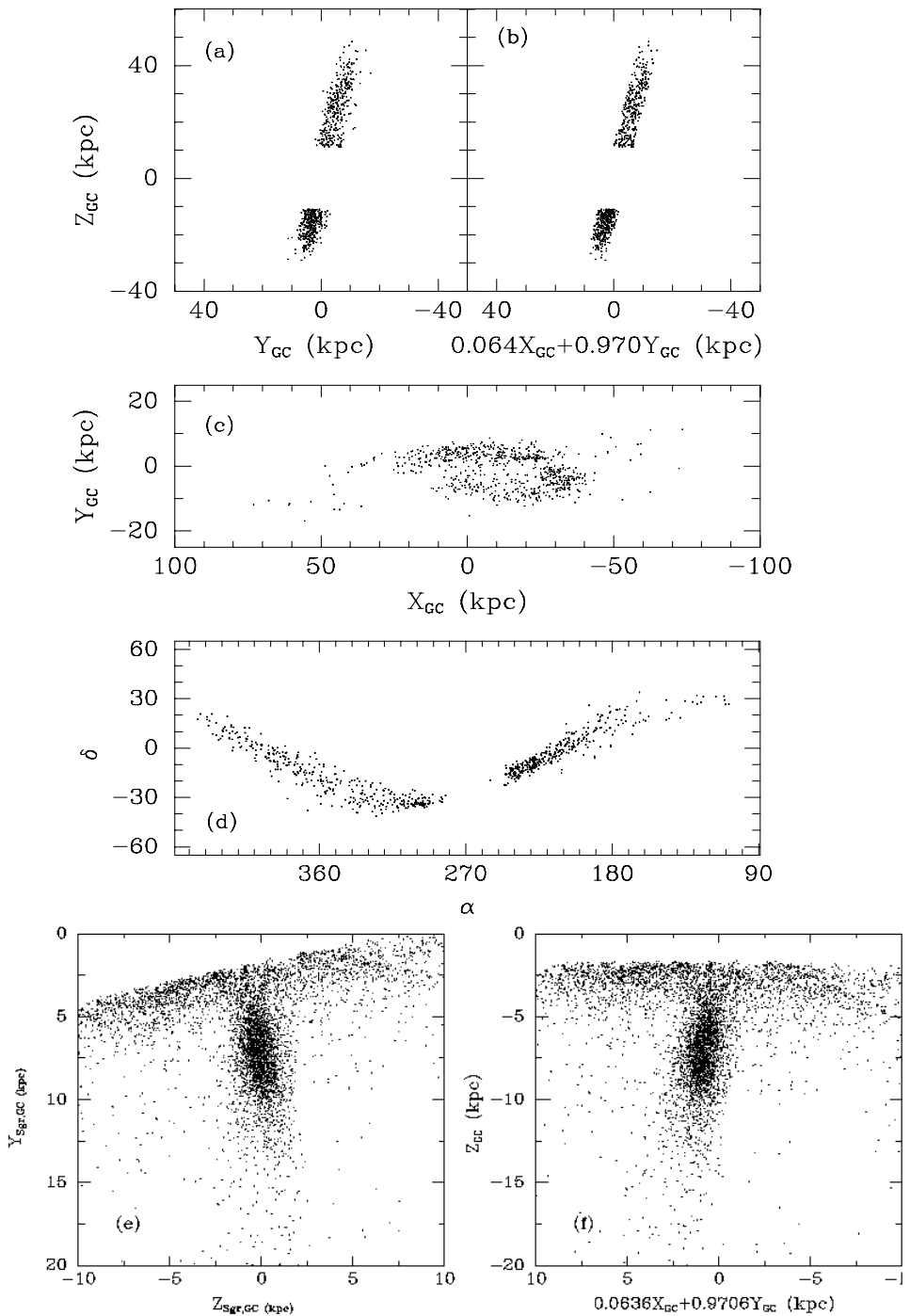


Fig. 7.— In panels (a)-(d) the points used to define the Sgr orbital plane are used to show various projection effects. (a) The Galactic  $Y_{GC} - Z_{GC}$  plane. (b) The plane shown in panel (a) but rotated by  $3.8^\circ$ . This projected plane is perpendicular to the derived best fitting plane. By definition, the width of the material is narrower as well in Figure 7b compared to Figure 7a. (c) A projection parallel to the Galactic plane. (d) The projection on the sky in celestial coordinates, showing the foreshortening effects of varying proximity to the Sun. In panels (e) and (f) we show edge-on views of the best-fitting Sgr plane all stars with  $(J - K_s)_o > 1.0$  and  $E(B - V) < 0.555$ , but restricted to the far side of the Galactic Center ( $R_{GC} \sin(\Lambda_{GC} + 21.60^\circ) > 9$  kpc) to highlight the Sgr core. Both figures are edge-on to both the Galactic plane and to the Sgr plane, but the coordinate system in (e) has the best-fitting Sgr plane along  $Z = 0$ , while panel (f) is rotated so that the Galactic plane is at  $Z_{GC} = 0$ . Canting of the Sgr main body with respect to both these planes is evident.

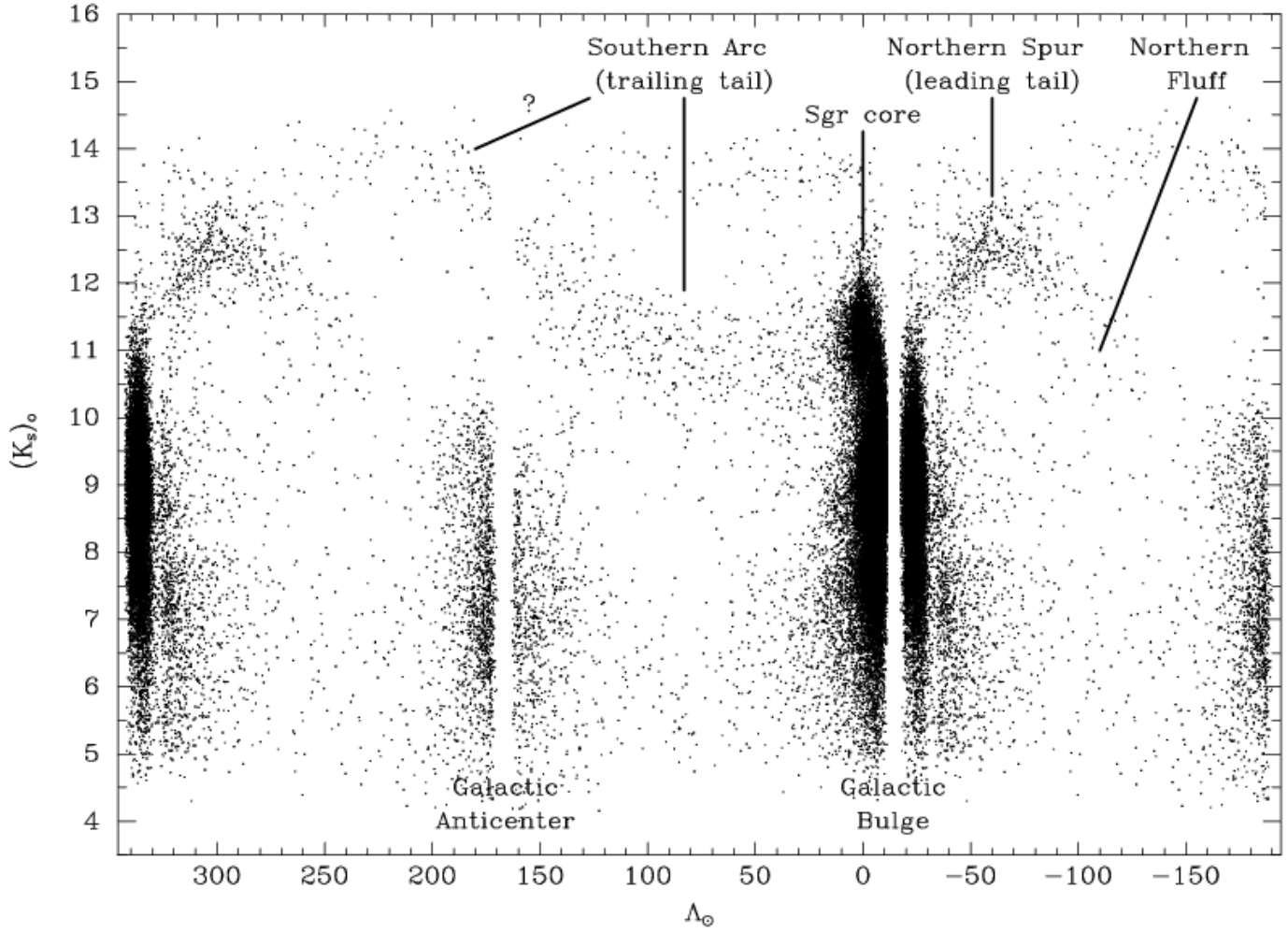


Fig. 8.— Dereddened  $K_s$ -band magnitudes for M giant candidates with  $(J - K_s)_o > 1.00$  shown as a function of Sgr longitude,  $\Lambda_\odot$ , along the great circle in the sky defined by the Sgr debris (Sgr orbit). Only candidates within Sgr latitude range  $-10^\circ < B_\odot < +10^\circ$  are shown. For clarity, we remove sources with  $E(B - V) > 0.555$ . The Sgr core is at  $(\Lambda_\odot, [K_s]_o) = (0^\circ, 11.25 \text{ mag})$ . Other features and possible features of the Sgr debris stream are indicated.

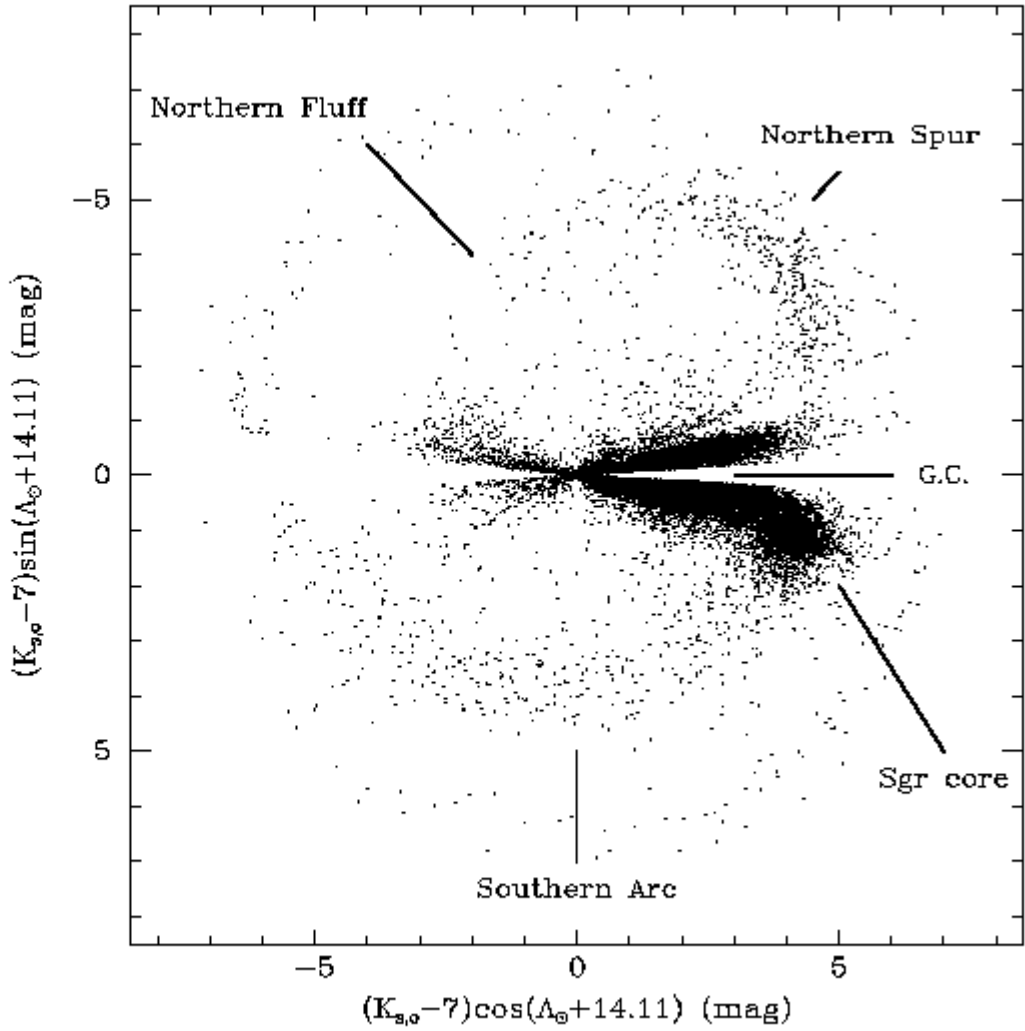


Fig. 9.— Same as Figure 8, but shown in a cross-sectional plot of the Sgr orbital plane (that is, the approximation of that plane given by the  $[\Lambda_\odot, B_\odot]$  coordinate system), where  $(K_s)_o$  magnitudes of M giant candidates are shown radially (after subtraction of 7 mag). Stars with  $(K_s)_o$  have been left out of the figure. The term  $(\Lambda_\odot + 14.11^\circ)$  ensures that the Galactic plane is horizontal across the center of the figure. The direction of  $\Lambda = 0$  is the direction towards the Sgr core (to the right and below the Galactic plane) and  $\Lambda_\odot$  increases counterclockwise. We show the same sample of stars as given in Figure 8.

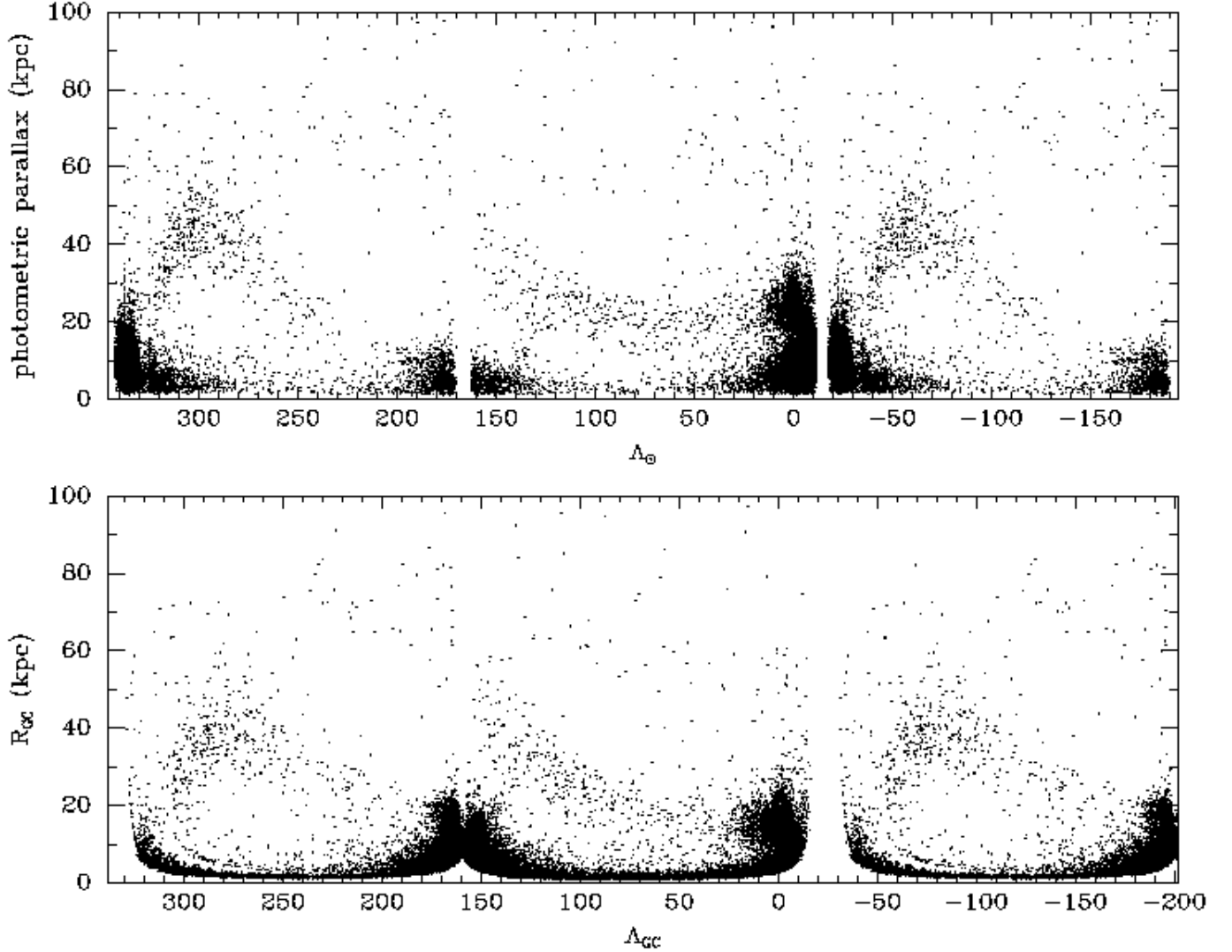


Fig. 10.— (Top) Same as Figure 8, but for photometric parallaxes (in kpc) after assigning each M giant candidate an absolute magnitude according to its  $J - K_s$  color. Stars within Sgr latitude range  $-10^\circ < B_\odot < +10^\circ$  are shown. (Bottom) The perspective from the Galactic Center point of view. After calculation of photometric parallaxes, distances from the center of the best fit plane from Section 5.2 are calculated. For this panel, we have adopted a stellar sample with  $(J - K_s)_o > 1.00$  and  $E(B - V) < 0.555$ , as in the top panel, but here we show stars with  $-10^\circ < B_{GC} < +10^\circ$ . To remove additional contamination at large distances (where the adopted  $B_{GC}$  latitude range translates to a broad spatial range) we impose the additional constraint that stars lie within 7 kpc of the best fit Sgr plane.

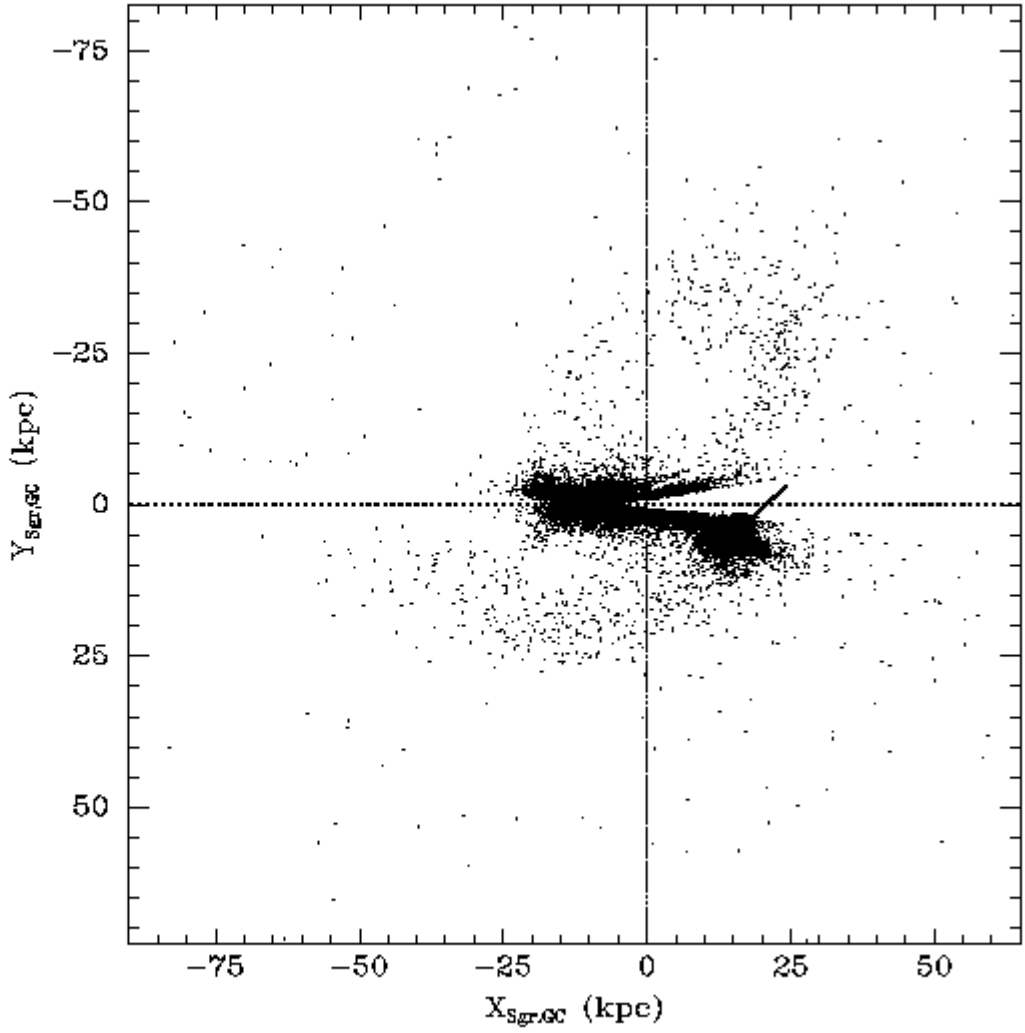


Fig. 11.— Similar to Figure 9, but the radial dimension now shows distances from the Galactic Center derived from the photometric parallaxes, and the plane shown is the best-fit plane from Section 5.2 (the plane shown is slightly tilted from a traditional  $[X_{GC}, Z_{GC}]$  projection – see Table 2). The center of the coordinate system is actually given by  $(X_{GC}, Y_{GC}, Z_{GC}) = (-8.51, -0.21, -0.05)$  kpc (see Section 5.2). The stellar sample is the same as that shown in the lower panel of Figure 10. The nominal position of the Sgr core and the direction of motion is shown by the filled circle and line. The Sgr proper motion and radial velocity are from Ibata et al. (1997). The continuity of the Northern Spur and Southern Arc, and their association with the Sgr core, is evident in this projection, despite obscuration by the Galactic disk. The reader is reminded that the width of Sgr features in this plot are artificially broadened by  $\sigma_d/d = 0.17$  because of the “standard candle” scatter (see Section 5.2).

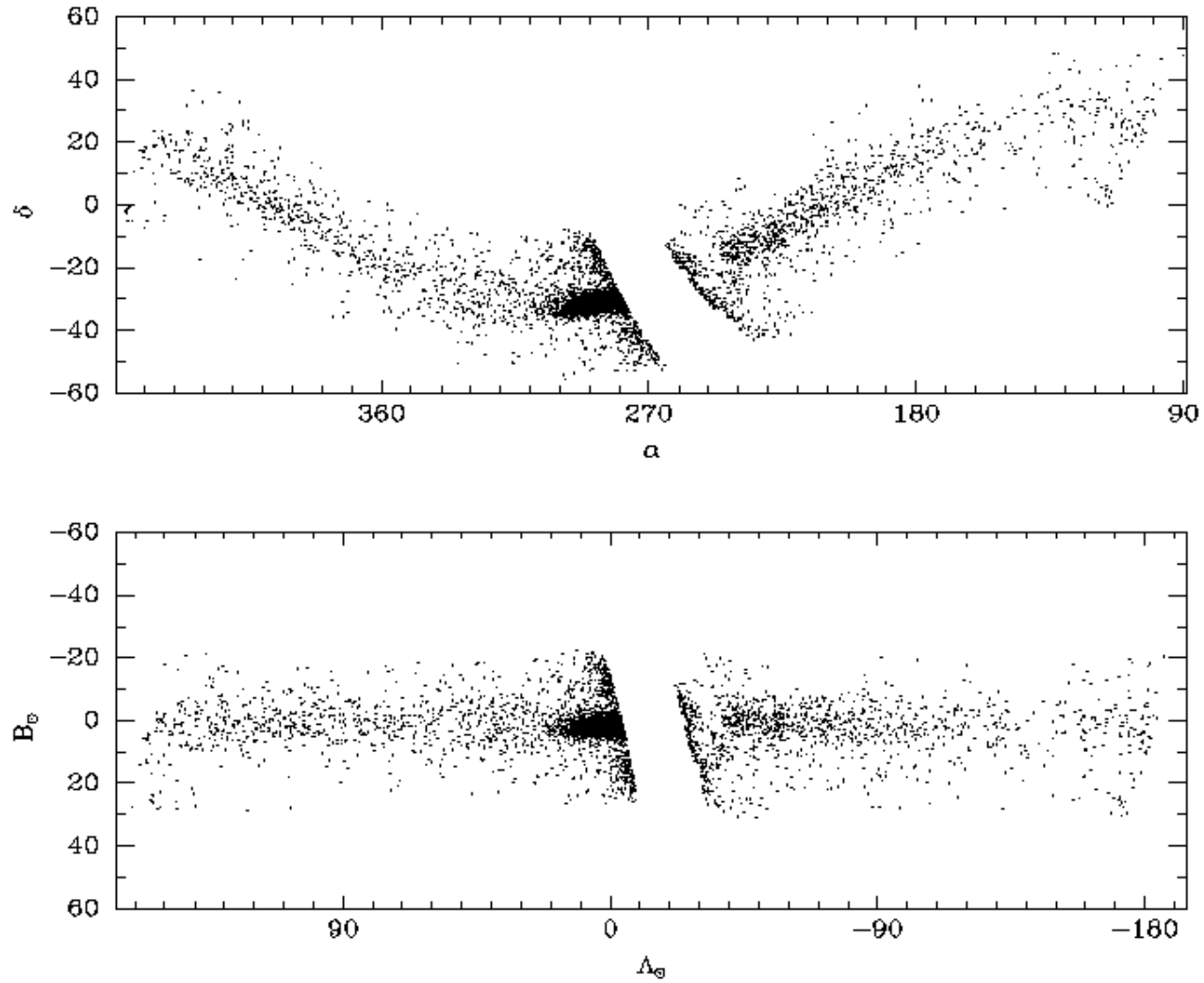


Fig. 12.— The  $-7 < Z_{Sgr,GC} < 7$  kpc sample explored in the next Figure shown in equatorial and Sgr coordinates.

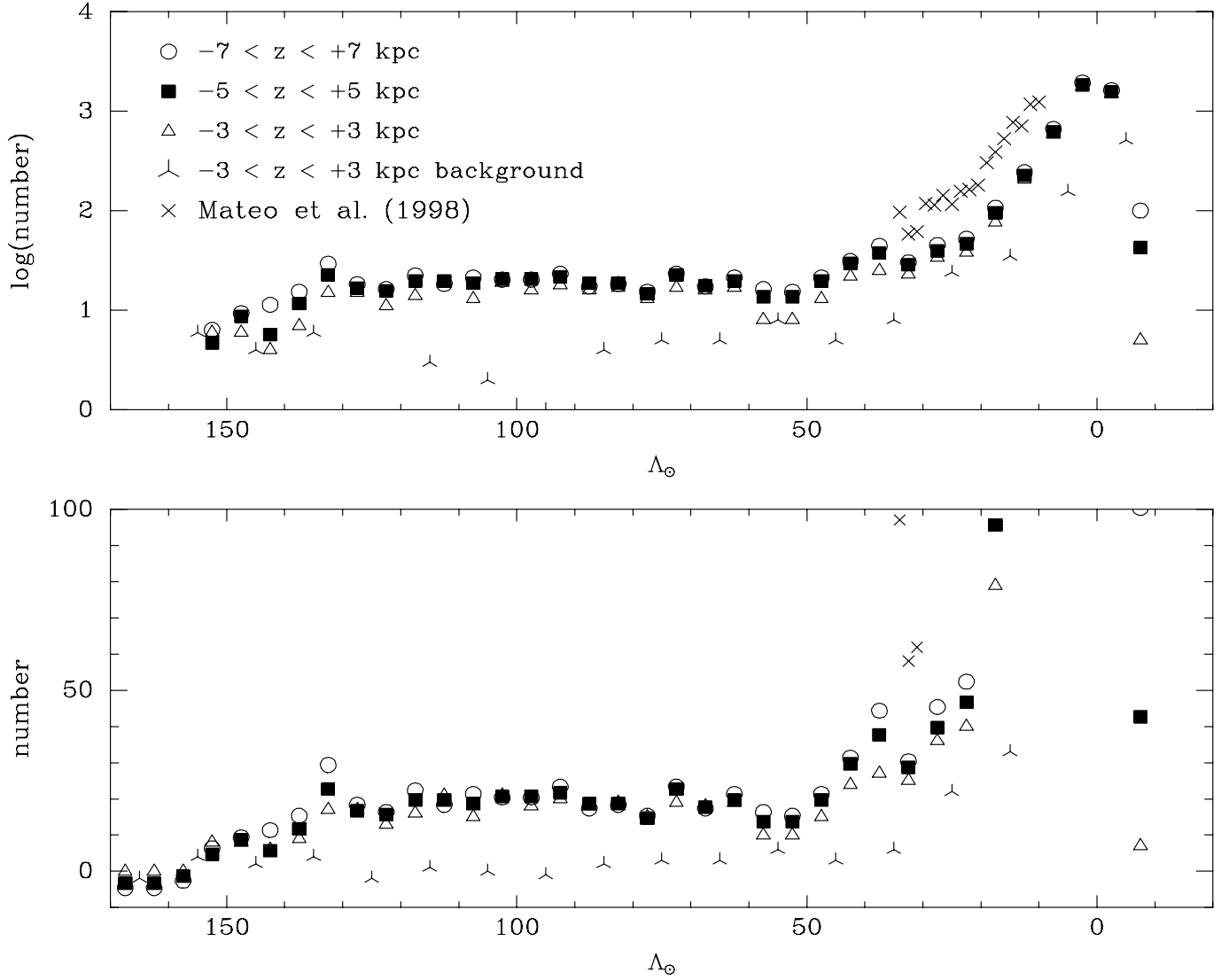


Fig. 13.— Background-subtracted counts (per  $5^\circ$  of longitude) of  $0.95 \leq (J - K_s)_o \leq 1.10$ , trailing tail M giants as a function of longitude  $\Lambda_\odot$ . Counts for different allowed ranges of distance,  $z$ , from the best-fitting Sgr mid-plane are shown. To improve statistics, the background points are shown for  $10^\circ$  longitude bins, rather than the  $5^\circ$  bins shown for the Sgr tail data.

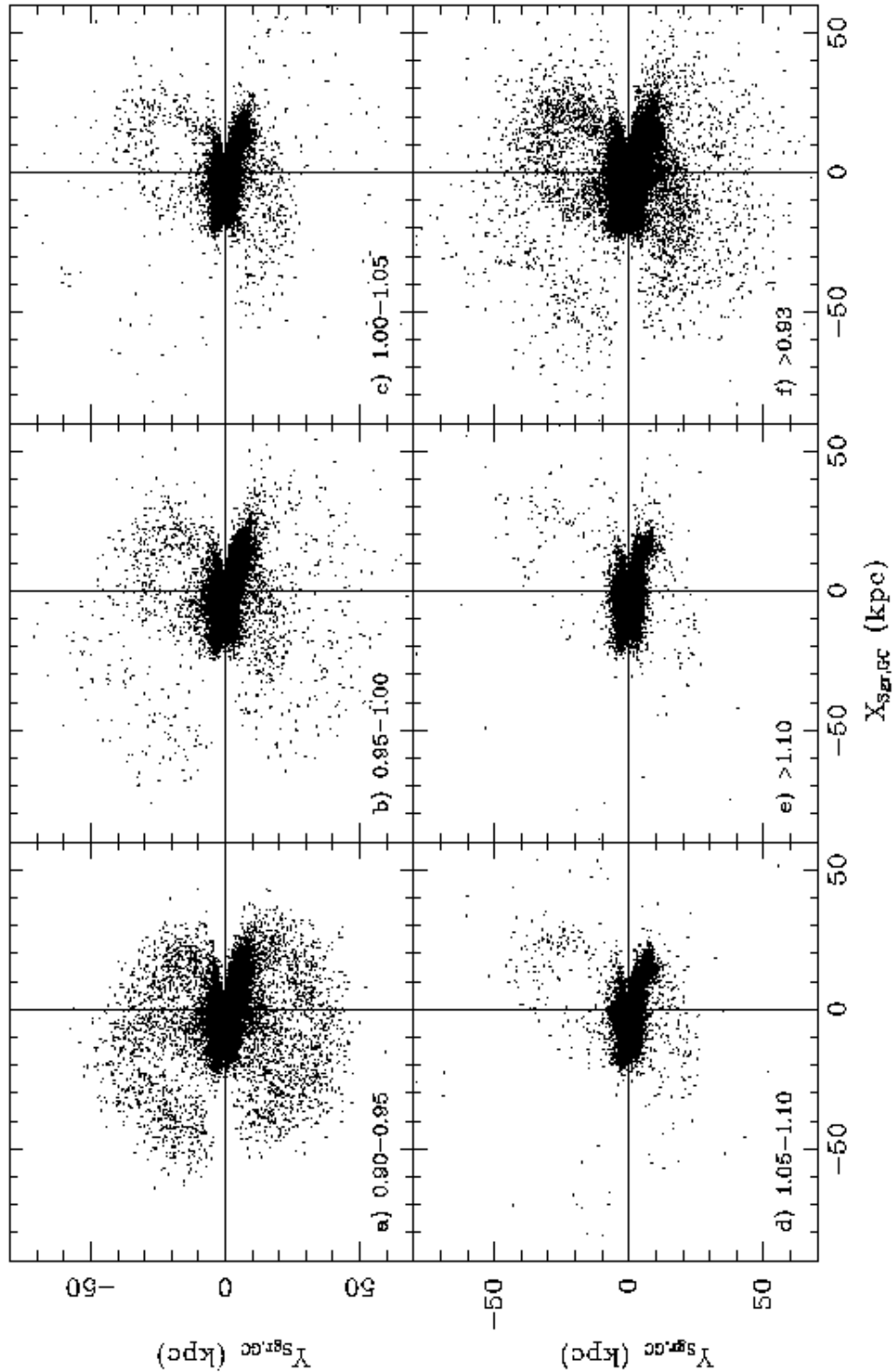


Fig. 14.— The  $-7 < Z_{Sgr,GC} < 7$  kpc late type giant candidate sample shown by various  $(J - K_s)_o$  color bins. All stars with  $E(B - V) \geq 0.555$  have been removed from the sample. The solid lines mark the approximate location of the Galactic Center.

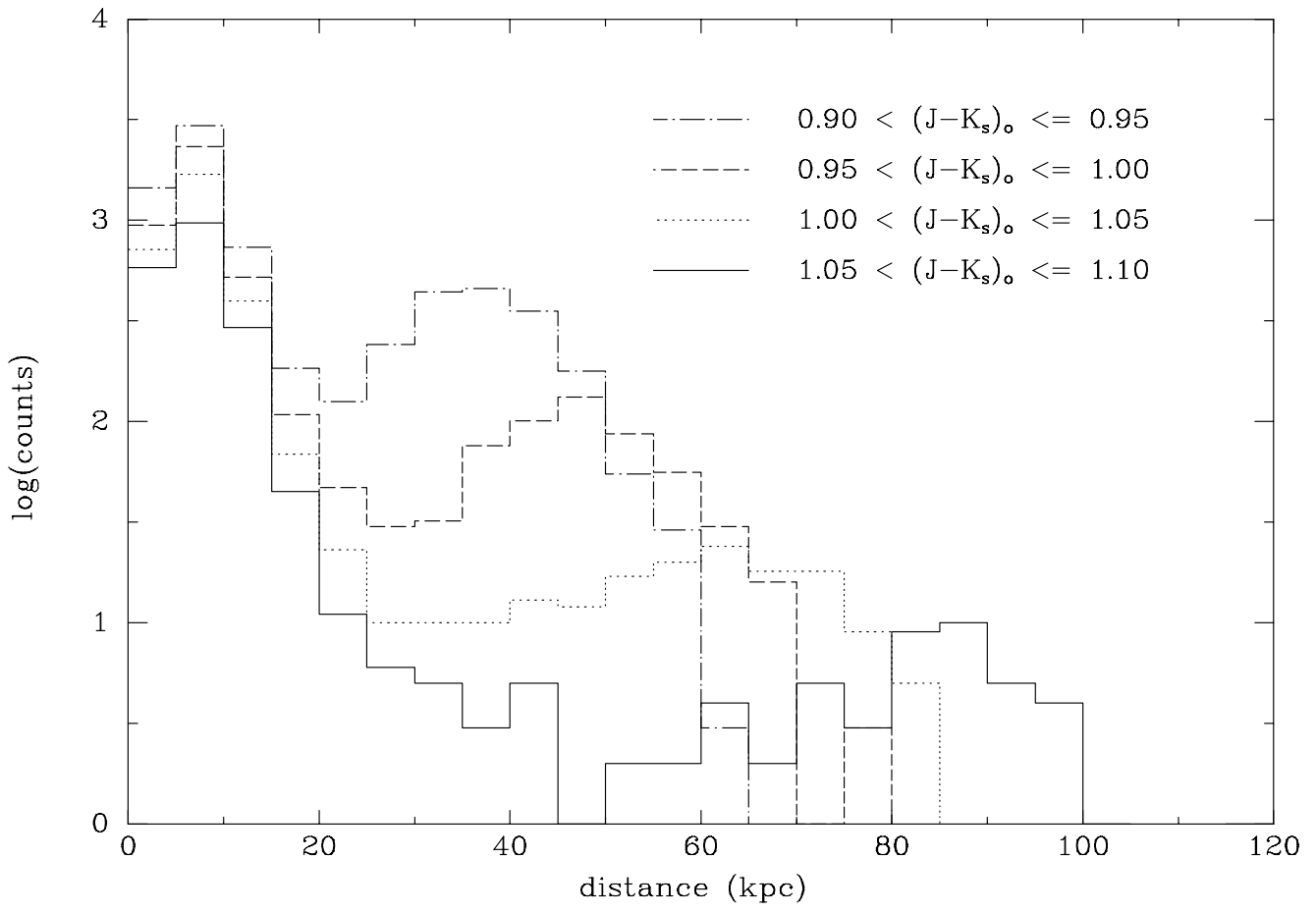


Fig. 15.— Starcounts as a function of radius in a wedge ( $Y_{GC} > 0, Z_{GC} > 0, Z_{GC} > Y_{GC}$ ) more or less free of Sgr and the Magellanic Clouds for various  $(J - K_s)$  color bins. All stars with  $E(B - V) \geq 0.555$  have been removed from the sample.

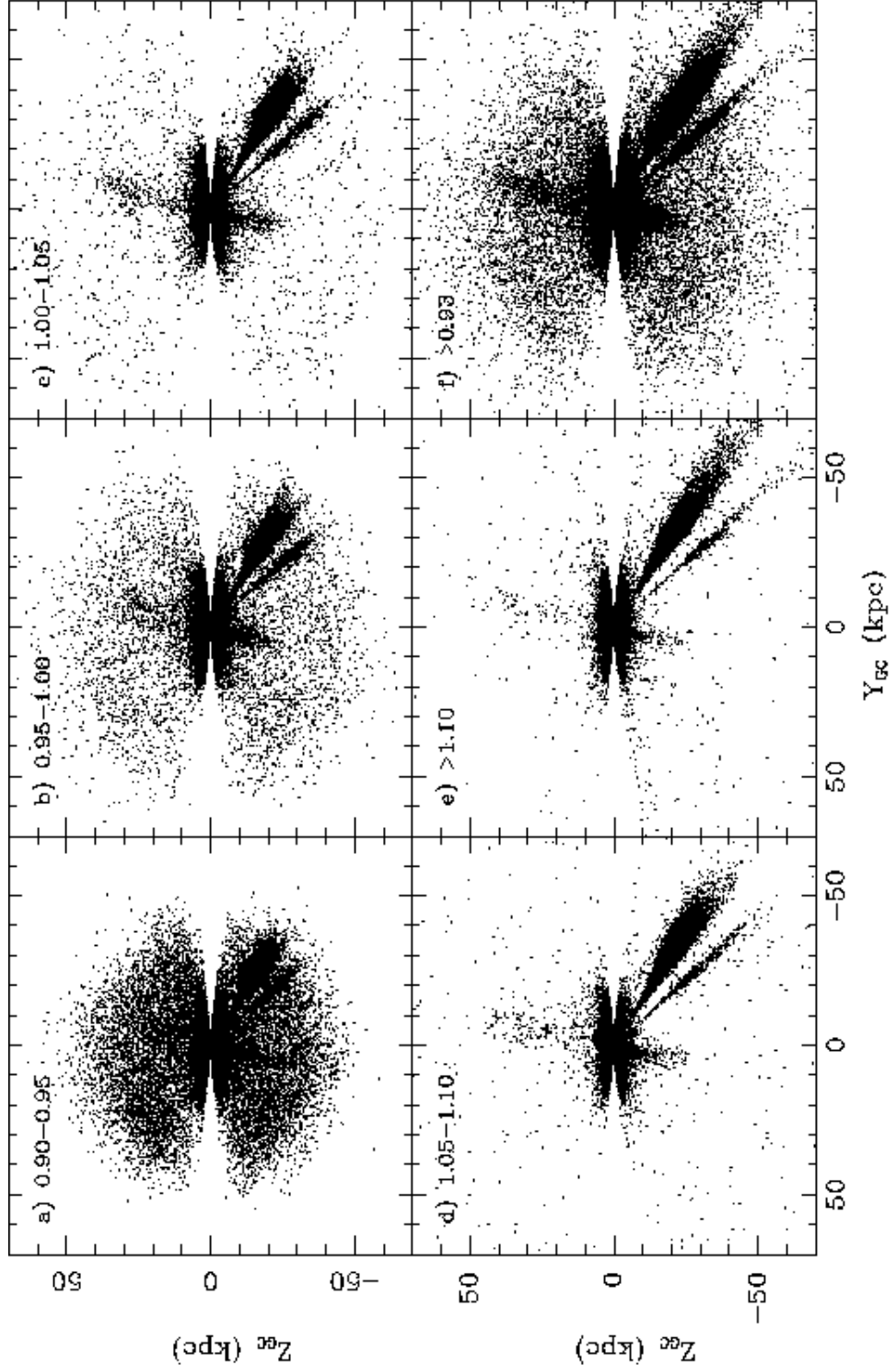


Fig. 16.— Views of the Milky Way distribution of 2MASS late type giant candidates in projection on the Galactic  $YZ$  coordinate system. The panels show the distribution by various  $(J - K_s)_o$  color bins. All stars with  $E(B - V) \geq 0.555$  have been removed from the sample. The “bowing” of the Sgr plane is due to the Galactocentric parallax effect described in Section 5.2.

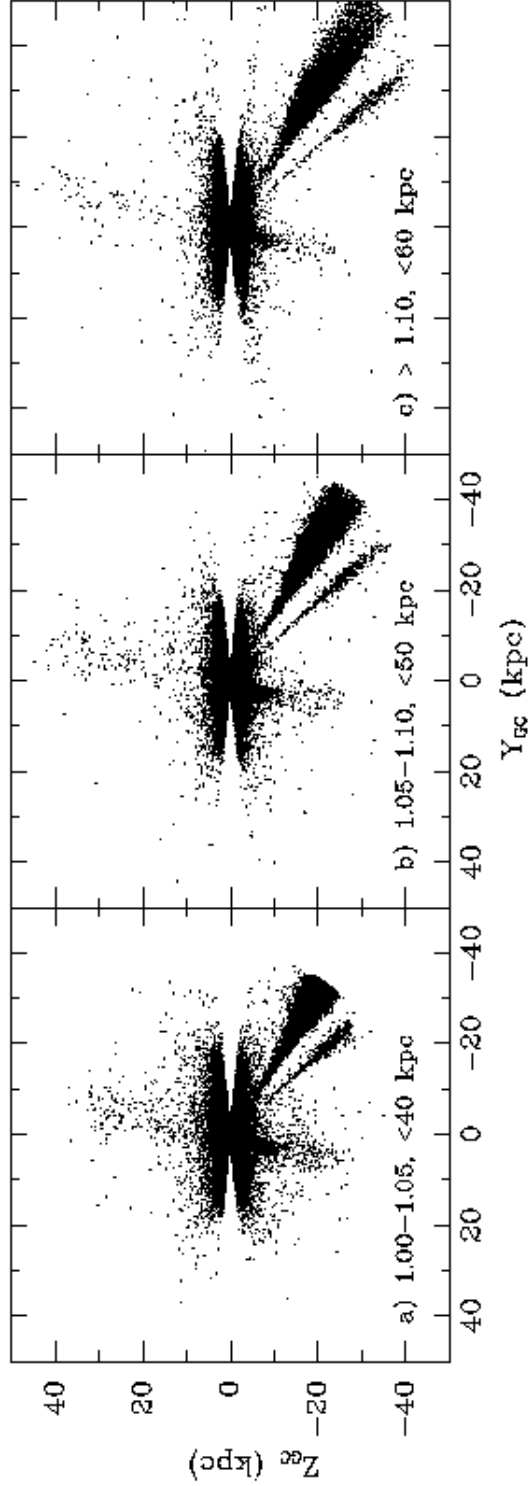


Fig. 17.— Same as Figures 16c-e, but, in order to improve the signal-to-noise contrast, with the samples pruned to stars with projected photometric parallaxes less than 40 kpc, 50 kpc, and 60 kpc in the  $(J - K_s)_o$  samples shown in panels a), b) and c), respectively. Note that the end of the Northern Loop is slightly truncated by these distance limits.

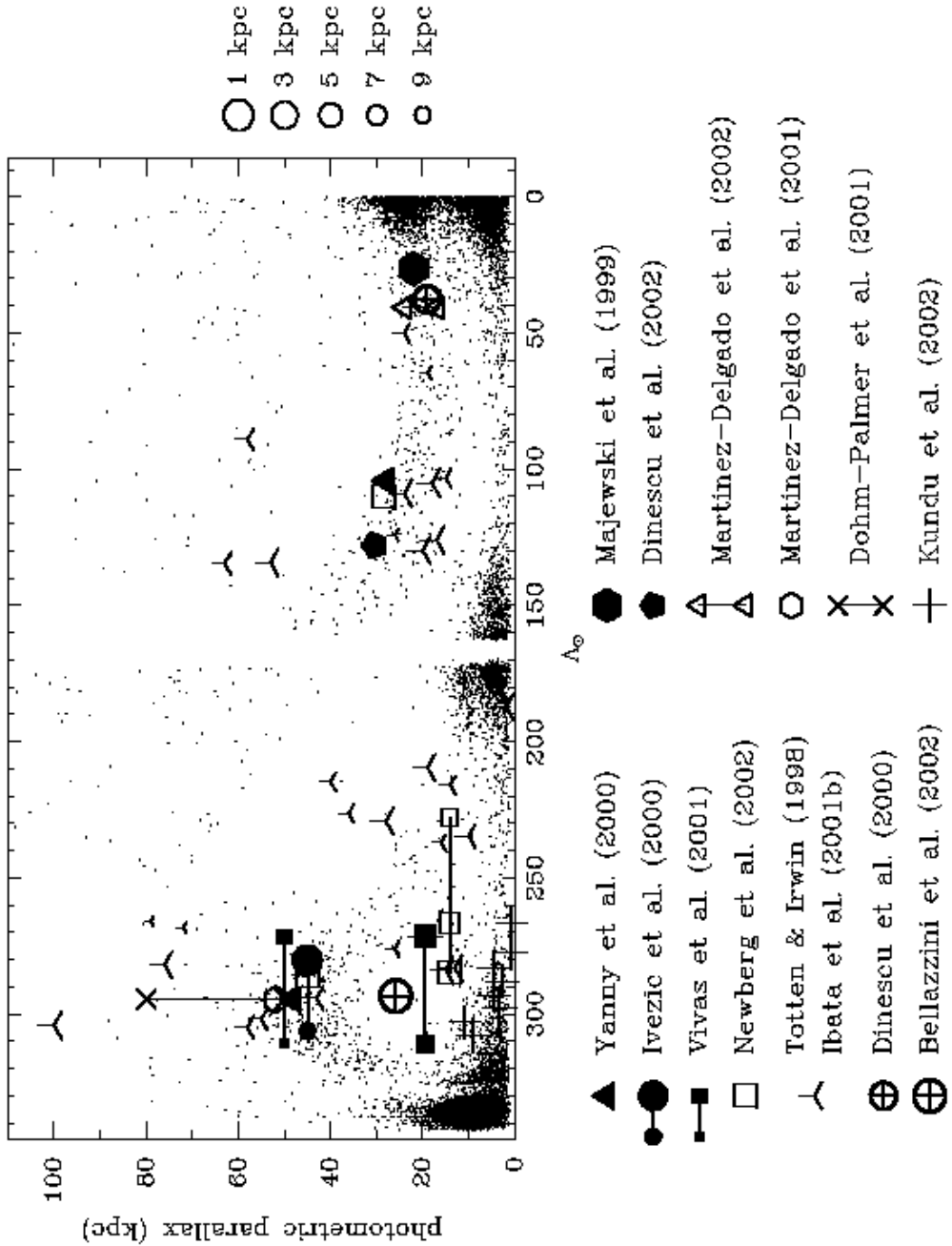


Fig. 18.— Summary of previous claims or suggestions of Sgr debris detections. Only detections near or outside the tidal radius are shown. Solid symbols are used for detections based on horizontal branch stars. Open symbols denote detections making use of main sequence stars. Cross-like symbols are detections based on red giant branch or asymptotic giant branch (i.e. carbon) stars. The clusters Pal 12 (Dinescu et al. 2000) and NGC 5634 (Bellazzini et al. 2002) are shown by circled plus symbols. In some cases the papers cited give either a range of distance, an uncertainty of distance, or a range of longitude for their Sgr detections. These ranges are indicated by solid lines connecting points. In each case, the symbols are sized to indicate relative proximity of the detection, at the cited distance, to the  $\Lambda_{GC}$  Sgr midplane (an approximate size scale is shown in the legend to the right). In the case when ranges of values are shown, the endpoint sizes correspond to the relative  $Z_{Sgr,GC}$  distance at that point. The Martinez-Delgado et al. (2002) and Dinescu et al. (2000) symbols have both been shifted by one degree of longitude away from each other, respectively, for clarity. To reproduce the Ibata et al. (2001b) carbon star sample, only Totten & Irwin (1998) carbon stars with  $11 < R < 17$  and having radial velocities are used, and this sample is trimmed to only stars within 12 kpc of the Sgr plane. Obviously dusty carbon stars for which only an upper limit to distance has been given by Totten & Irwin (1998) have been left out.

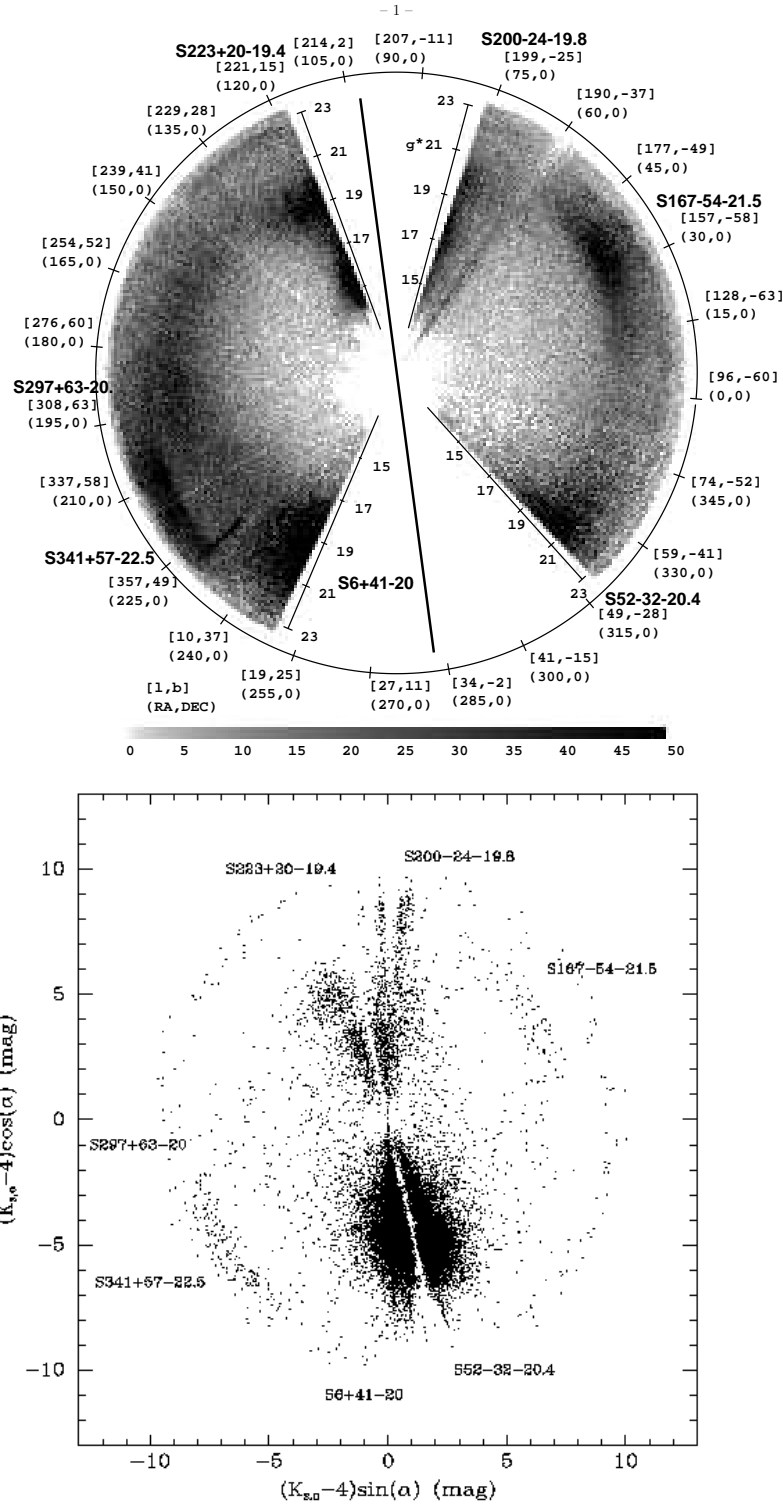


Fig. 19.— *Upper panel:* Main sequence turnoff stars from the Sloan Digital Sky Survey equatorial slice by Newberg et al. (2002), reprinted by permission of Heidi Newberg. *Lower panel:* Celestial Equator slice of the 2MASS Mgiants for comparison to the Sloan Digital Sky Survey (Newberg et al. 2002, Figure 1). All stars within  $10^\circ$  of the equator, and having  $1.00 < (J - K_s)_o < 1.10$  from the color-color selected catalogue are used in this rendition. We exclude stars with  $|b| < 5^\circ$ . The azimuthal directions of features identified by Newberg et al. (2002) are indicated. Two spikes appearing at the very top of the figure are from inexact dereddening at this low latitude.

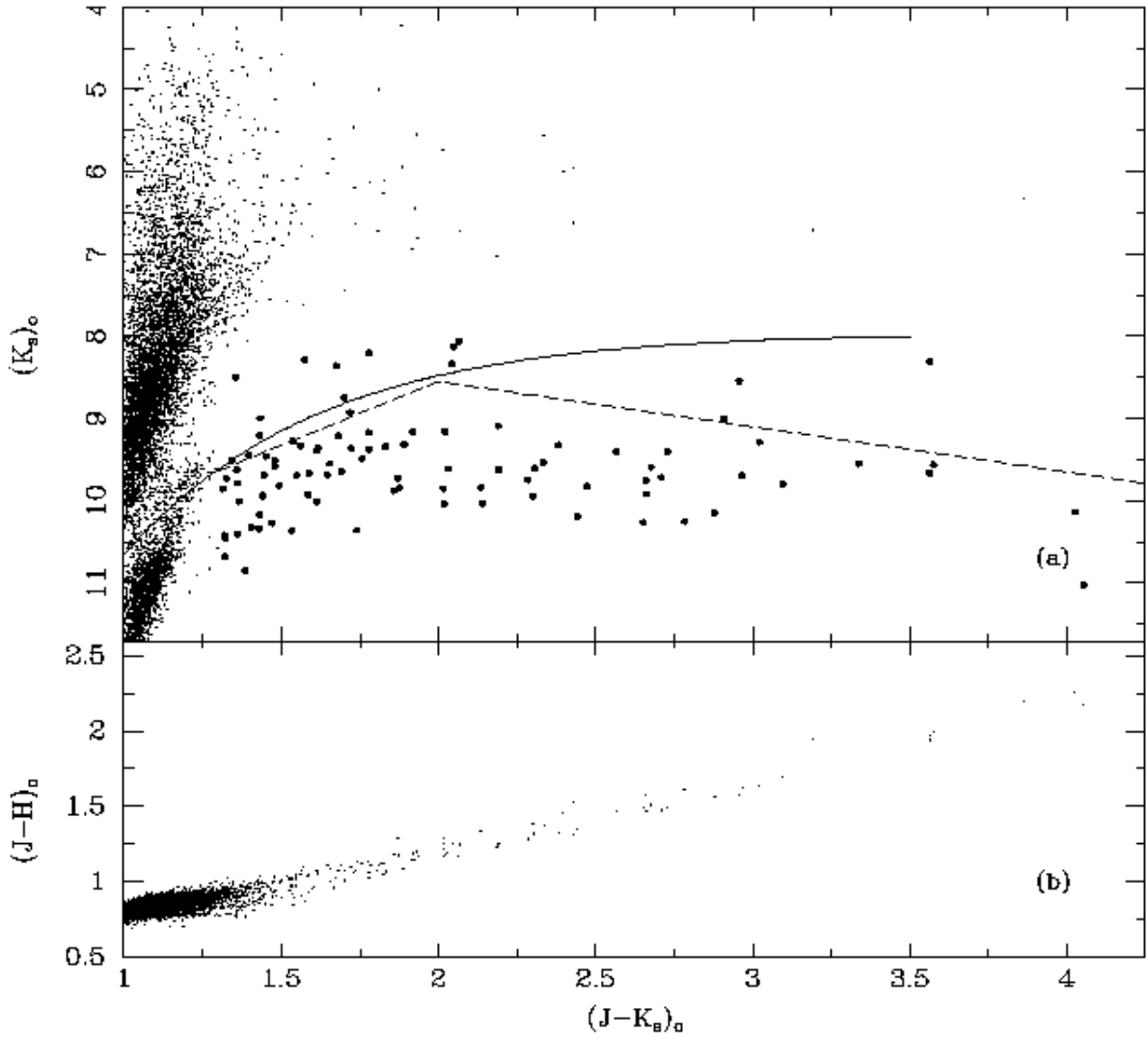


Fig. 20.— Color magnitude diagram of stars within 5 degrees of the Sgr core (Table 1) and highlighting the carbon star population. The *solid line* is the mean carbon star color-magnitude relation from Totten, Irwin & Whitelock (2000) derived as a fit to the NIR photometry of a sample of carbon stars from Milky Way satellite galaxies, converted to 2MASS colors (Carpenter 2000) and shifted to the Sgr distance modulus ( $m - M = 16.9$ ). The *dashed line* shows the approximate ridge line for LMC carbon stars in Weinberg & Nikolaev (2001), shifted 1.65 mag brighter to account for the distance modulus difference between Sgr and the LMC. Points used in the various fits discussed in the text are marked with larger points. Stars in this plot also obey the following dereddened color criteria:  $(J - H) > 0.40(J - K_s) + 0.25$  and  $(J - H) < 0.561(J - K_s) + 0.36$ .

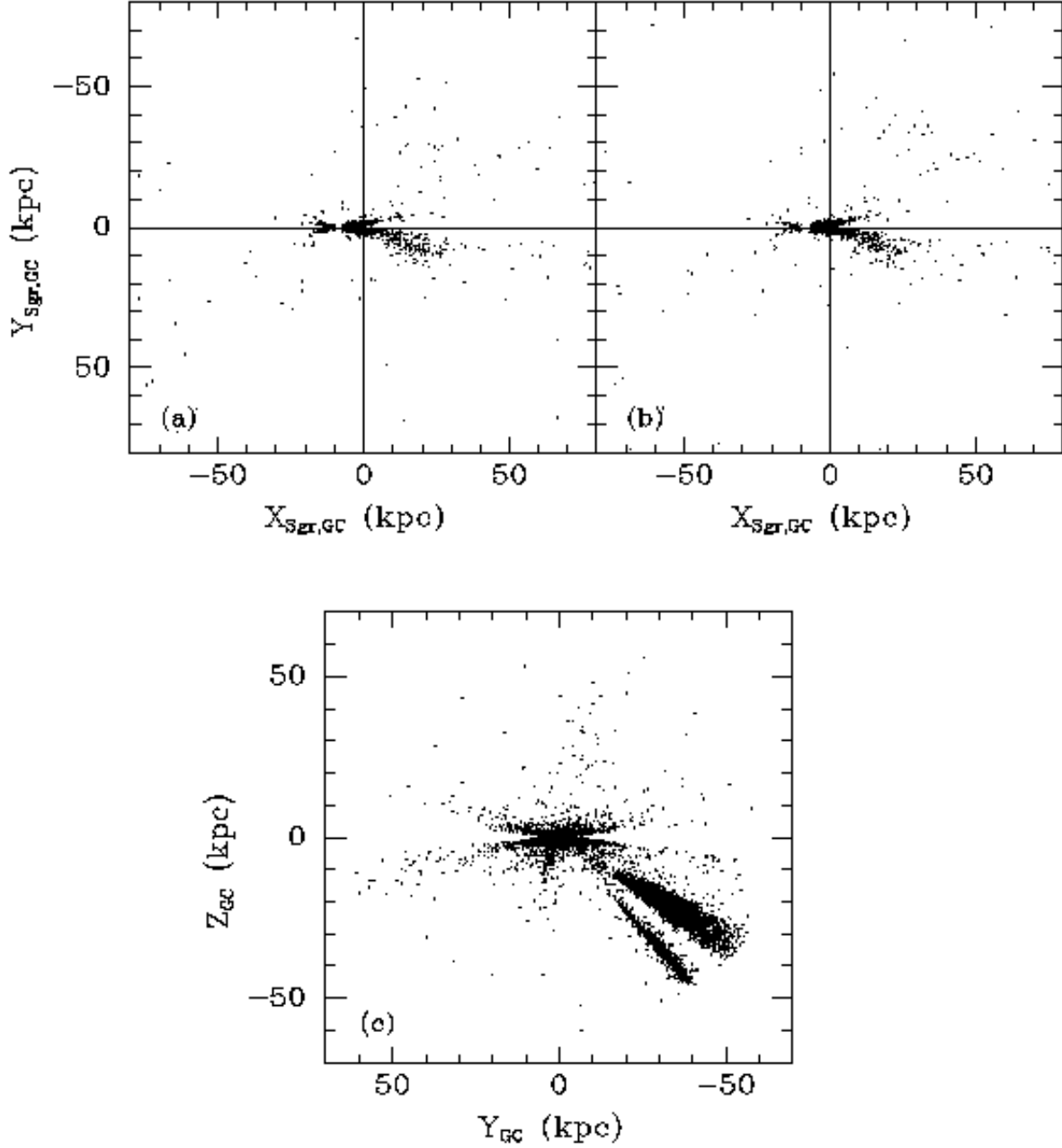


Fig. 21.— Planar distribution of all carbon star candidates within  $|B| = 10^\circ$  of the  $\Lambda_\odot$  plane and  $(J - K_s)_o \geq 1.3$ . (a) Distribution after applying the Weinberg & Nikolaev (2001) LMC ridge lines, adjusted to the distance modulus of Sgr and dimmed an additional 0.5 mag. (b) Distribution after assuming all carbon stars have  $M_{K_s} = -7.31$ . In both panels, a large number of stars - likely contaminants - have projected photometric parallaxes beyond the bounds of the region shown. A small hole in the distribution near the Sun is from carbon stars incompleteness at the bright end of the catalogue used here. (c) Nearly edge-on view of carbon star sample with distances as in panel (b). In this panel all carbon star candidates with  $(J - K_s)_o \geq 1.3$  are shown, but, for clarity, the sample has been limited to  $(K_s)_o < 11.75$ .

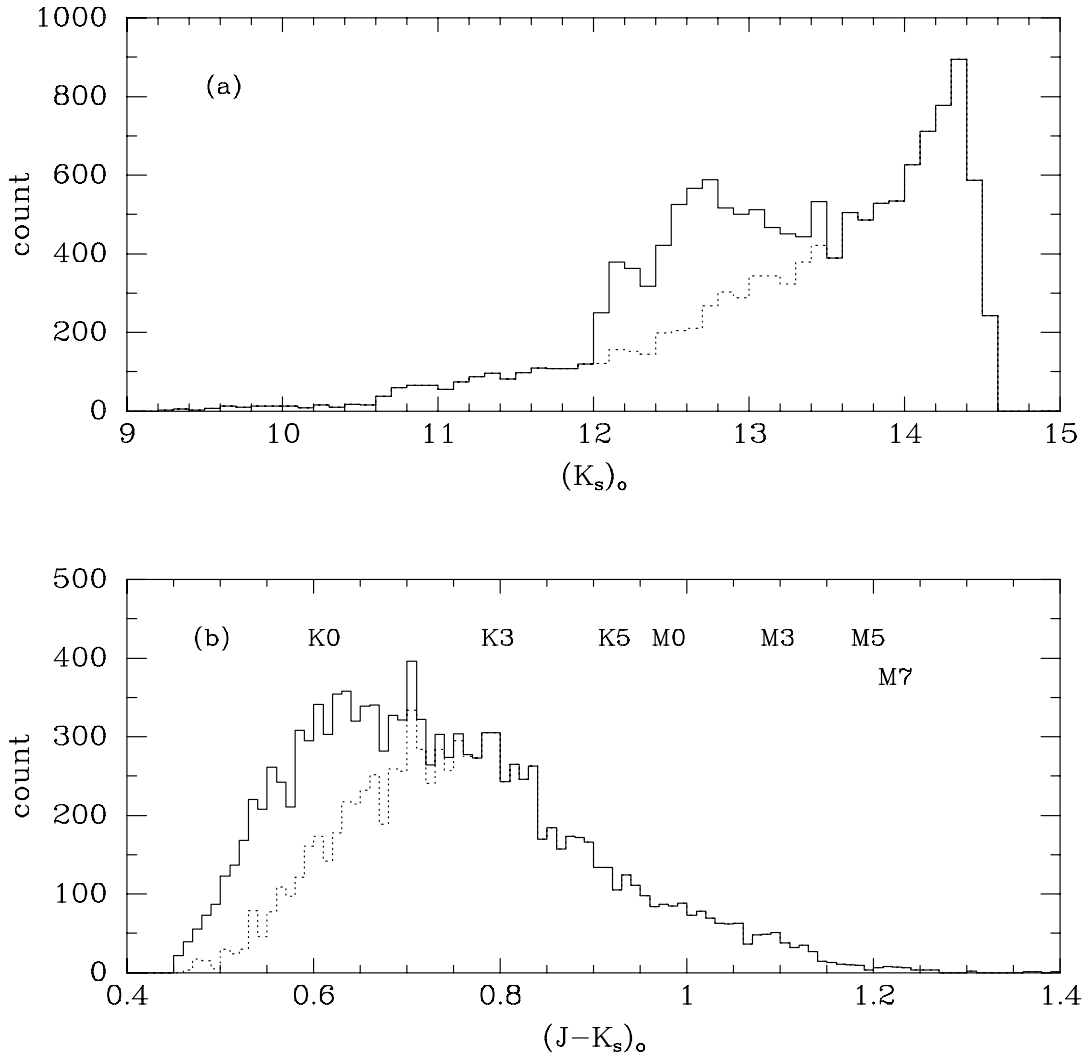


Fig. 22.— (a) Luminosity function for evolved Sgr stars shown in Figure 1c. *Dotted line*: Luminosity function for the RGB only, isolated by the relation  $(K_s)_o > -7.22(J - K_s)_o + 17.64$ . *Solid line*: RGB plus red clump, where the latter is defined by  $(J - K_s)_o > 0.45$  and  $12 < (K_s)_o < 13.5$ . (b) Color function for stars with  $(K_s)_o < 14.3$ . Lines as in panel (a). The color function becomes incomplete for *RGB stars* bluer than  $(J - K_s)_o \sim 0.80$ . Approximate colors (ignoring metallicity effects) for spectral types for luminosity class III objects from Bessell & Brett (1988) are indicated (converted to the 2MASS system using Carpenter 2001).

Table 1: Profile Fits to the Sgr Main Body

parameter	King Profile Fit	Power Law + Core Fit
$\alpha_{center}$ (deg)	$283.7467 \pm 0.0133$	$283.8313 \pm 0.0034$
$\delta_{center}$ (deg)	$-30.4606 \pm 0.0256$	$-30.5454 \pm 0.0114$
$\alpha_{center}$ (2000)	$18:54:59.2 \pm 00:00:03.2$	$18:55:19.5 \pm 00:00:00.8$
$\delta_{center}$ (2000)	$-30:27:38 \pm 00:01:32$	$-30:32:43 \pm 00:00:41$
$l$	5.6193	5.5690
$b$	-14.0660	-14.1665
background (stars arcmin <sup>2</sup> )	$1.422 \times 10^{-5}$	$2.016 \pm 0.623 \times 10^{-6}$
position angle (deg)	$104.3 \pm 0.6$	$100.2 \pm 0.6$
ellipticity	$0.65 \pm 0.01$	$0.62 \pm 0.01$
core radius (arcmin)	$224 \pm 12$	$234 \pm 10$
King radius (arcmin)	$1801 \pm 112$	...
Power Law index, $\nu$	...	$1.44 \pm 0.03$

Note. — The errors for all parameters given have been derived using a Metropolis Markov Chain algorithm (see Ostheimer et al. 2002).

Table 2: Eulerian Transformations to the Sagittarius Coordinate Systems

System	Euler angles			rotation center		
	$\phi$ (deg)	$\theta$ (deg)	$\psi^a$ (deg)	$X_{GC}$ (kpc)	$Y_{GC}$ (kpc)	$Z_{GC}$ (kpc)
$(\Lambda, B)_\odot$	183.8	76.5	194.1	0.0	0.0	0.0
$(\Lambda, B)_{GC}$	183.8	76.5	201.6	-8.51	-0.21	-0.05

Note. — a - Adopted as  $180.0^\circ$  for some figures in order to keep the intersection of the Sgr and Galactic planes parallel to  $X$ -axis.

Table 3: Color of the RGB Tip for Sgr Populations

age (Gyr)	[Fe/H]	$(J - K_s)_{2MASS}$
10-11	-1.3	0.968
5	-0.7	1.035
0.5-3	-0.4	0.665-1.114

---

Note. — RGB tip colors from Bertelli et al. (1994) with conversions from Bessell & Brett (1988) colors to 2MASS colors using transformations in Carpenter (2001).

Table 4: Counts of Stars in Sgr Core by Spectral Type and Color

Spectral type	Adopted $(J - K_s)_o$ Range	Counts
>M0III	> 0.980	1000
K3III-M0III	0.797 – 0.980	3009
K0III-K3III	0.611 – 0.797	> 4678
red clump	see text	2978

---

Note. — Color definitions from Bessell & Brett (1988) translated to 2MASS system using Carpenter (2001).